WHITE **PAPER**

cadence®

5G Communications

Featuring Cadence AWR Software

This white paper examines the recent advances that the modeling, simulation, and design automation capabilities in Cadence® AWR® software are helping designers develop the antenna and RF front-end components that are making 5G a reality. This primer offers a breadth of application notes on the innovative wizards and synthesis technologies that enable engineers designing 5G communications systems to deliver cost-effective, high performance, and high-reliability products to market.

Contents

Overview

5G new radio (NR) is driving many of the requirements for wireless products today. Achieving the aggressive goals of 5G is being addressed in several key areas. Spectral usage, which includes variations on orthogonal frequency division multiplexing (OFDM)- based waveforms and inter-and intra-band carrier aggregation (CA) is important, especially for spectrum below 6GHz. Another goal is enhancing over-the-air (OTA) efficiency with the expansion of multiple-in-multiple-out (MIMO) and beam-steering technologies. A final goal is moving to higher frequencies, particularly above 6GHz and into the centimeter- and millimeter-wave (mmWave) range. As 5G pushes into these higher frequencies, beam-steering antennas will be required to direct radiated energy from the base station antenna array to the end-user while overcoming the higher path losses that occur at these frequencies.

Figure 1: Mobile devices sending out radio waves which spread out in a crowd of people

Regarding the RF and microwave hardware components that support these different systems, three main trends will continue to be true. First, performance such as bandwidth, linearity, and efficiency will be critical and will have a major impact on devices like power amplifiers (PAs), filters, and antennas. Second, the integration of multi-technology modules and embedded devices will be critical for bringing high-performing, cost-effective communications products to market quickly. Third, the escalating cost of product development for complex systems will require in more coordinated engineering efforts. Recent advances in the modeling, simulation, and design automation capabilities AWR software are helping designers develop the antenna and RF front-end components that are making 5G a reality.

Basics of Design: Raising the Levels of 5G mmWave Signals

Fifth-generation (5G) wireless network technology is being touted as the true "next generation" of wireless communications, capable of performance levels far beyond the limits of current Fourth Generation (4G) Long Term Evolution (LTE) wireless networks. While 5G wireless networks have not yet been designed or standardized, most global system- level planners agree on the need for more bandwidth to increase data capacity, and much of that additional bandwidth is expected to come from the mmWave frequency range, such as 60GHz for high-data-rate, short-haul wireless links. The use of mmWave signals has proven quite successful in 77GHz automotive radars as part of collision-avoidance safety systems, and the large bandwidths available within the mmWave frequency range (30 to 300GHz) hold the promise of increased network capacity compared to 4G/ LTE which is quickly reaching its limits. Building 5G networks that leverage mmWave bandwidths, however, requires mmWave signals at sufficient signal strength and that will depend on the availability of practical mmWave PAs.

Designing a mmWave PA is not trivial. Signals at those frequencies are so-named for the fact that their wavelengths are only 1 to 10 mm long. Given the physical connection between frequency, wavelength, and various circuit features needed to support operation at those high frequencies, such as resonators and transmission line structures, design challenges arise from the extreme miniaturization of mmWave circuits and the need to conserve signal power as much as possible by minimizing forward and reflected signal losses.

The Promise of 5G

Expectations are great for 5G networks, even before the infrastructure has been built (Figure 2). Earlier- generation wireless/ cellular networks were based on supporting voice communications, although that started to change with 2G and 3G systems. The nature of modern communications has changed, largely due to the influence of the internet, and has become very data-centric, with network performance defined in terms of data transfer speeds and data capacity.

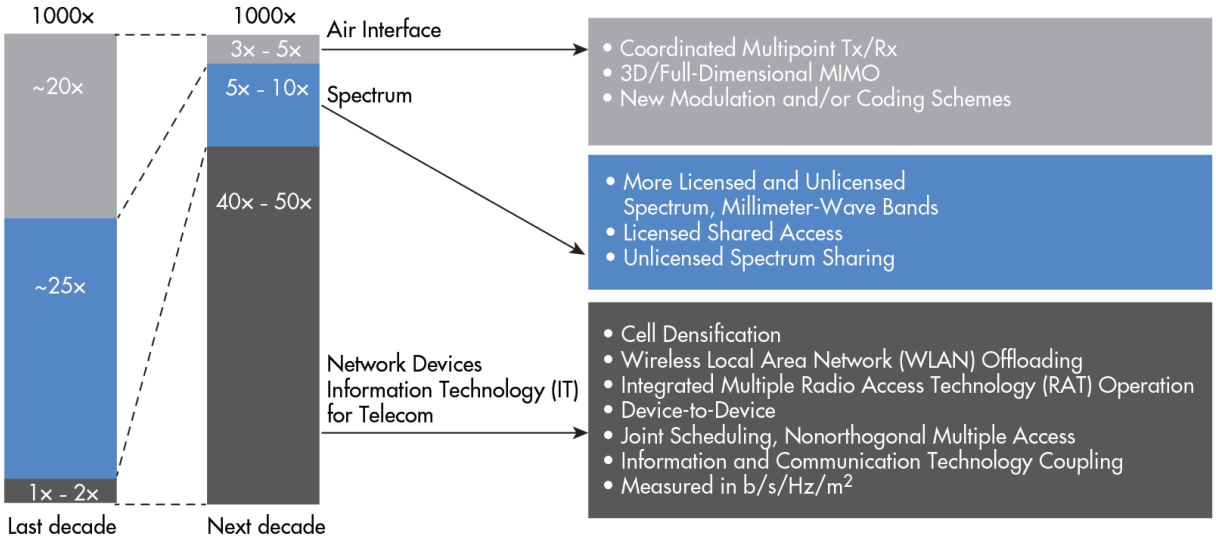

Figure 2: The need for bandwidth to transfer large amounts of data through wireless channels makes the use of mmWave frequencies in 5G wireless networks inevitable. (Image courtesy of National Instruments)

The increasing use of internet of things (IoT) devices, for example, will create a need for wireless networks with much higher data capacity and devices with low power consumption. Many of these devices are "always-on" and "always connected" to the internet via wireless network bandwidth. This is in contrast to a smartphone, which may sit idle for long periods with no consumption of network capacity. But many IoT devices will need to remain connected, such as for medical and health-care monitoring and that expected network capacity must be available in 5G systems. Projections vary on the number of IoT devices that will require wireless network access in the next few years, but numbers as high as several trillion devices suggest huge bandwidth/data-capacity requirements just based on IoT devices, without even considering a growing number of smartphones on the same networks.

The inevitability of 5G wireless networks is due to the fact that current 4G networks are limited in data capacity and speed. Compared to 3G wireless networks, 4G networks achieved performance improvements by means of enhanced spectrum efficiency, typically through the use of advanced modulation and coding techniques. Antenna techniques such as MIMO schemes also helped increase spectrum efficiency in 4G systems as well as the use of novel radio technologies, such as OFDM, to make better use of the available spectrum. These improvements have made possible relatively fast data transfer rates in 4G/LTE systems, as fast as 1Gb/s for stationary devices and about 100 Mb/s for moving mobile devices communicating through the network. But proponents of 5G wireless networks note the capacity requirements of so many IoT devices and the growing demands for fast data transfers and streaming video, with the expectation that 5G systems will operate at 10 times the speed of 4G/LTE networks, or at 10Gb/s.

The capacity of a wireless network is affected by a number of factors, including the available bandwidth, the number of communications channels, the number of cells, and the signal-to-noise level of the system. By adding bandwidth in the form of mmWave frequencies, 5G wireless networks can gain capacity, but system planners hope to do so without a significant increase in energy consumption, a requirement that will impact the design of PAs for 5G networks, whether at mmWave or lower frequencies (Figure 2).

Power Amplifier Basics

In general, a PA can be characterized by a number of performance parameters, including gain, gain flatness, output power, linearity, efficiency, input and output VSWR, and noise figure (NF). The usable frequency range of a given PA is determined by an amplifier's capabilities to deliver acceptable RL levels of performance for the greatest number of performance parameters over a given frequency range. Gain, for example, tends to be highest at an amplifier's lowest frequencies and lowest at its highest frequencies, with the variations in gain across frequency RL summarized by an amplifier's gain-flatness specification. A value of ±1dB, for example, denotes no more than 2dB variation in gain across the frequency range.

Output power is a function of the input signal power, the gain, and the acceptable amount of gain compression at the output. For most RF through mmWave amplifiers, output power capability is measured and listed at the 1dB compression point, often abbreviated as P1dB. More output power may be possible, by increasing the level of the input signal power, at the cost of linearity, such as when the amplifier is represented by the signal distortion that occurs, for example, when the amplifier is driven to output power at 3dV compression. An amplifier with the highest linearity would be one in which the output signals are most proportional to the input signals in terms of waveform shape, differing in amplitude level as a function of gain. With the digital modulation schemes proposed in 4G and 5G networks, the peak-to-average power ratio (PAPR) is considerably higher than in earlier wireless communications standards. A higher PAPR results in an amplifier operating well into its compression region, unless the amplifier is operated considerably below its compression point (this is achieved by using a larger-periphery active device). As a result, amplifiers may be characterized and model details specified at higher compression points or determining impedance- matching requirements or design activity is focused on optimizing matching networks for output-power backoff operation.

High linearity for most PAs is achieved by operating with lower-than-maximum input power signal levels so that the active devices operate without gain compression. On the other hand, most amplifiers are most efficient when operated with input power levels that cause compression, at a point where an amplifier is considered at saturation and its highest output-power level because an increase in output power no longer follows an increase in input power.

Linearity is a key parameter for 5G PA designers due to the need for maintaining high signal integrity (SI) and low signal distortion for the complex modulated signal waveforms used to achieve high-data-rate communications. Amplifier linearity traditionally comes at the cost of power consumption, such as in a Class A or Class AB linear amplifier in which the active devices are always supplied with input power levels to avoid nonlinear operation.

In a 5G wireless network, however, the mmWave and lower-frequency amplifiers must also operate with high efficiency, so that the energy consumption of a base station or microcell is minimized. Similarly for microwave and mmWave amplifiers that are integrated into smartphones and other mobile/portable wireless devices that are powered by batteries, high linearity must be achieved without sacrificing high power-added efficiency (PAE)— two amplifier parameters that have traditionally been viewed as tradeoffs.

Various amplifier design techniques are available to improve linearity or efficiency. For enhanced efficiency, Doherty amplifier configurations have been used, in which the amplifier essentially consists of two separate amplifiers, operating under different bias conditions (Figure 3). Input signals are split between the two amplifiers and combined at the outputs of the amplifiers, to achieve the best use of bias energy based on waveform shape and level. Envelope-tracking (ET) power-supply techniques are also used to boost PA efficiency, in which the power supplied to the PA follows the shape of the waveform to be amplified, with DC power increasing or decreasing as needed to maintain output power at a certain level.

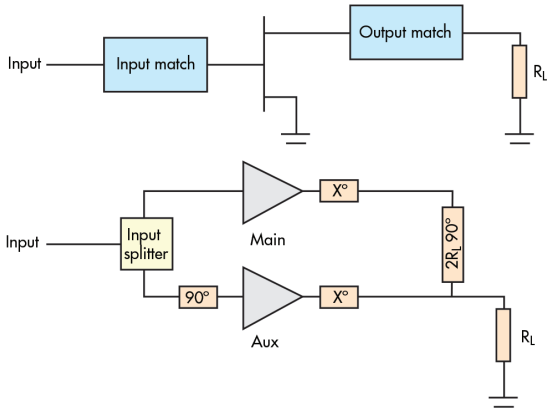

Figure 3: These block diagrams compare a single-ended (one-transistor) Class AB amplifier to a two-way Doherty amplifier

Digital predistortion (DPD) techniques are often used to provide high PA linearity while also achieving reasonable efficiency. Since an amplifier is most efficient when it is operating near saturation, DPD techniques help shape the modulated waveforms to be amplified so that an amplifier can operate with high efficiency but without causing distortion or nonlinearity.

Sorting Through Semiconductors

Amplifiers for 5G and other mmWave applications employ a number of different semiconductor technologies, including transistors fabricated on silicon-germanium (SiGe), gallium-arsenide (GaAs), indium phosphide (InP), gallium-nitride (GaN), and devices on substrates of different materials, such as GaN on silicon (GaN-on-Si) and GaN on silicon carbide (GaN-on-SiC), which has excellent thermal properties for effective dissipation of heat.

Silicon laterally diffused metal oxide semiconductor (LDMOS) devices are well established as high-power active devices in 3G and 4G base stations, capable of generating the transmit power levels required. Silicon semiconductor PAs based on silicon-on-insulator (SOI) CMOS devices have also delivered lower power levels when multiple transistors are used in stacked configurations. Output power levels approaching 1W with linear gain have been achieved at frequencies as high as 28GHz, with diminishing power levels at frequencies extending into the higher mmWave range, demonstrating that low-cost silicon substrates may still be a viable semiconductor material candidate for 5G handset applications at mmWave frequencies.

The choice of semiconductor material for a 5G PA will likely be determined by whether the PA will be used in a handset or a base station and the operating frequency range since a number of different frequency bands have been allocated by regulatory organizations around the world. Frequencies from 4 to 6GHz and 24 to 86GHz have been considered for different portions of 5G networks, with different PA output-power requirements ranging from as little as 0.2W at higher frequencies to as much as 30W in the lower- frequency range.

A key characteristic for any semiconductor material as a starting point for 5G PAs is relatively high electron mobility, so that different device structures will provide higher than unity gain at mmWave frequencies. A variety of different device topologies have been fabricated. All of these substrate materials offer higher electron mobility than ever-popular silicon substrate materials, making them attractive substrate materials for mmWave active devices. Many different device topologies have been fabricated on these high-frequency substrate materials, including MESFETs, heterojunction bipolar transistors (HBTs), and high-electron-mobility transistors (HEMTs), each with its own gain and power characteristics in support of mmWave PAs.

GaN in its various forms has gained favor among PA designers at RF and microwave frequencies and GaN mmWave devices are starting to become more practical. Whereas semiconductor substrate materials such as SiGe, InP, and GaAs are capable of supporting transistors with cutoff frequencies (fT) of 300GHz and higher, GaN substrates support active devices with much higher power densities, making it possible to fabricate discrete devices or monolithic microwave integrated circuit (MMIC) amplifiers at higher power levels and smaller sizes than amplifiers made from the other semiconductor substrates.

Design Strategies

As noted, the design of an effective mmWave PA for 5G applications requires achieving a balance among a number of competing performance parameters, such as linearity and efficiency. Depending upon the capabilities of a particular active device technology, a designer has a choice of many different amplifier topologies, from single-stage amplifiers to multistage designs. The design will be dictated by the final set of performance requirements, such as frequency range, gain, output power, linearity, and PAE.

Achieving the optimum performance from the active devices in a PA requires matching the complex source and load impedances of a given device to the 50Ω characteristic impedance of a 5G system. This is typically done by means of measurements of device S-parameters using a vector network analyzer (VNA) with suitable frequency range for the device under test (DUT) for small-signal (and input impedance matching) and a source/load-pull tuner capable of presenting a wide range of impedances to a DUT with a fine-tuning resolution for large-signal (nonlinear) output impedance matching. Optimum source impedance will usually enable a PA to deliver low NF performance while optimum load impedance is required for nonlinear performance, such as for acceptable levels of output power, PAE, and linearity, including adjacent channel power ratio (ACPR) and error-vector magnitude (EVM), as shown in Figure 4. Because a large number of measurements may be required to determine the optimum source and load impedances, the use of an automated load-pull measurement system from companies such as Maury Microwave and Focus Microwaves as well as test system software programs such as LabVIEW from National Instruments can dramatically reduce the time needed to characterize an active device in preparation for developing PA matching networks.

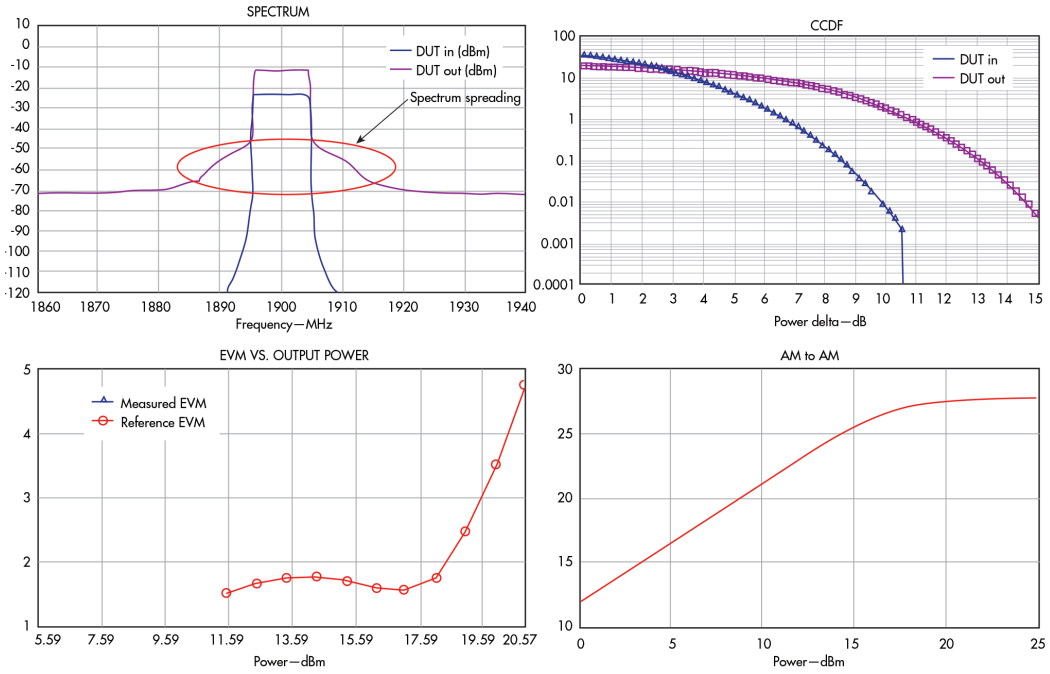

Figure 4: Many current mmWave PA designs incorporate waveguide interconnections to minimize input and output interface losses. (Photo courtesy of Millitech Corp.)

Amplifier design in AWR Design Environment® platform, specifically AWR Microwave Office® circuit design software, can either be based on a compact or behavioral model representing the transistor(s). An alternate design approach is to develop matching circuits based on the results of load-pull data (measured or simulated from a compact model). To make use of the large data sets that may characterize the power transistors used in communications amplifiers, circuit simulation tools such as AWR Microwave Office software support dedicated RF design features that help the engineer plot critical performance metrics via contour mapping and develop impedance-matching networks through self-guided design utilities. The circuit simulation engines (linear and harmonic balance) combine with integrated EM simulation (2.5D and 3D) to enable "what-if" type analyses of a circuit design, to predict the effects of different transmission-line lengths and configurations of passive devices, even different impedance-matching networks on the output power and gain possible from a particular device. In support of amplifier designers, the company recently made available an application note on designing high-efficiency Doherty amplifiers: "Designing a Modified Three-Level Doherty Amplifier for Use in Next-Generation Communications Systems," (available for download at www.awr.com/resource-library/designing-modified-three-level-doherty-amplifier-use-next-generation-communication).

Depending on the specific application (mobile or base- station), a 5G power amplifier will need to address a given frequency range, power level, efficiency, and linearity specifications. Standard linear simulations are used to derive many of these amplifier performance metrics such as gain vs. frequency, return loss, etc. The advanced measurements associated with 4G/5G operations require simulation testbenches that can replicate standard defined modulated waveforms. AWR Design Environment provides the simulation technology, 5G modulation waveforms (the major proposed techniques including CP-OFDM) and preconfigured testbenches (Figure 5) to simulate performance such as the ACPR, a measure of spectral regrowth due to amplifier nonlinearity or EVM, another linearity measurement that describes the error vector in the I-Q plane between the ideal constellation point and the point recovered by the receiver.

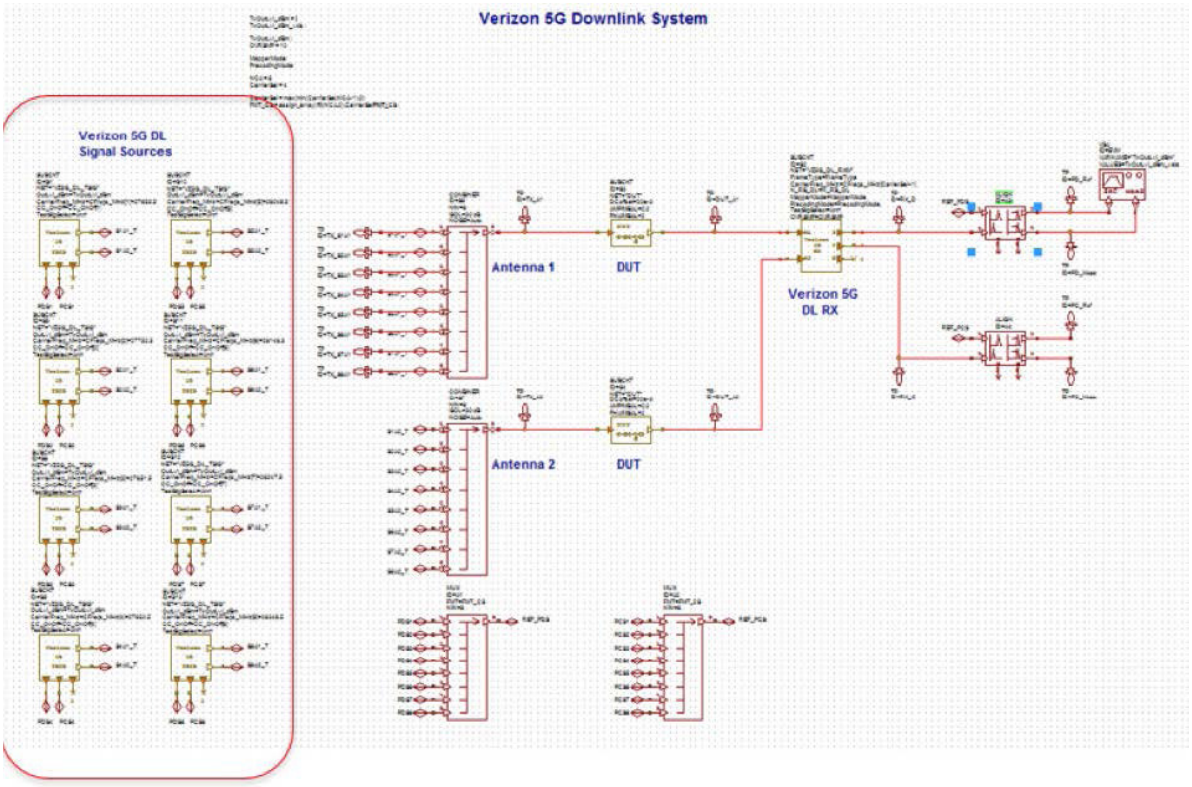

Figure 5: Microwave Office enables simulations of critical PA performance parameters such as error vector magnitude (EVM, RMS% and absolute) based on transistor model or measured load-pull data

Although mmWave frequencies represent enormous amounts of bandwidth for 5G networks and other EM-based applications, such as automotive radar/safety systems, the PAs for those applications will most likely be needed and designed for relatively narrow bandwidths. For one thing, channel allocations by organizations such as the FCC refer to relatively narrow frequency bands around a center frequency, such as 24, 28, or 60GHz, so that wide bandwidths are not needed for these wireless channels. In addition, the impedance-matching networks needed for optimum PA performance are much easier to design at narrow bandwidths than at wider bandwidths, especially as the center frequency of the amplifier increases well into the mmWave range.

Note: This Basics of Design is reprinted with permission from Penton Publications.

Designing a Narrowband 28GHz Bandpass Filter for 5G

5G will increase network capacity, reduce latency, and lower energy consumption through a number of innovative technologies aimed at enhancing spatial and spectral efficiency. The use of CA, mmWave spectrum, base station densification, massive MIMO and beam-forming antenna arrays will combine to support the goals of 5G communications at the cost of more signals operating in close spectral and spatial proximity.

These enabling technologies place new demands on the filters required to mitigate signal interference across a dense network of base-stations and mobile devices. This article examines the factors driving the physical, electrical, and cost restraints for 5G filters. To address these challenges, a narrowband filter design methodology using classic filter network theory, parameterized EM simulation, and port-tuning techniques is presented in this article. The approach is demonstrated using the AWR Design Environment platform to develop a narrowband 28GHz bandpass cavity filter targeting mmWave backhaul applications.

5G Applications and Filter Requirements

5G will be deployed in stages to address three main thrusts; enhanced mobile broadband (EMBB), massive machine-type communications (mMTC), and ultra-reliable and low-latency communication (URLLC) for remote sensing and control for medical and autonomous vehicle applications. On the infrastructure side, densely populated urban environments will utilize mmWave-frequency spectrum for higher data rates. Wireless backhaul is likely the most cost-effective and versatile solution to connect 5G base stations to the core network. Filters developed for wireless backhaul application will face challenging cost and volume concerns, which must be considered early in the design stage.

Design Approaches and Filter Specifications

Ideal filter responses are well defined by math functions, which has led to the development of numerous commercial synthesis tools that can generate circuits for an exact filter response based on ideal element values. However, the parasitic behavior of the filter components must be considered early in the design stage. For this reason, synthesis is excellent for accelerating the initial design phase and generating mathematical filter solutions to serve as a starting point to define ideal lumped or distributed networks. However, synthesis can be limited in its ability to generate a physically-realizable filter. In this case, the synthesis tool provides critical coupling coefficient and external Q targets, but the ideal electrical design has limited usefulness for this particular design.

Synthesis tools such as iFilter™ filter synthesis within AWR software can perform the math to exactly produce ideal LC filters and distributed designs such as edge coupled, hairpin, interdigital, and combline, based on ideal distributed microstrip and stripline models. Figure 6 shows several types of narrowband filters that can be synthesized based on microstrip technology with ideal distributed models that do not incorporate manufacturing limits and tolerances. Addressing this uncertainty can be very difficult without a process for converting ideal designs into physically realizable ones.

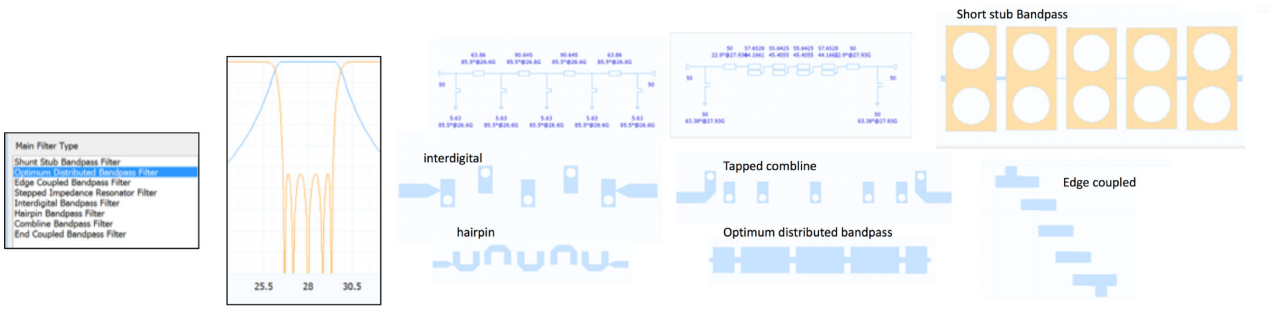

Figure 6: Several types of narrowband filters that can be synthesized based on microstrip technology

The method used in this design is based on a technique introduced by Dishal and adopted for use with modern circuit and EM simulation by co-author Dan Swanson. EM modeling is used to efficiently determine three fundamental filter properties: the unloaded Q of the internal resonators, the coupling between two adjacent resonators, and the external Q of the two resonators that will form the input and output connections. Parametric studies with EM analysis will be critical in modifying the physical structure in order to obtain specific values for these filter properties, which are determined by the Dishal method. Port tuning is then applied using circuit simulation and optimization with ideal lumped-element components, specifically capacitors that are placed in strategic locations. Port tuning is used to guide adjustments that need to be made to the final physical design.

Design by Optimization

General purpose optimizers are not particularly efficient for filter design unless they are able to take advantage of the mathematical foundation that defines a filter's optimal response. For a lossless Chebyshev filter, the optimal behavior is an equal ripple insertion and return loss response in the passband. So, if the optimizer can consistently find this equal ripple response, optimization can reliably be used. The optimizer that is used in this project is available as an add-on module to the AWR Design Environment platform using the software's API COM interface to integrate fully with Microwave Office circuit design software and AWR AXIEM® and AWR Analyst™ EM simulators.

Designing a Physically Realizable 5G Filter

The design methodology follows a set of well-defined steps that scale for the desired frequency and bandwidth. There are specific design steps, which are shown in Figure 7.

Figure 7: Steps for designing a physically realizable 5G filter

The process starts with specification of the filter requirements, including bandwidth, passband return loss, and stopband rejection, from which the filter order is determined, and the low-pass Chebyshev parameters are determined and scaled to the required frequency.

An EM model of a single resonator is built, and its length for a desired resonant frequency and unloaded Q can be determined. Additional EM models are created to generate the coupling coefficient and external Q curves that guide the determination of key physical dimensions such as resonator spacing and tap height. These individual components are then assembled, and port tuning is used to tweak the design for the optimum equal ripple response using optimization.

Narrowband Bandpass Filter Design

The filter is designed with a center frequency of 28GHz (3GPP band n257). The construction is based on a single in-line cavity, using an interdigital arrangement of is to achieve 30dB of rejection at 800MHz off-center frequency and an in-band return loss of 20dB. This sets the in-band ripple at 0.044dB. From these specs, the expected insertion loss and the necessary filter order are determined.

The mathematical foundation for an ideal filter response is very well established, with parameter values derived for an ideal lowpass Chebyshev filter response based on a cutoff frequency normalized to 1Hz (Figure 8.).

Chebyshev Lowpass Prototype: 0.044 dB ripple, 20 dB return loss, 1.22 VSWR

N	g_0	g_1	g_2	g_3	g_4	g_5	g_6	g_7	g_8	g_9	g_{10}	$\Sigma g_1 - g_N$
2	1.0000	0.6682	0.5462	1.2222								1.2144
3	1.0000	0.8534	1.1039	0.8534	1.0000							2.8144
4	1.0000	0.9332	1.2923	1.5795	0.7636	1.2222						4.5727
5	1.0000	0.9732	1.3723	1.8032	1.3723	0.9732	1.0000					6.4989

Figure 8: Ideal Chebyshev lowpass filter response based on cutoff frequency normalized to 1Hz

Once the prototype ripple level has been determined from the desired in-band return loss, the filter order N can be estimated based on the desired stopband rejection, as shown in Equation 1. A 5th order filter is needed to achieve the desired selectivity and bandwidth.

$$N > \frac{Rejection\,(\mathrm{dB}) + RtnLoss\,(\mathrm{dB}) + 6}{20\log_{10}(S + \sqrt{S^2 - 1})}$$

$$Rejection = \text{Stopband Insertion Loss}$$

$$RtnLoss = \text{Passband Return Loss}$$

$$S = \frac{\text{Reject Bandwidth}}{\text{Filter Bandwidth}}$$

Equation 1

Design Details

The design is based on an interdigital configuration made up of coupled resonators with the open ends on a substrate or cavity alternately pointing in opposite directions. The length of the resonators determines the resonant frequency and the coupling between resonators is controlled by their separation. The width of the housing, for a cavity filter should be λ/4 at the operating frequency.

In addition to the cavity dimensions, another early concern is to determine the cross-sectional dimensions of the resonator post. The resonator cross-section in relation to the outer cavity wall determines the characteristic impedance of the resonator. For a coaxial resonator, the literature indicates an optimum resonator characteristic impedance of around 77Ω, as determined by the resonator cross-section, resulting in a post-to-cavity width ratio of about 33% (Figure 9). In this case, the optimum Q_u was not achieved due to physical constraints. A coax transmission line calculation approximates the resonator Z_o ~ 46Ω.

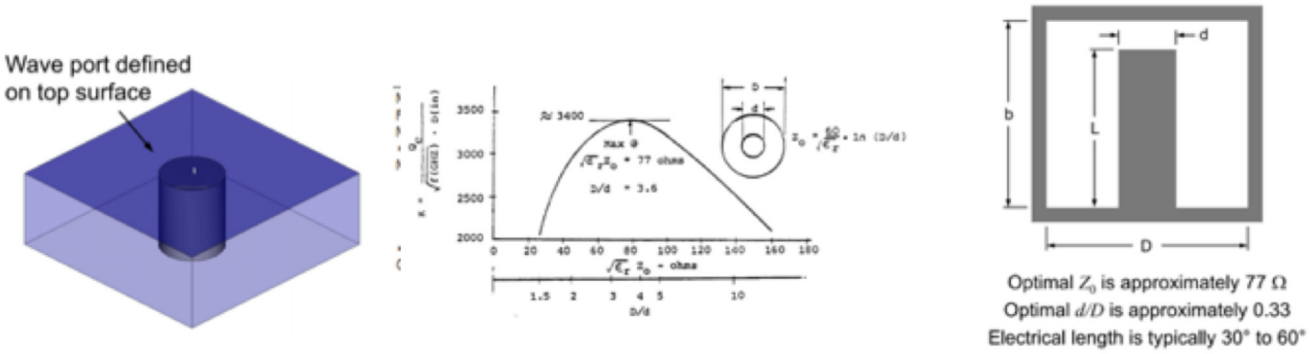

Figure 9: The resonator cross section in relation to the outer cavity wall determines the characteristic impedance of the resonator

Simulate Resonant Frequency and Q_u

With the cavity and resonator cross-section dimensions determined, an EM model of this single resonator is defined with the resonator length parameterized so that the resonant frequency can be controlled, as shown in Figure 10.

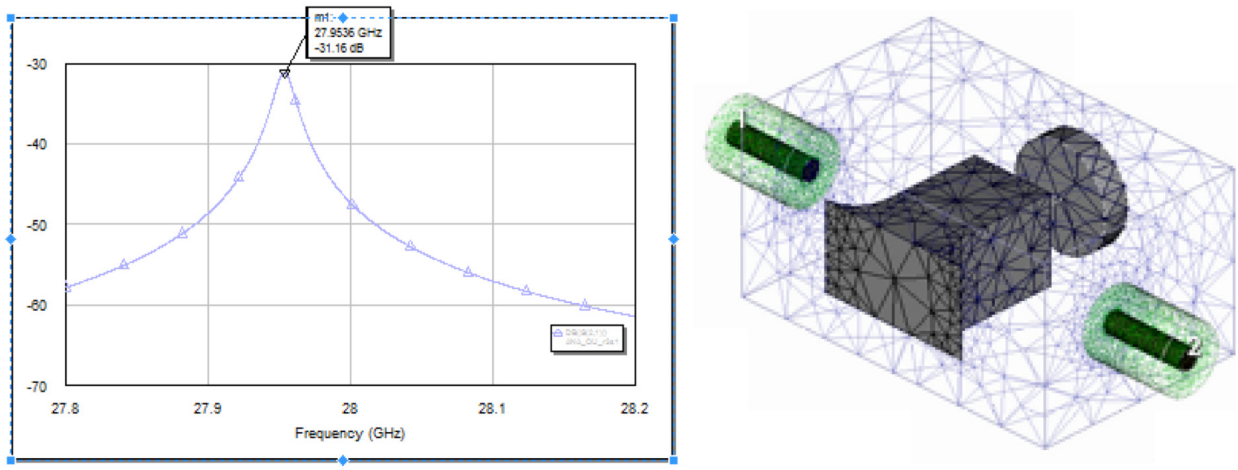

Figure 10: The EM model uses two coax feed structures that are loosely coupled to the waveguide cavity to act as the input and output ports.

The frequency response is shown for several different resonator lengths (Figure 11), demonstrating that the resonant frequency increases with a shortening of the resonator.

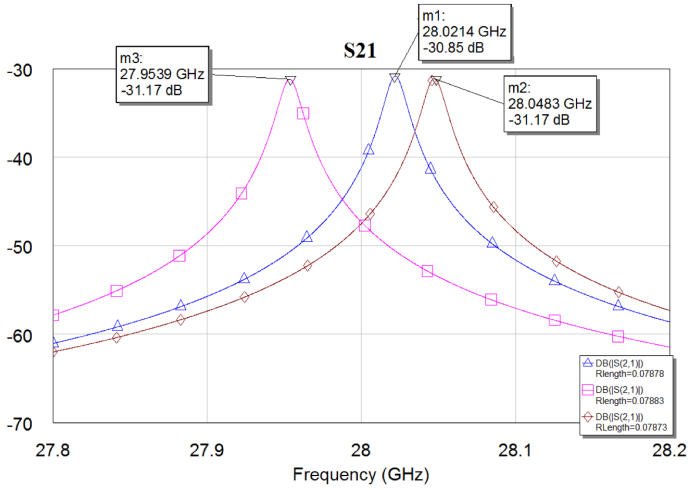

Figure 11: Simulation results of resonator EM analysis

The unloaded Q of an individual resonator is calculated from the simulated time delay and insertion loss using Equation 2.

$$Q_u = \pi f_0 \, t_d \frac{10^{IL(dB)/20}}{10^{IL(dB)/20} - 1}$$

Equation 2

For the low-pass Chebyshev parameters, ripple bandwidth, center frequency, and simulated unloaded Q (Table 1), the expected insertion loss can be calculated for the entire filter at mid-band using Equation 3. The estimated insertion loss is ~0.25dB.

R length	F0 (GHz)	Qu
0.07883”	27.9535	1975.2
0.07878”	28.022	2040.6
0.07773”	28.043	1978.1

Table 1

$$Loss(f_0) = \frac{4.343 f_0}{\Delta f \, Q_u} \sum_{i=1}^{N} g_i \text{ (dB)},$$

Equation 3

Where

Δf: is the equal ripple bandwidth of the filter

$Q_{u:}$ is the expected average unloaded Q for the resonators

g_i: normalized lowpass filter element values, calculated for a given ripple in Table 1.

An accurate accounting of manufacturing factors such as surface roughness and plating details are missing from the model used for EM simulation and the in-band insertion loss will likely be higher than this initial estimate. The model approximated 80% of the ideal conductivity as a starting point. The quality of the silver plating is very process dependent. The measured data from the manufactured and tested filter can be used to adjust model conductivity information.

Simulate Coupling Coefficients

From the Chebyshev low-pass filter parameter values (g) in Table 1, the external Q and the coupling coefficients (kij) for the resonant pairs were calculated based on Equations 3 and 4, respectively, using a 2.85% bandwidth.

$$Q_{ex} = \frac{f_0 \cdot g_0 \cdot g_1}{f_2 - f_1} = \frac{g_0 \cdot g_1}{BW}$$

$$K_{ij} = \frac{(f_2 - f_1)}{f_0 \sqrt{g_i \cdot g_j}} = \frac{BW}{\sqrt{g_i \cdot g_j}}$$

$$f_0 = \frac{f_1 + f_2}{2} \qquad BW = \frac{f_2 - f_1}{f_0}$$

f_1 = bandpass filter lower equal ripple frequency

f_2 = bandpass filter upper equal ripple frequency

f_0 = bandpass filter center frequency

BW = percentage bandwidth

g_i = prototype element value for element i

Note: Equations assume Qu is infinite.

Equations 3 and 4

These calculated values provide the targets for physical design. The next step is to build the coupling coefficient design curves using an EM model of the coupled resonators in order to determine the necessary spacing.

Two resonators based on the initial resonator study are enclosed in a metal cavity and loosely coupled to the input and output ports, as shown in Figure 12.

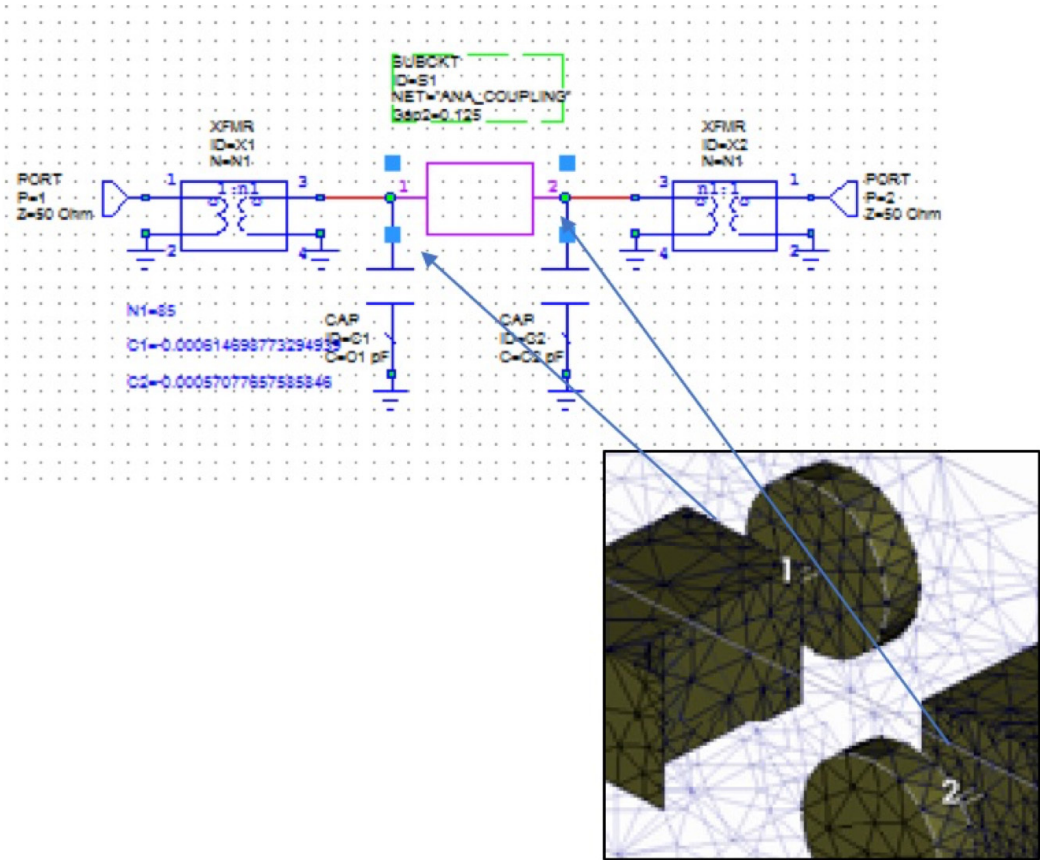

Figure 12: Simulation results of resonator EM analysis

The two resonators are identical and resonate at frequency f_0. The coupling between the resonators results in a displacement Δf of the resonance frequencies, which is known as the coupling bandwidth. By dividing the coupling bandwidth by the ripple bandwidth of the filter, the normalized coupling coefficient is obtained. The normalized coupling coefficient divided by the center frequency provides the Chebyshev lowpass coupling coefficient. The resonant frequency occurs at the mid-point between the two peaks, as shown in Figure 13.

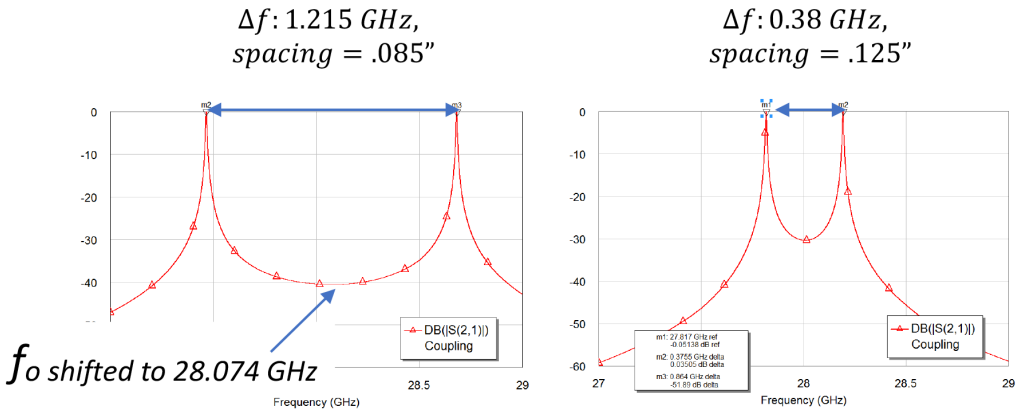

Figure 13: Simulated transmission characteristics of two resonators enclosed in a metal cavity and coupled to the input and output ports

The more closely the resonators are spaced, the farther apart the peaks are, which corresponds to higher coupling. As the resonators move farther apart the coupling gets progressively weaker and the two peaks merge at the original resonant frequency. It can also be seen that the center frequency between the peaks on the plot to the left has shifted upward 74MHz for the case where the resonator spacing has been reduced to 85mils.

The admittance versus frequency for these two ports is simulated and the capacitor values are optimized to zero out the admittance at 28GHz, which will recenter the resonant frequency of the coupled pair (Figure 14). The impact of the small amount of capacitance added or removed in order to center the coupled resonance can then be replaced by adjusting the resonator length to add/remove an equivalent amount of capacitance.

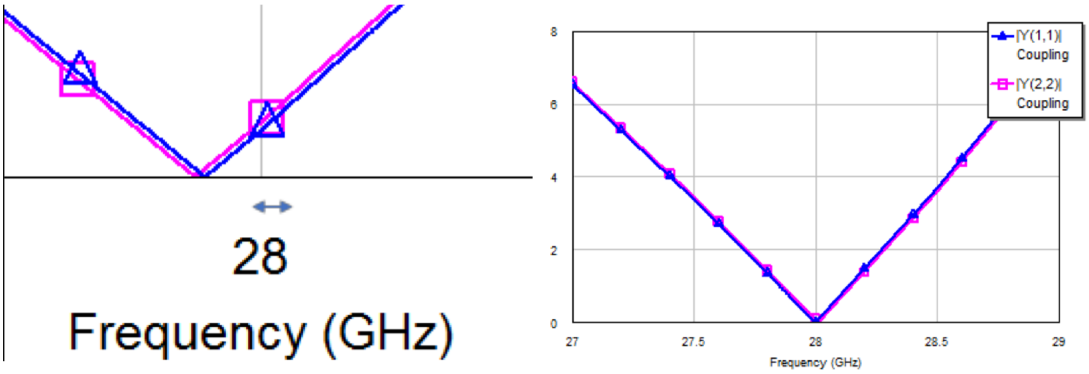

Figure 14: The f_o shift is addressed through tuning c1 and c2 values using optimization

Calculating Kij Curves From Parametric EM Analysis

Dividing the normalized coupling coefficient by the 28GHz center frequency provides the coupling coefficients that are needed to match up to the lowpass Chebyshev parameter values.

From Kij calculations:

- [K1,2],[K4,5] = 0.02466
- [K2,3],[K3,4] = 0.01812
- Coupling bandwidth [1,2][4,5] = 690MHz
- Coupling bandwidth [2,3][3,4] = 507MHz
- (= Kij x 28GHz)

By parameterizing the spacing and tweaking the resonator length through port tuning, a curve relating coupling coefficients to a very accurate resonator spacing based on EM analysis can be calculated. From this curve, the spacings necessary to achieve the required coupling can be determined. The curve in Figure 15 shows the anticipated inverse relationship between the amount of coupling between resonators and their spacing.

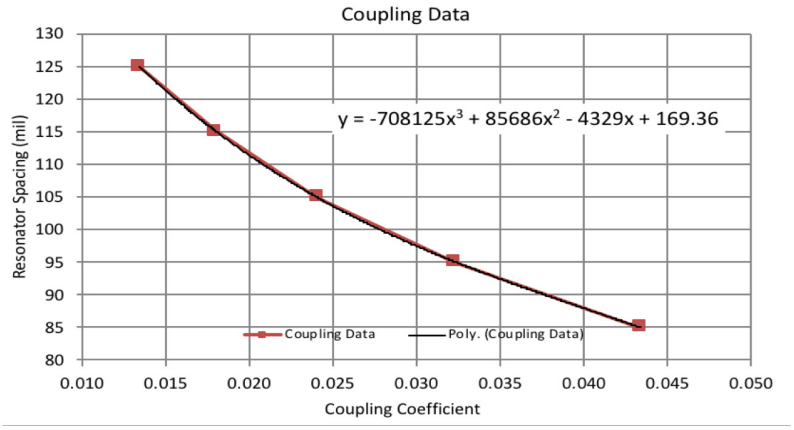

Figure 15: The anticipated inverse relationship between the amount of coupling between resonators and their spacing

Parametric Modeling of the Tapped Resonator

The next step is to determine the physical details of the tapped resonators that will provide the input/output to the filter. The external Q can be determined by the ratio of the center frequency to the 3dB bandwidth of the tapped resonator or by measuring the group delay (Figure 16). The external coupling is found by measuring the 3dB bandwidth of the resonance curve - denoted Δf3dB. The external Q is: Qext = Qloaded = f0 / Δf3dB. It is also possible to determine the external Q by measuring the group delay of S11.

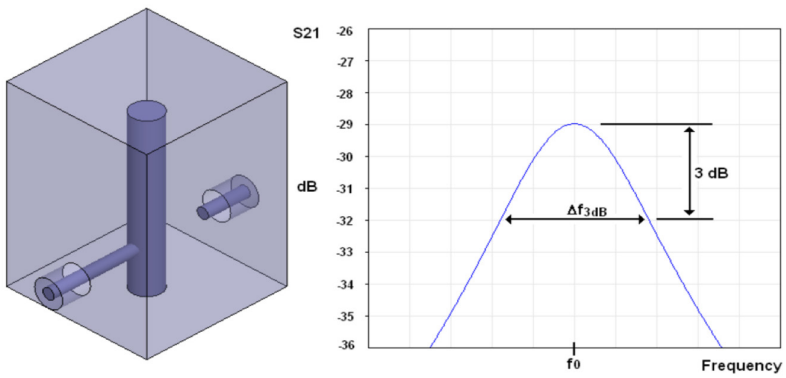

Figure 16: The external coupling is found by measuring the 3dB bandwidth of the resonance curve

A parameterized EM model that includes a coax feed that taps into a single resonator is created and the distance from the bottom of the housing to the center of the coax tap is parameterized so that it can be adjusted to different heights to achieve the external Q calculated from the Chebyshev lowpass parameter. A lumped port is also placed between the resonator and tuning screw to support port tuning to address any shifts in the resonator frequency due to the tap (Figure 17). EM analysis of the tapped resonator provides the time-delay response as a function of frequency for different tap heights (Figure 18).

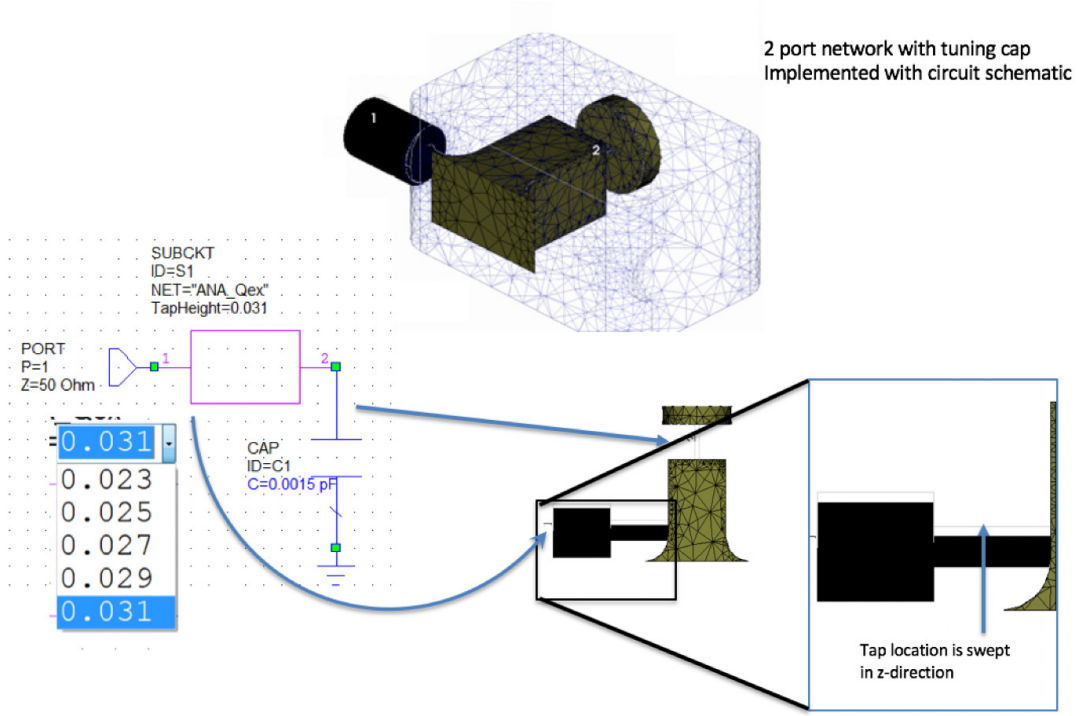

Figure 17: The single resonator EM model includes a coax feed with a parameterized tap feed height to adjust the external Q

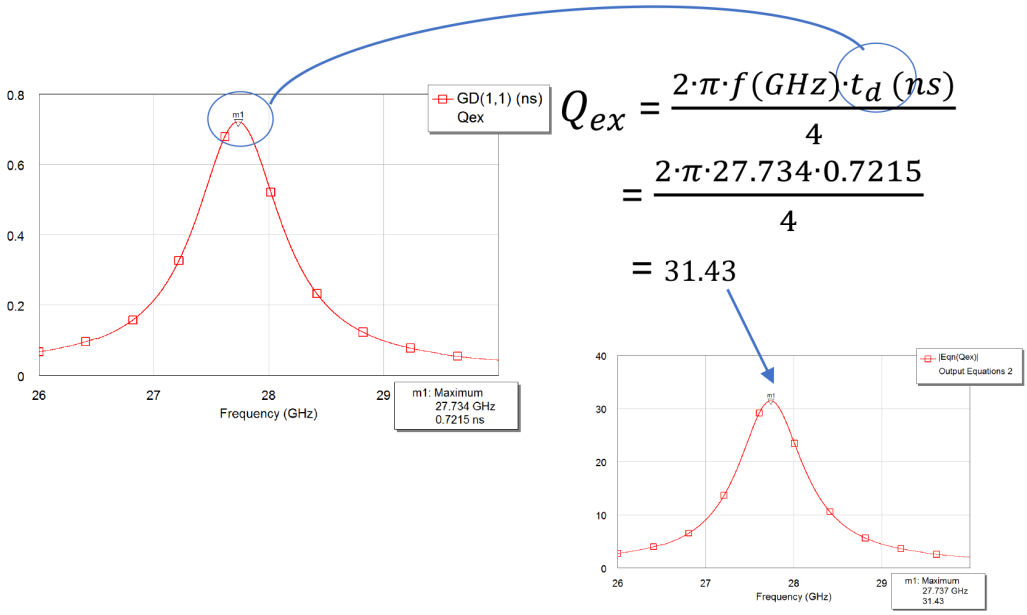

Figure 18: Simulated reflected delay for the tap height

The time delay response is used to derive the external coupling. Parametric simulation enables the generation of an external Q versus tap height curve, from which the tap height necessary for the required Qex can be directly chosen (Figure 19).

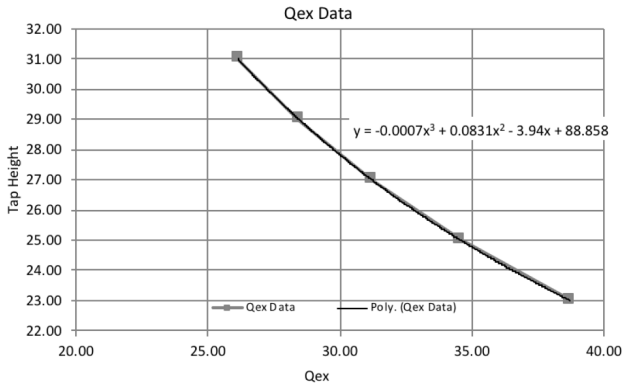

Figure 19: Resulting Qex vs. tap height based on parameterized swept EM analysis of the reflected time delay.

Port Tuning

Parameterization has been used to sweep values and generate the individual components that are combined to reproduce the entire filter and finalize the design through port tuning using the equal ripple optimization routine. While today's EM simulators are quite faster and powerful today, EM simulation times for low-order filters is still on the order of minutes or tens of minutes. Port tuning moves the optimization process from the EM domain to the circuit theory domain, where simulation times are much faster. Adding a port at each resonator enables rapid tuning of each resonator and the coupling between resonators (Figure 20).

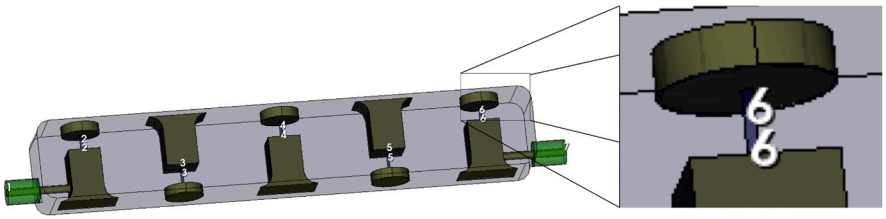

Figure 20: Adding a port at each resonator enables the designer to tune the frequency of each resonator and the coupling between resonators

With each resonator loaded with a 50Ω port, the raw coupling between resonators (not coupling coefficients per se) is being simulated and the S-parameter variation across the simulation domain is quite smooth (Figure 21). In fact, for a narrowband filter, only 5-10 discrete frequencies across the simulation domain are required for the circuit simulator to generate a smooth frequency response plot through interpolation.

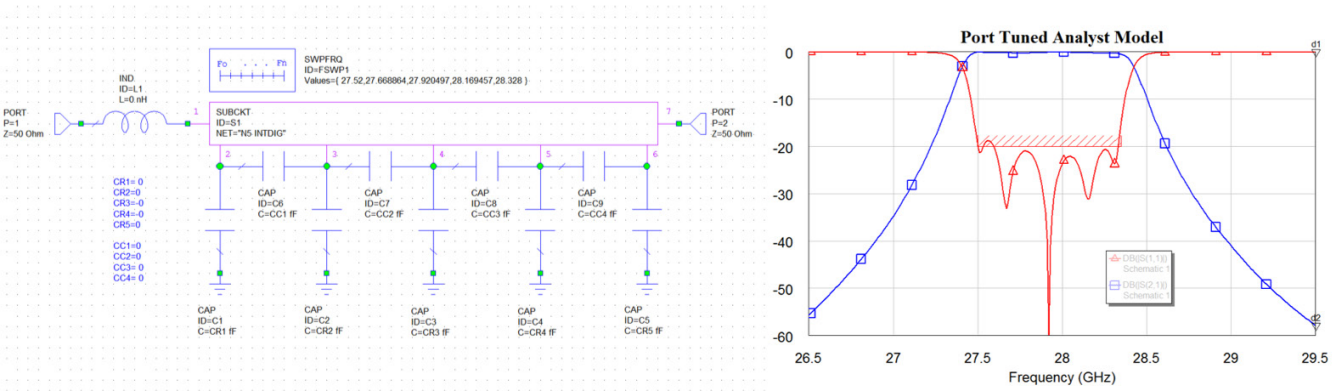

Figure 21: The raw coupling between resonators is simulated and the S-parameter variation across the simulation domain is quite smooth

With port tuning, the resulting capacitance values reveal the tuning requirements for the 3D EM model. Both positive and negative capacitance values can be used in circuit simulation. For the resonator tuning (port to ground capacitors), a negative capacitance value indicates that the resonator (EM model) is tuned too low. Positive capacitance represents a resonator that is tuned too high. For adjusting the coupling (port to port capacitors), a positive series capacitance indicates that the coupling is too strong in the EM model (the resonators are too close).

The process is repeated until the capacitances become sufficiently small. Convergence is guaranteed if the changes are not too large. Once the resonator sensitivities (kHz per mm) are known, capacitance values can be converted into physical changes of the structure. Figure 22 shows the dimensions for the final design, derived from the port tuning.

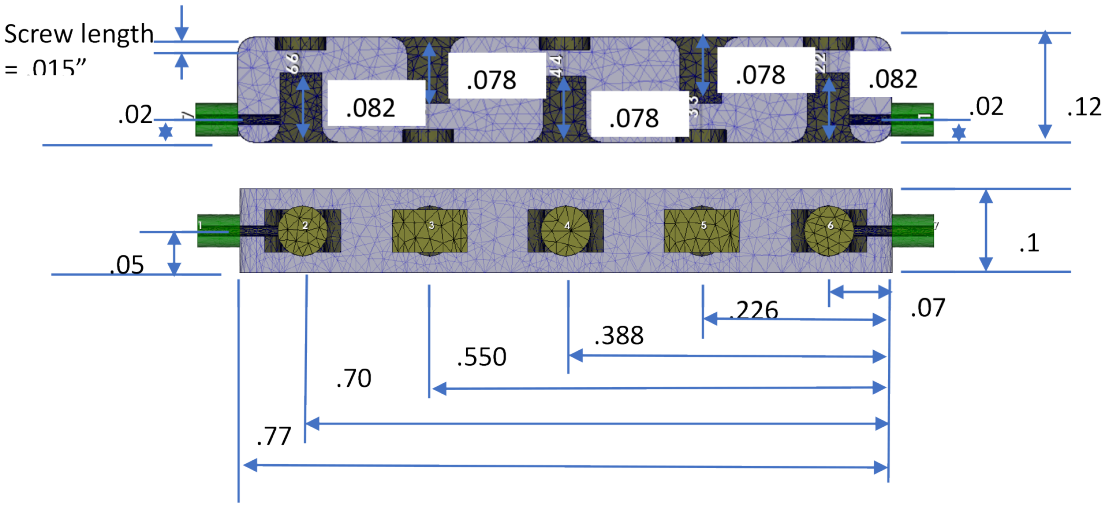

Figure 22: Final dimension of the filter design, derived from port tuning

Simulated Versus Measured Results

From this design, the filter manufacturer (Reactel, Inc.) built and tested the cavity filter, shown without the cover on the left in Figure 23. The frequency response of the measured filter and simulated model is shown to the right in Figure 18. As designed, the target response was achieved with moderate screw tuning. More exact tuning could be applied to better replicate the optimized, simulated result.

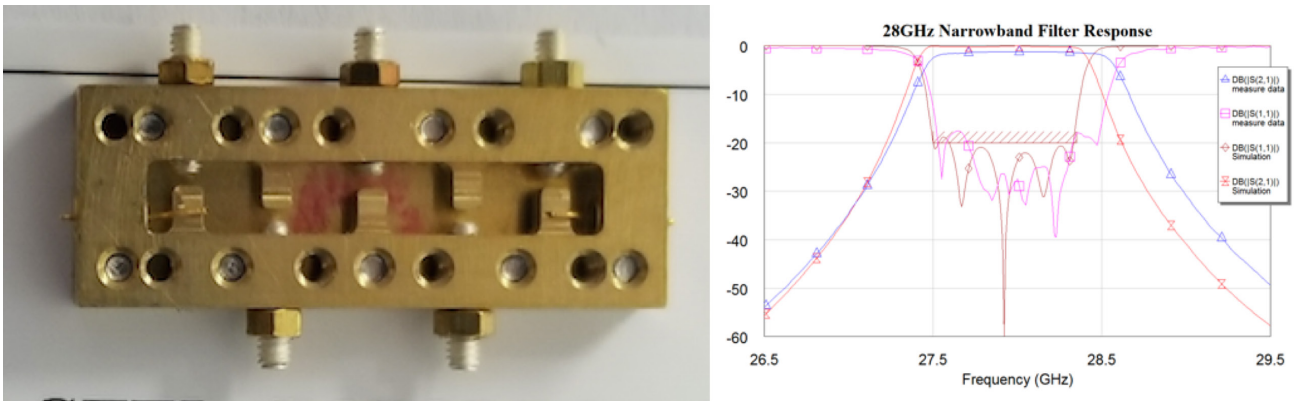

Figure 23: Pre-plated cavity (left) and simulated vs. measured results (right)

Manufacturing Tolerances and Yield Analysis

Modern CNC machines offer 0.0002" tolerances, not including tooling and fixturing. The relationship between 3D EM model and port tuning capacitors (resonators and coupling) can be used to perform yield analysis using the circuit simulator, allowing physical tolerances from manufacturing process to be translated into capacitor tolerances for yield analysis.

Yield analysis of microwave circuits is often done with a Monte Carlo-type analysis with a large number of iterations. Running these iterations in the EM domain is prohibitive, but if the computed sensitivities convert a capacitance to a physical dimension, yield optimization is possible through the circuit simulation. Figure 24 shows yield analysis performed on a similar cavity filter using AWR Microwave Office software and EM co-simulation with CST.

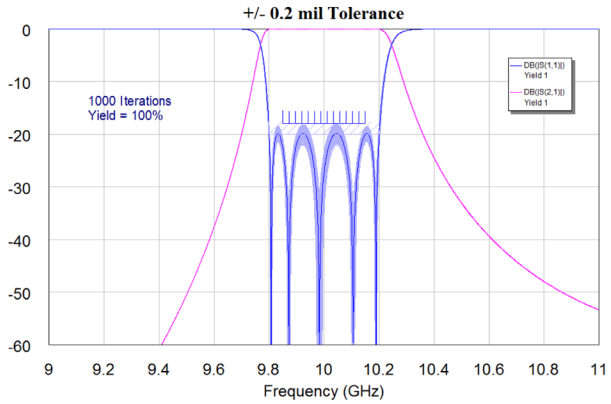

Figure 24: Yield analysis of a similar cavity filter performed using Microwave Office software and CST

A practical design method that is independent of filter type/construction has been demonstrated, showing a robust equal ripple filter optimization that is a fast and intuitive alternative to design by synthesis and a key component for port tuning complex EM-based filter models. EM tools continue to mature and add capabilities/speed, making it practical to include in an optimization loop. This technique has been used to address the challenge of designing highly sensitive mmWave filter designs.

AWR Visual System Simulator Testbench for Verizon 5G Technical Forum Downlink

Current 4G waveforms are not capable of supporting escalating demand for faster, more robust communication. What is needed is more spectrum, more and smaller cells, power efficiency, new modulation schemes, higher data rates, high-directivity antennas, and lower latency.

The ideal waveform for the 5G next generation of communications will be capable of supporting high data-rate and wide-bandwidth communications. It will enable energy-efficient operation, have low latency for long and short-burst transmission modes, and will be capable of fast switching between the uplink and downlink.

From several proposals in May 2017, the 3GPP standards organization, as well as Ericsson, are now converging towards using cyclic-prefix OFDM (CP-OFDM) as the waveform of choice for 5G New Radio (NR). CP-OFDM is used by LTE and ranks best on the performance indicators that matter most: compatibility with multi-antenna technologies such as MIMO, high spectral efficiency, and low implementation complexity. It is less susceptible to phase noise and Doppler effects than other multicarrier systems and has a high peak-to-average power ratio (PAPR) like other OFDM signals. Verizon 5G (VZ5G) Technical Forum has also chosen CP-OFEM, a key difference being that Verizon's CP-OFDM has a variable 15-120kHz carrier spacing.

In anticipation of the need for AWR Design Environment users to have the ability to simulate Verizon 5G signals, AWR Visual system Simulator™ (VSS) system simulation software now offers a Verizon 5G testbench that allows designers to simulate 5G DUTs in the Verizon downlink system and, alternatively, perfom EVM and ACPR measurements.

AWR VSS VZ5G Downlink System Testbench

This application example demonstrates the VZ5G downlink transmission, which includes the physical broadcast channel (PBCH), physical downlink control channel (PDCCH), and physical downlink shared channel for data (PDSCH). The corresponding transmitter and receiver have already been set up, along with a behavioral amplifier DUT in between, as shown in Figure 25 The example has been configured to enable the user to perform various measurements.

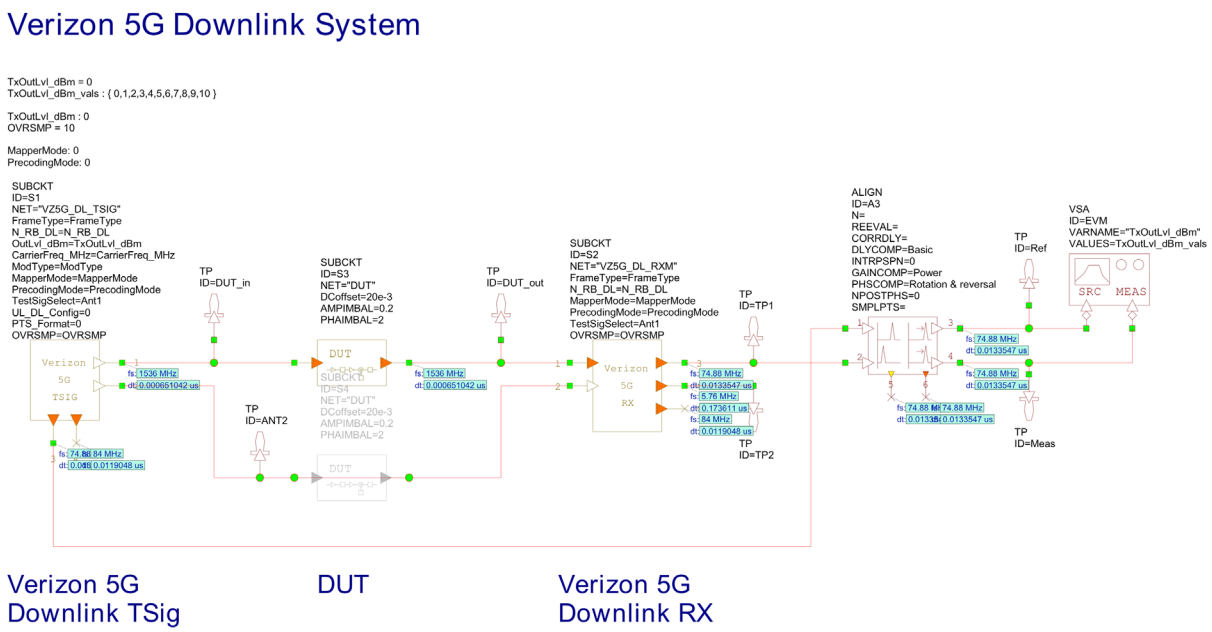

Figure 25: VZ5G downlink system with corresponding transmitter and receiver setup

Figure 26 (left) is a 100MHz-wide signal before and after the DUT. Some spectral regrowth can be seen at the output of the spectrum. Some complementary cumulative distribution (CCDF) measurements have been set up in Figure 26 (right), and the input and output to the DUT are shown in Figure 27 (left). There is also a parallel power sweep measurement being performed on the signal operating on the AM-to-AM curve. The IQ constellation plot in Figure 27 (right) shows the received demodulated IQ constellation for both the xPDCCH and xPDSCH.

Figure 28 (left) shows ACPR measurements at the 100MHz and 200MHz offset, which represent the channels for the VZ5G specification. The EVM versus input power and output power sweep measurement in Figure 28 (right) shows the EVM characteristics as a function of output power.

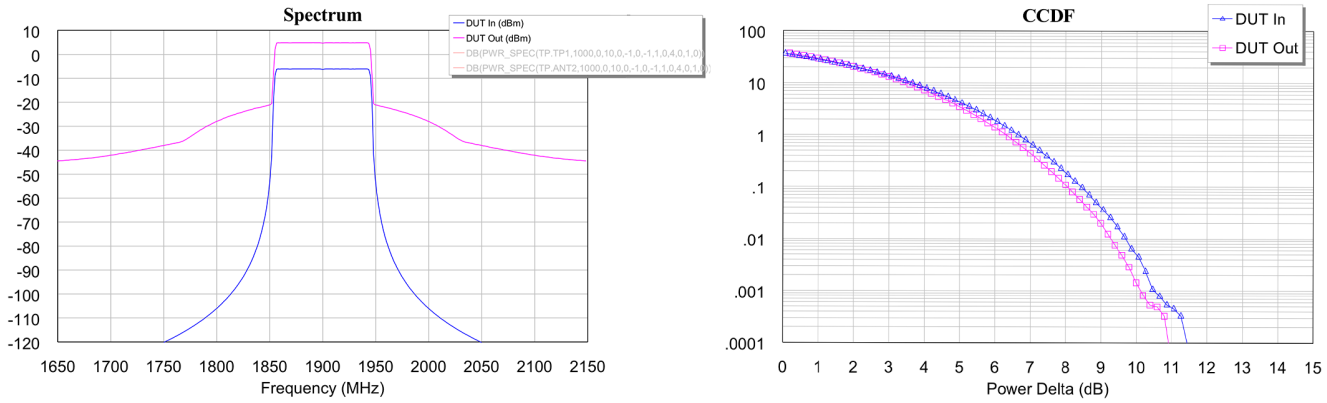

Figure 26: 100MHz-wide signal before and after the DUT and CCDF measurements with input and output to the DUT

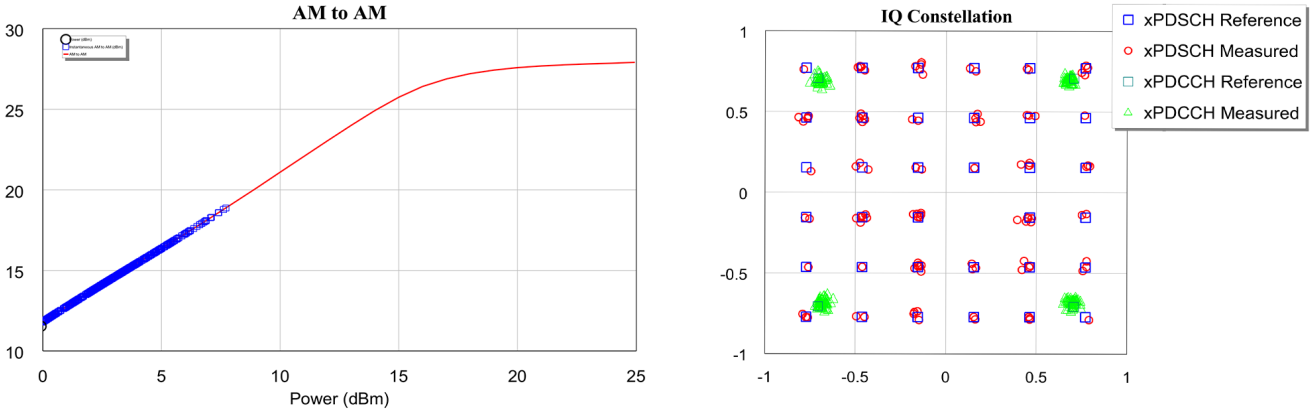

Figure 27: CCDF measurements with input/output to the DUT and Plot of received demodulated IQ constellation for both xPDCCH and xPDSCH

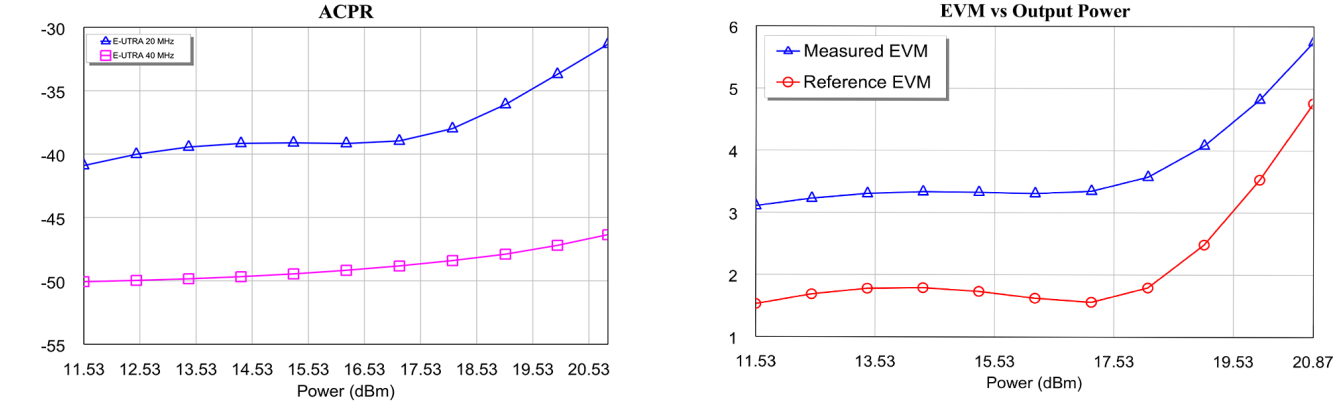

Figure 28: ACPR measurements that represent the channels for the VZ5G specification and EVM versus output power sweep measurement showing EVM characteristics as a function of output power

By replacing the DUT element in the diagram with the user's DUT element of choice, this example can be quickly turned into a VZ5G-based testbench to evaluate system performance according to VZ5G specifications (Figure 29).

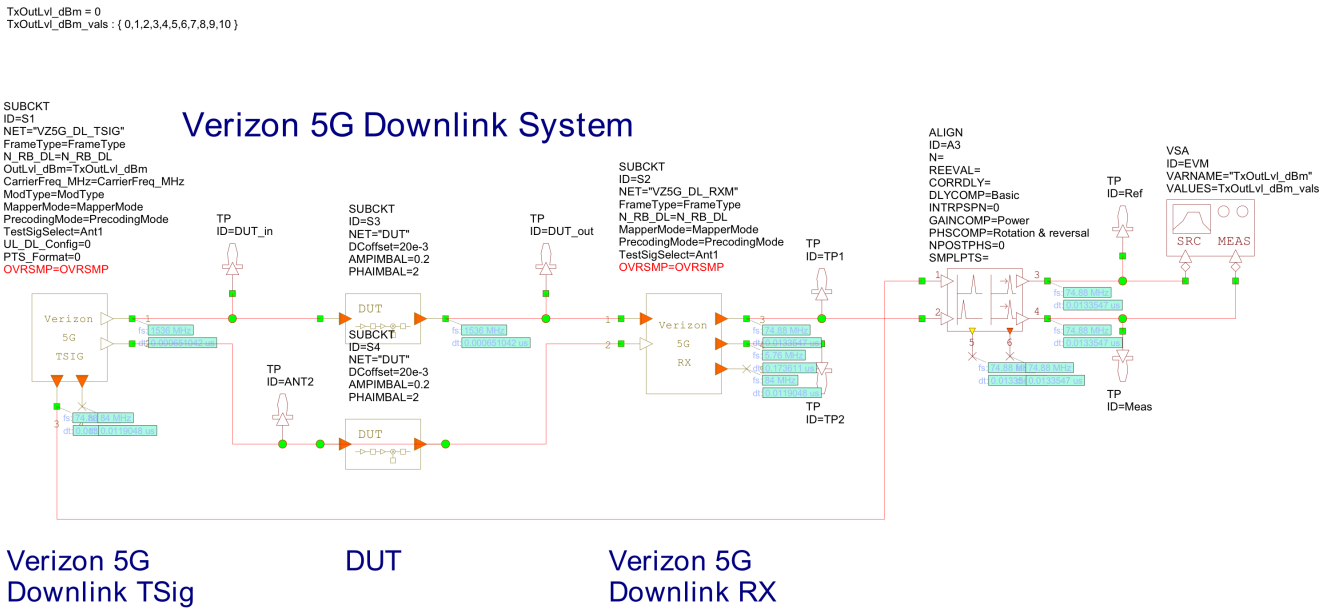

Figure 29: Example testbench where the DUT can be replaced by a DUT of choice in order to evaluate system performance according to VZ5G specifications

The VZ5G downlink system testbench within VSS software enables designers to simulate 5G DUTs in the Verizon downlink system and also perform EVM and ACPR measurements. Because VZ5G specifications are in the early stages and therefore changing constantly, the current implementation in AWR VSS software will be updated according to developments. The advantage of the AWR VSS signal generator is that it is built from basic building blocks, so when specifications change, the parameters in the root blocks can be updated without having to change hard code. When final specifications are made, the current AWR VSS signal channel model (SCM) in the 5G channel model will be updated to the final configuration defined in 3GPP.

Product Flow for 5G/LTE Envelope-Tracking PAs

Next-generation communication systems, made possible through innovative high-frequency electronics, will be responsible for a rich ecosystem of future wireless connectivity. The technologies being introduced to achieve anywhere, anytime instantaneous data will rely on complex system architectures that will lead to design challenges at the component level. The AWR Design Environment platform is continually advancing to help RF/microwave engineers meet these challenges with system/circuit/electromagnetic co-simulation and a streamlined path to NI test solutions for design verification. This chapter examines the use of ET, digital predistortion, and impedance matching via load pull to improve the efficiency and linearity performance of RF power amplifiers targeting 4G and 5G applications.

LTE PA Design Challenges

5G represents the next big milestone in the evolution of mobile communications, targeting more traffic (10,000x), increased capacity (1,000x), substantially lower latency (<1 millisecond), and lower energy consumption (10% reduction) by the year 2020 (Figure 30). Until then, operators have been addressing immediate demand for greater data capacity and throughput with various medium-term technologies, such as multiple-input MIMO, beamforming, and CA, a feature first introduced with LTE Advanced (3GPP Release 10).

Carrier Aggregation

With CA, operators can make better use of available fragmented spectrum allocations by combining component carriers (CCs) from a single intra-band CA or multiple intra-band CAs, allowing the combination of up to five separate carriers to enable bandwidths up to 100MHz, although current long-term evolution A (LTE-A) implementations target an aggregate bandwidth of 40MHz (two carriers with 20MHz bandwidth each) for the uplink and four CAs (80MHz) on the downlink.

The earliest and most straightforward CA implementations, as defined by release 11 of the 3GPP LTE-A standard, call for aggregated contiguous CCs within the same frequency band (intra-band) for TD-LTE in the uplink. Inter-band CA configurations refer to the aggregation of component carriers in different operating bands, where the carriers aggregated in each band can be contiguous or non-contiguous, as shown in Figure 30. This can lead to CA combinations that cover a broad spectrum and is clearly a more challenging PA design problem.

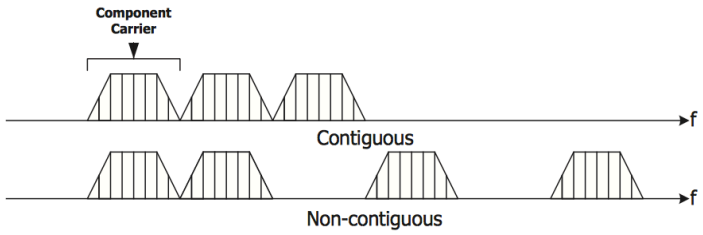

Figure 30: Contiguous and noncontiguous carrier bands

Operation across two or more bands has historically required separate amplifiers and an assembly of low-pass filters (LPFs) and a multiplexer (Figure 31 [left]). A single wideband amplifier and a low-loss switch (Figure 31 [right]) could replace multiple amplifiers, offering a lower cost solution than multiple band-specific amplifiers and consume less circuit board area. However, the configuration based on a wideband PA must offer higher power and efficiency to offset increased insertion loss of the switch. CA also requires higher power output to enable simultaneous transmission on multiple component carriers.

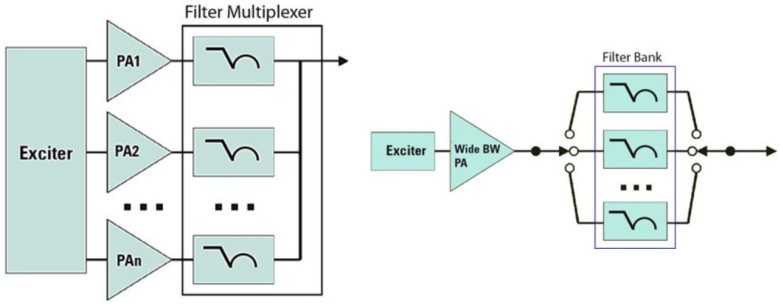

Figure 31: Multi-band front-end configurations based on (left) narrowband PA/filter chains and (right) wideband PA/switch filter bank

In addition to high power and wideband requirements, PAs must offer sufficient linearity and power efficiency to reduce operating costs for the base station and extend operating time/reduce battery size and weight for the mobile device.

Beyond CA, operators are researching additional methods, informally referred to as 4.5G or pre-5G, to provide higher data rates. 3GPP is introducing an LTE-Advanced Pro standard that extends LTE to unlicensed bands, evolves LTE time-division duplex (TDD) and frequency-division multiplex (FDD) frame structures, aggregates across more carriers, diverse spectrum types, and different cells, and enables more MIMO-based antennas at the base station (up to 64 antenna elements). MIMO increases data rates and network capacity by transmitting multiple spatially separated data streams over the same frequency band, using multiple antennas on base stations and user devices. 4.5G will introduce much higher-order MIMO (2.5 to 2.7GHz, 3.4 to 3.8GHz, and 5 to 6GHz bands) to further enhance network capacity with up to 256 simultaneous data streams.

OFDMA, SC-FDMA, PAPR, and Efficiency

Maintaining signal integrity (low distortion) in a crowded frequency spectrum allocation is especially critical as the increasing demand for higher data rates has been met with the use of larger signal bandwidth and modulation schemes with noncon-stant envelope and high PAPR. High linearity is required in these communication systems in order to minimize signal distortion, reduce BER, improve spectral efficiency, and reduce adjacent channel interference (ACI). Linearization techniques such as digital predistortion (DPD), discussed later in more detail, are being employed to reduce signal distortion that leads to spectral regrowth (Figure 32). Spectral regrowth, CCDF, EVM, and am-to-am conversion vs. input power are simulated in AWR Design Environment platform, specifically AWR VSS system design software.

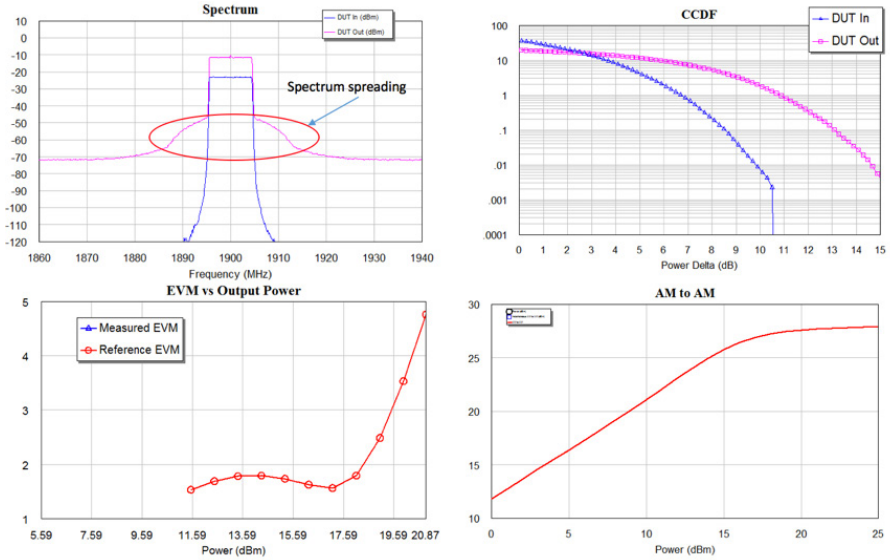

Figure 32: Various aspects of signal distortion and impact on the system arising from nonlinearities

The efficiency of the PA determines the power consumption, size, and battery lifetime of the radio. Various techniques, including ET, have been explored to increase the efficiency of PAs for high PAPR signals such as those utilizing OFDM.

In LTE, the base station uses OFDMA for downlink, transmitting the data over a large number of narrow sub-channels (15KHz each) or 180kHz channels with logical groupings of 12 subcarriers (12x15kHz=180kHz), as opposed to spreading one signal over the complete 5MHz carrier bandwidth, as shown in Figure 33. This multicarrier approach enables better spectral efficiency and reduces the impact of multipath reflections on the receiver's ability to demodulate the signal.

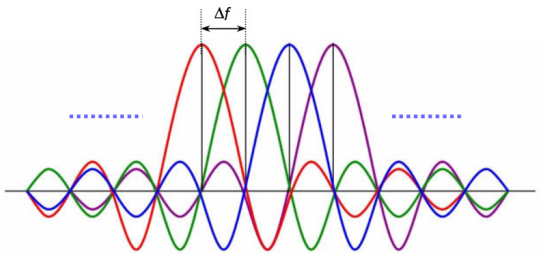

Figure 33: OFDM subcarrier spacing

Multiple access is achieved by assigning subsets of subcarriers to individual users, which are transmitted in parallel, thereby increasing the symbol duration and lowering the symbol rate which allows the use of a guard interval between symbols, making it possible to eliminate inter symbol interference (ISI). Channel equalization is simplified because OFDM uses many slowly modulated narrowband signals rather than one rapidly modulated wideband signal. In addition, OFDMA offers robustness against severe channel conditions compared to single-carrier schemes. Despite their many benefits for high data rate transmission, OFDMA transmit signals can have high peak values in the time domain since many subcarrier components are added via an inverse fast Fourier transformation (IFFT) operation. As a result, OFDM systems are prone to have high PAPR or envelope fluctuations when compared to single-carrier FDMA (SC-FDMA) used for uplink by the mobile unit.

High PAPR can drive a power amplifier deep into saturation (nonlinear operating region) leading to distortion that results in spectral spreading of the signal causing ACI. The linearity problem can be overcome with a variety of methods, including the use of high compression-point PAs and/or amplifier linearization techniques. PAPR dictates the PA's minimum output backoff (OBO) from saturated power to ensure that the maximum power stays within the linear region of the power amplifier (Figure 34). This results in a reduction in the mean transmission power and directly impacts (lowers) the amplifier efficiency, since the PA spends less time in efficient saturated mode. The energy consumed by the backed-off PA during transmission increases dramatically due to the lower efficiency, in turn raising the operating costs for the base station. If a PA operates at only 35% efficiency, 65% of the energy is wasted as heat. The heat produced also causes reliability issues and requires large heat sinks, which increases the overall product size.

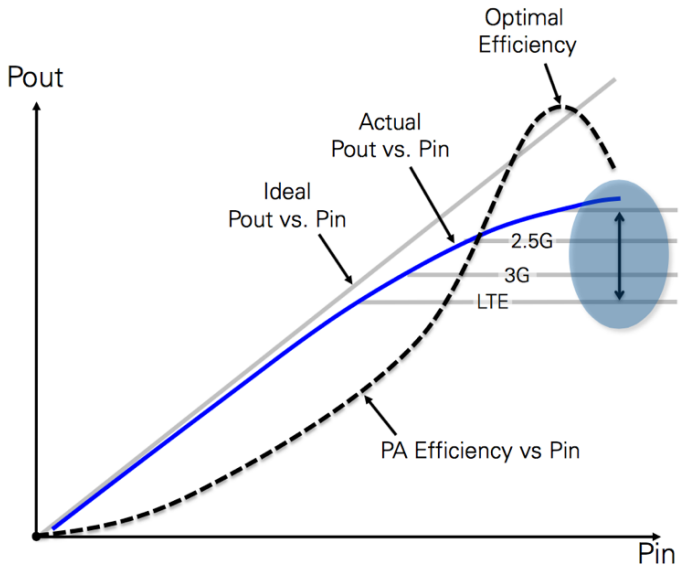

Figure 34: P_{out} and PAE vs. input power for an RFPA showing the power compression and optimal efficiency for saturated amplifier.

Load Pull and Matching Network Design

Engineers developing PAs must incorporate a wide breadth of simulated and/or measured data into their analysis and design verification in order to explore their design options in pursuit of optimum performance. Simulation data must accurately predict critical circuit metrics such as gain, linearity, efficiency, output power, and more as a function of operating conditions such as frequency, input power, bias, and source/load impedances.

After determining an appropriate semiconductor technology such as GaAs, GaN, SiGe, or laterally diffused metal oxide semiconductor (LDMOS) and circuit architecture and/or class of operation, the design effort typically turns to developing the impedance matching network. PA circuit design often starts with development of a nonlinear (compact) transistor model which can be used to create load-pull performance contours, which map a specific performance metric such as P_{out}, PAE, or ACPR, to corresponding source/load impedances. Alternatively, direct measurement of the transistor (or PA) using a load-pull measurement system can be used to generate these contours (Figure 35).

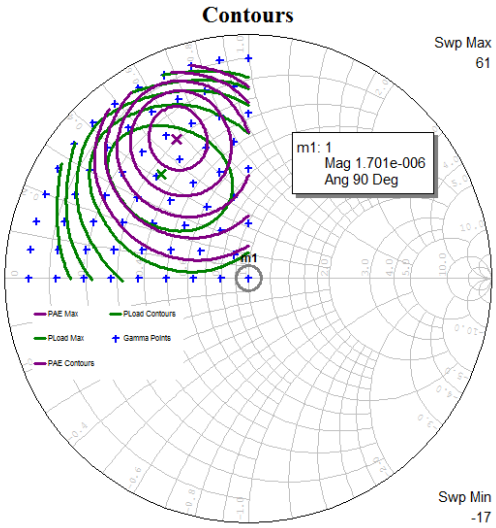

Figure 35: Gamma points, P_{load} and PAE contours

The AWR Design Environment platform supports the generation of load-pull contours from either compact models or through importing multidimensional load-pull measurements in the form of SPL and CST files from Maury Microwave and LPD files from Focus Microwaves. The AWR software load-pull formats offer engineers access to an extensive array of data manipulation functions and intuitive post-processing of data. This unique capability enables PA designers to work with dense data sets, such as multiple gamma points, frequencies, and power steps, for greater understanding of design tradeoffs and performance across operating conditions.

PAs for LTE, LTE-A/Pro and 5G must address stringent power, efficiency, and linearity requirements. For the high PAPR of these systems, the PA must be backed off from compression, possibly in addition to other linearization techniques, in order to achieve the necessary linearity requirements. Designers need to keep this in mind when they specify the operating conditions under which they characterize the active device to determine its optimum load. The load-pull data sets used in AWR software support multi-dimensional load-pull data across swept operating conditions such as frequency, power, and bias. This allows designers to directly observe optimum termination impedances for a range of potential output backoff operating conditions.

With simulated or measurement-based plots generated in the software, designers can dynamically track changing contour plots as a function of operating conditions. In Figure 36, a marker points to a specific input power level, with the contours for that power level plotted on the right. When the marker is moved, another set of contours will be shown corresponding to that power level. If the marker is moved again, a third set of contours is obtained, and so on, providing designers with multiple views of the one aspect of a PA circuit design's behavior—a much more comprehensive analysis tool than possible with older single-point local files. Alternatively, the same link could exist for any simulated/measured data including gain compression, current/voltage output waveforms, spectral regrowth, adjacent channel leakage ratio (ACLR), and more. Conversely, instead of choosing an input power level and plotting contours, users can choose a gamma point or impedance value and plot swept data for that data point.

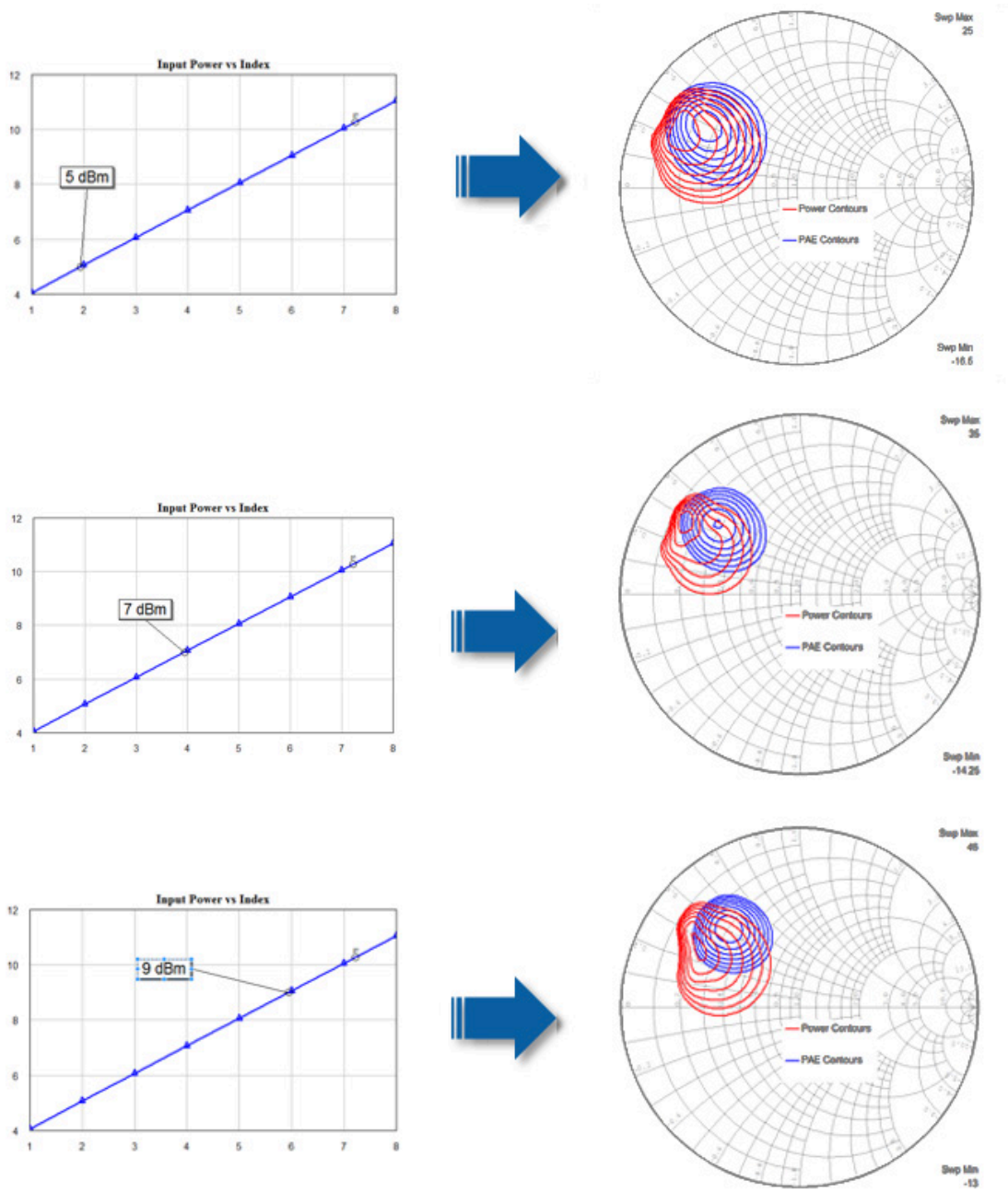

Figure 36: Swept load-pull data sets and linked data plots (shown: P_{in}/P_{out} and P_{out}/PAE contour graphs) allow designers to dynamically view changing load-pull contours as a function of operating conditions (P_{in}) simply by dragging the marker in one plot and observing the changes in the linked plots

Figure 37 shows how gain compression curves can be plotted by choosing a gamma point from the impedances in a data file. The plots show both gain-compression curves for all the gamma points in the file, as well as the gain-compression behavior for a gamma point selected with the marker. If the marker is moved to another gamma point, the gain-compression curve changes to reflect the performance at the new impedance.

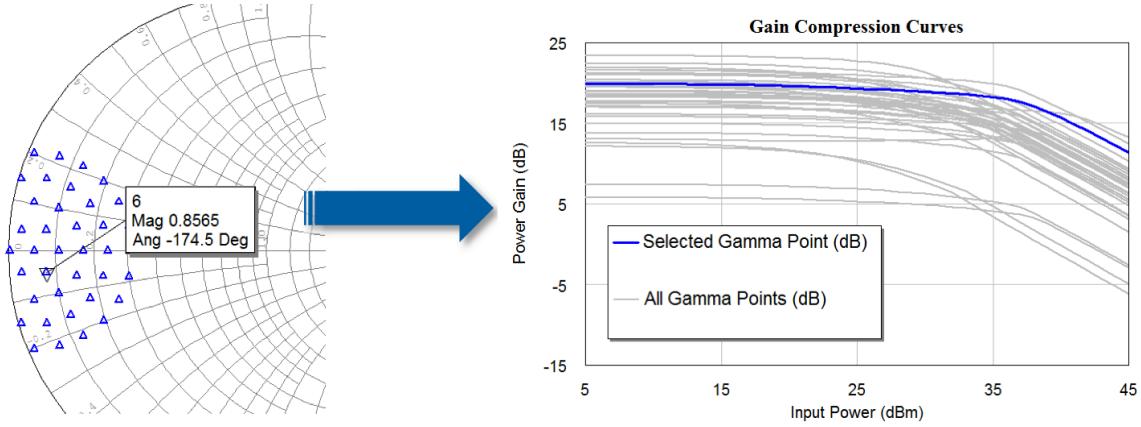

Figure 37: Gain compression curves (vs. input power) for discrete load impedances

The input and output matching networks are then designed based on the target impedance(s) indicated by the load-pull data. By comparing the simulated performance data with the design goals for the circuit, a circuit designer can adjust the matching networks to achieve optimized performance levels that are as close as possible to the design goals.

System Simulation Defines PA Requirements

In LTE-A, CA will drive up the PAPR by another 2.5 to 3dB, pushing PAPR demands higher than the levels currently required by LTE. Different OBO levels related to PAPR requirements are required depending on the number of aggregated component carriers (CCs) and the CA configuration. To calculate OBO specification, it is normally sufficient to apply 0.01% CCDF of the waveform.

For a random signal, PAPR is a statistical quantity. In OFDM systems, the large number of subcarriers periodically (and somewhat randomly) add to or subtract from one another, thus creating waveforms with a nearly Gaussian distribution of power variation. As a result, OFDM signals tend to have a PAPR ranging from 10 to 13dB (Table 2).

Standard	Modulation Type	Typical Uplink PAPR
GSM	GMSK	0dB
EDGE	8-PSK	3 - 4dB
UMTS	QPSK	3 - 5dB
HSUPA	16-QAM and 64-QAM	5 - 7dB
LTE	Vairous (SC-FDMA)	6 - 8dB
General OFDM	Various (OFDM)	10 - 13dB

Table 2: PAPR for various cellular technologies

AWR VSS system design software can be used to calculate CCDF and determine PAPR and OBO specifications (Figure 38). Also, by simulating complex digital waveforms directly applied to an RFPA circuit model, designers can optimize performance based upon PAPR, ACLR, EVM, or any number of performance metrics. EVM measurements can be made in individual subcircuits and/or over the entire OFDM symbol, while ACI analysis can be easily performed. This allows designers to effectively evaluate the in-situ performance of the PA within the end-to-end system. Alternatively, PAs can be represented with various behavioral models to determine design goals such as am-to-am and am-to-pm requirements.

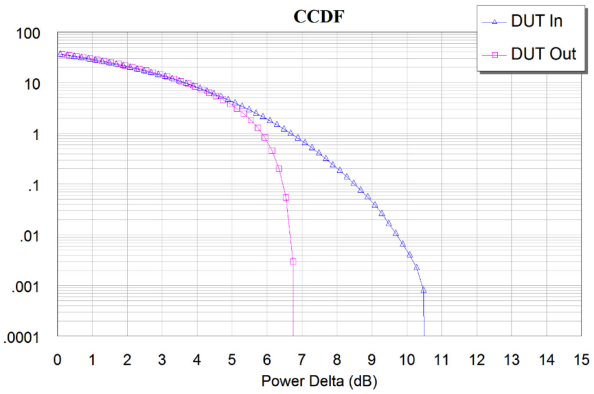

Figure 38: Simulated CCDF vs. input power for LTE DL TDD transmitter

LTE supports three modulation schemes in both the downlink and the uplink: quadrature phase-shift keying (QPSK), 16QAM, and 64 quadrature-amplitude modulation (QAM). The constellation diagram of the 16 and 64QAM modulation scheme are illustrated in Figure 39. As the figure illustrates, 16QAM has 16 discrete combinations of phase and amplitude, while 64QAM has 64. As a result, LTE transmissions achieve the highest data rate when using 64QAM. The LTE standard uses adaptive modulation techniques, which allow the eNodeB to choose the specific modulation scheme, depending on the channel conditions. Depending on channel conditions, some UEs might receive a more robust transmission (QPSK) and others might receive higher data-rate transmissions (64QAM or 16QAM).

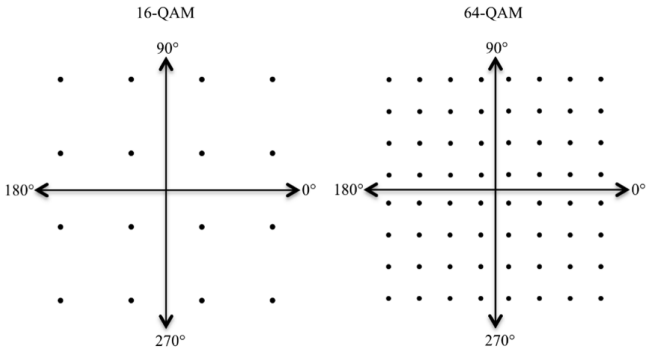

Figure 39: 16-QAM and 64-QAM symbol map

These modulators are standard in VSS software, along with modulators found in virtually all communication standards, including new modulation schemes being considered for 5G such as CP-OFMD, FBMC and GFDM, which will be available in version 13 of the software. In addition, VSS software has LTE downlink and uplink signal sources with parameter settings that are self-explanatory, allowing RF engineers to set up their simulations immediately without having to manually set up sources. The downlink and uplink sources are built from the ground up as subcircuits using easy-to-understand building blocks, enabling baseband engineers to drill down into sources to verify and possibly modify physical layer (PHY) 1 specifications.

Critical performance measurements can be performed without the use of difficult-to-understand testbenches, extending simulation analysis directly to PA circuit designs via circuit/system co-simulation or to a physical DUT in the laboratory via the use of LabVIEW and/or TestWave software. AWR Design Environment platform and test solutions were used in the development of a PA utilizing ET and DPD technology for improving the efficiency and linearity of a reference design targeting LTE Band 1 (2.14GHz) micro-cell base station applications.

ET and DPD Enhance Efficiency and Linearity

As a result of the increased PAPR and peak power requirements of LTE-A and CA, linearization and efficiency enhancement techniques such as DPD and ET will be even more crucial to the future of cellular standards than they already are for LTE today. DPD allows designers to operate in the efficient yet nonlinear region of an amplifier while retaining the transmitted signal linearity required of most digital modulation formats. DPD does not produce dramatic improvements in PA efficiency, but it does improve the quality of a signal that a PA produces when operating at its peak efficiency point. The approach to DPD can range from simple solutions such as a basic look-up table (LUT) to more complex real-time signal processing approaches.

To linearize a PA via a LUT, the measured or simulated output power and phase of the PA must be characterized as a function of input power, as shown in Figure 40 (simulations performed in AWR Microwave Office software based on shown PA circuit). These measurements produce the am-am and am-pm responses used to create a LUT that relates every input power/phase combination to the power/phase required to produce the desired linear output. By predistorting the input waveform, the PA can essentially be linearized.

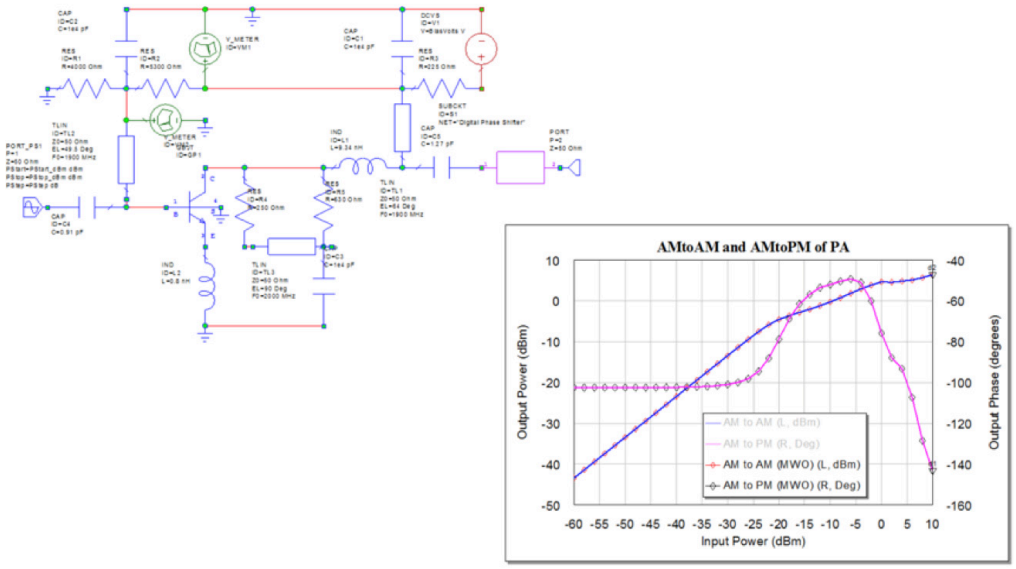

Figure 40: Simulated AM-AM and AM-PM response plots for a PA driving into compression

Figure 41 shows the compression of a nominal (64QAM) waveform, which produces a constellation where the peak portions of the signal experience less gain than other portions.

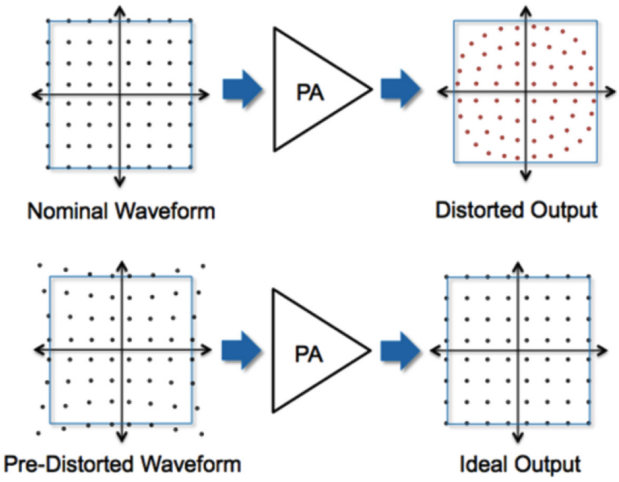

Figure 41: Predisortion reverses the nonlinear behavior of the PA

Thus, by predistorting the waveform such that the higher power symbols are amplified (gain expansion), the nonlinear behavior of the PA actually corrects the predistorted waveform. The resulting PA output using a predistorted waveform produces a more reasonable constellation.

With NI software and test solutions, the LUT can be developed into hardware through a combination of simulated and measured data, progressively replacing simulation models/results with hardware and measured data (Figure 42). The LUT is initially implemented in AWR VSS software and used to predistort the waveform, exciting a simulated PA with nonlinearities represented with a behavioral model using measured or simulated data. Comparison of the original PA input/output power response (showing compression) and the response after predistortion is shown in Figure 43.

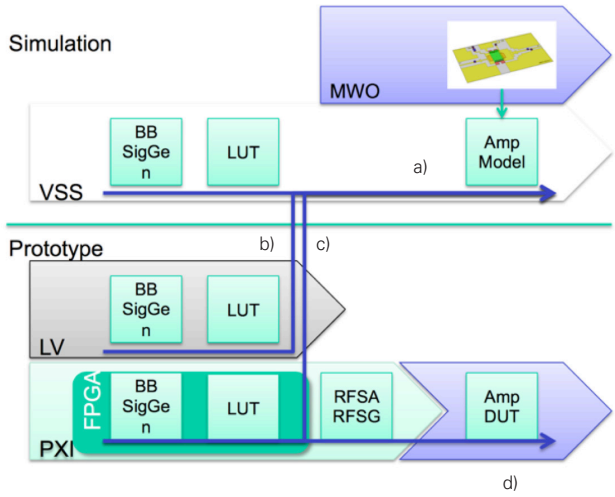

Figure 42: LUT DPD development flow based on a) full simulation in AWR VSS b) LabVIEW modeling of the LUT with simulated PA c) LUT implemented in PXI hardware co-simulation with AWR Microwave Office PA model d) PXI-based LUT predistortion of waveform driving actual PA

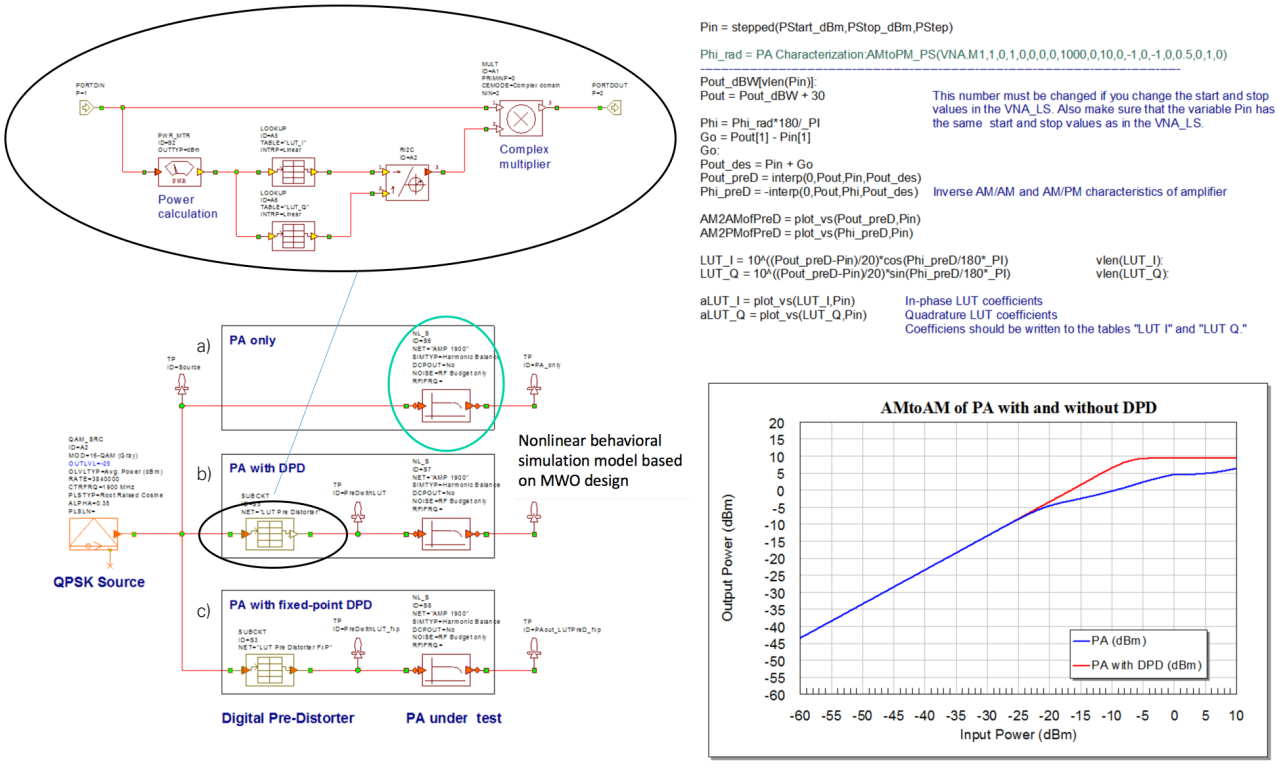

Figure 43: AWR VSS implementation of three simulations of PA a) without DPD b) PA with LUT c) PA with fixed-point LUT and resulting P_{out} vs. P_{in}

ET technology enables operators to utilize only as much power as is necessary to provide the amplified output. This technology reduces energy consumption, thus significantly lowering operating costs while providing environmental sustainability. In addition, from the hardware system perspective, this means a smaller form factor, higher reliability due to lower junction temperatures, and much lower weight due to reduced battery and energy requirements. The principle behind ET is to operate the amplifier in compression as often as possible. This technique makes use of the fact that both the point-of-peak efficiency and the point-of-peak output power vary as the supply voltage changes.

To illustrate this point, Figure 44 displays PAE as a function of output power for several Vcc values. The output power of peak efficiency tends to increase with an increase in Vcc. The basic idea of ET is to map instantaneous output power to an optimal Vcc value, thereby maximizing the time the amplifier spends on the edge of compression. While the idea of modulating the Vcc signal to maximize PAE is good in theory, this is difficult to execute in practice. A consequence of varying Vcc as a function of output power is that the amplifier's gain will dynamically change as Vcc is changed, thus increasing am-to-am distortion. This effect can be reduced by using a smaller range of Vcc levels, which leads to a design tradeoff between PAE and am-to-am distortion. DPD algorithms can be applied to the baseband RF waveform in order to correct for additional distortion introduced by ET.

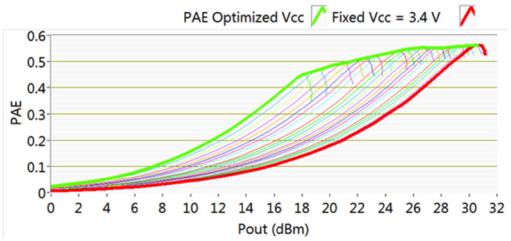

Figure 44: PAE vs. P_{out} across Vcc

Real-World Example: ET PA With DPD

MaXentric Technologies, LLC is a specialty R&D firm that provides product design, development, and manufacturing services for the military defense market, as well as telecommunications/broadcast commercial markets. MaXentric products include simple low-cost mmWave broadband wireless transceivers, passive radio-frequency identification (RFID) readers, and high-efficiency ETPAs. Typical applications include intelligence, surveillance, and reconnaissance (ISR) components, high-bandwidth wireless communications, electronic warfare (EW), broadband high-efficiency PAs, and more.

The engineers at MaXentric were focused on developing the world's first integrated circuit (IC)-based envelope modulator (MaXEA 1.0) for use in envelop tracking applications to improve the efficiency of PAs operating with high PAPR signals found in LTE, LTE-A, and 5G communication systems. The PA chosen for their reference design was a 6W GaN device, pre-matched for LTE band 1 (2.14GHz). At saturation, the PA provided 11.5dB of gain at 53% PAE. To provide the required linearity, the PA needed considerable backoff, operating at an output power of 0.5W (PAPR of 10.8dB) and a PAE of less than 10%. With DPD, the backoff was reduced, allowing the PA to operate at an output power of 2W and a PAE of approximately 25%.

Through the use of DPD, ET, and optimization of the output match using on-board tuning designed with Microwave Office software and measured load-pull data, the PA was able to operate at the saturated output power of 6 W, with a slight improvement in PAE of 54.6% and excellent linearity with a measured ACPR of 74.5dBc (Figure 45).

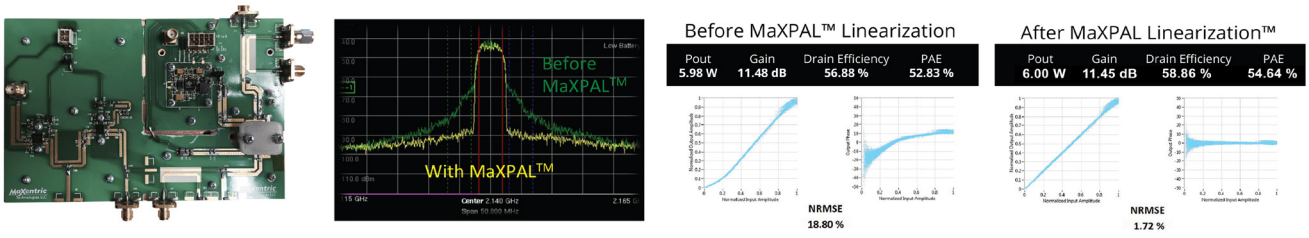

Figure 45: a) MaXentric ETPA with MaXEA, b) spectra before and after MaXPAL linearization, c) AM-AM and AM-PM before MaXPAL linearizaton, and d) AM-AM and AM-PM after MaXPAL linearization

The PCB output matching circuit and its frequency-swept impedance as seen from the output of the PA are shown in Figure 46. The design and its response were generated in AWR Microwave Office software by simulating a microstrip-based impedance transformer composed of transmission-line models and verified with the AWR AXIEM 3D planar EM simulator within AWR Design Environment. The software design's physical dimensions were determined through optimization to match the measured impedances of the load-pull tuners used to optimize the performance of the PA on the load-pull testbench.

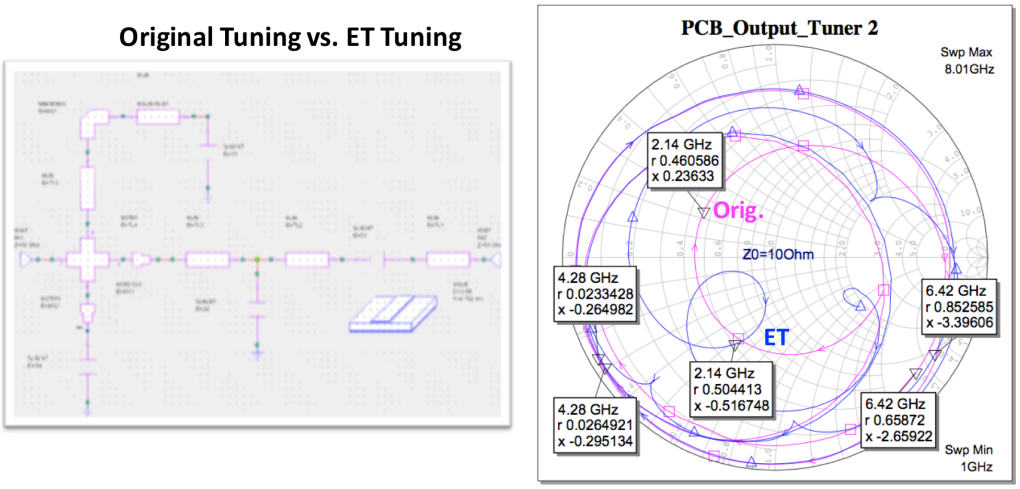

Figure 46: Retuning of the ETPA using AWR Microwave Office software

Test Solutions for ETPA Development

The success of this project was made possible by the development of an ETPA testbench capability for real-time efficiency and linearity measurements supporting the optimization of PA design utilizing ET and DPD, and the flexibility to accommodate different LTE and 5G signals. The testbench uses LabVIEW software to design and optimize the ETPA, along with the NI vector signal transmitter (VST) for RF signal generation and the NI arbitrary waveform generator (AWG) for envelope signal generation.

Traditional testbenches are made to test PAs with a constant supply voltage. In envelope tracking, a modulator is used as a dynamic power supply that varies as a function of the signal's envelope. This technique is deliberately designed for signals with high PAPR and hence, traditional PA tests cannot be used to optimize its performance. The average performance for a modulated signal is what needs to be evaluated in an ETPA, as opposed to continuous wave (CW) performance at the peak supply voltage. The problem is further complicated by the lack of accurate models over a wide range of supply voltages. Most device models are valid at the nominal constant supply voltage +/- 10%, while in ET the supply voltage can be 90% lower than the peak supply voltage. Hence, real-time performance measurements are highly desired for optimizing the ETPA.

There are many benefits to using PXI, VST, and AWG hardware for envelope tracking. Similar testbenches have been built in the past and have taken a year or more to complete. With the excellent integration in NI software and hardware and the use of LabVIEW, the designers were able to complete the NI envelope tracking testbench in less than two months. An important feature that PXI offers is the ease of synchronization between the equipment modules. Due to the nature of ET, it is critical that the supply envelope signal arrive at a specific time with respect to the RF signal.

Additionally, 5G PAs need to support various types of modulations, which the NI VST can easily generate. Another advantage to the NI VST is the widely tunable RF frequency it offers (65MHz to 6GHz). The second generation VST, introduced in the summer of 2016, provides even greater capabilities with an operating frequency range from 9kHz-6.5GHz, 1Ghz of instantaneous bandwidth, and large Virtex 7 onboard the FPGA for real-time signal processing such as real-time DPD. This covers most of the non-mmWave LTE bands of interest with 200MHz of instantaneous bandwidth, allowing system flexibility for various applications in addition to LTE. Because envelope tracking is inherently wideband in terms of tunable RF bandwidth, a wideband ETPA with this NI ET testbench can be used to test various LTE bands, GPS, and military applications, all on the same day with simply a click to change the RF frequency.

To develop a testbench for optimizing envelope tracking, various modules described in Figure 47 were used. Power source measurement units (SMUs) were used to allow for real-time DC power consumption measurements. RF power meters enable users to monitor the input and output power. In LabVIEW, these measurements are put together and calculations are done to enable instantaneous monitoring of the efficiency, gain, and output. The envelope signal was generated using the NI AWG. The NI VST served as the RF signal generator, as well as the RF feedback analyzer. Leveraging the feedback signal and the NI MathScript module, DPD was used to improve the linearity of the ETPA. The envelope shaping relationship between the true envelope of the signal and the supply voltage was optimized easily by simply loading a different equation.

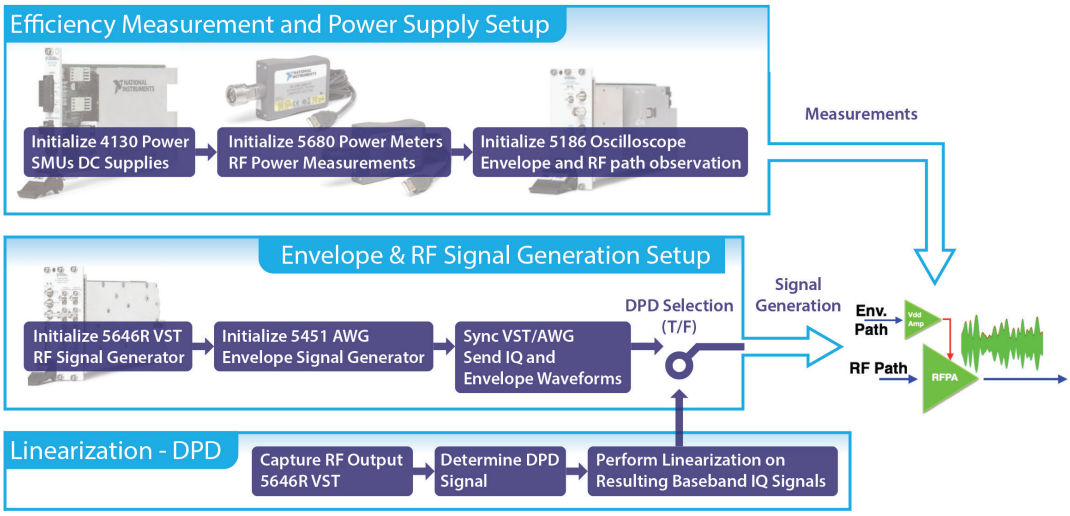

Figure 47: Test modules used in the development of an ETPA testbench

As mentioned earlier, impedance tuning for best performance can be done by load pulling and source pulling with external tuners and AWR Microwave Office software was used to apply the optimized tuning to the on-board ETPA. The reduced characterization time and ability to optimize the ETPA in real time offers a significant game changer for PA designers.

The time alignment of the amplitude signal and RF signal at the RF transistor is critical for optimizing the ETPA's performance. A time misalignment in these two signals will produce signal distortion, degrade ACPR performance, and reduce efficiency. Characterization of the time-delay difference between these two signal paths will allow for time alignment. This delay difference may vary with temperature or aging and therefore the system would need to compensate for this variation in order to ensure optimum performance. Using NI PXI, VST, and AWG hardware with LabVIEW software, the designers were able to visually see the improvement/degradation in linearity and efficiency as the alignment between the RF signal and the envelope supply was altered in real time (Figure 48).

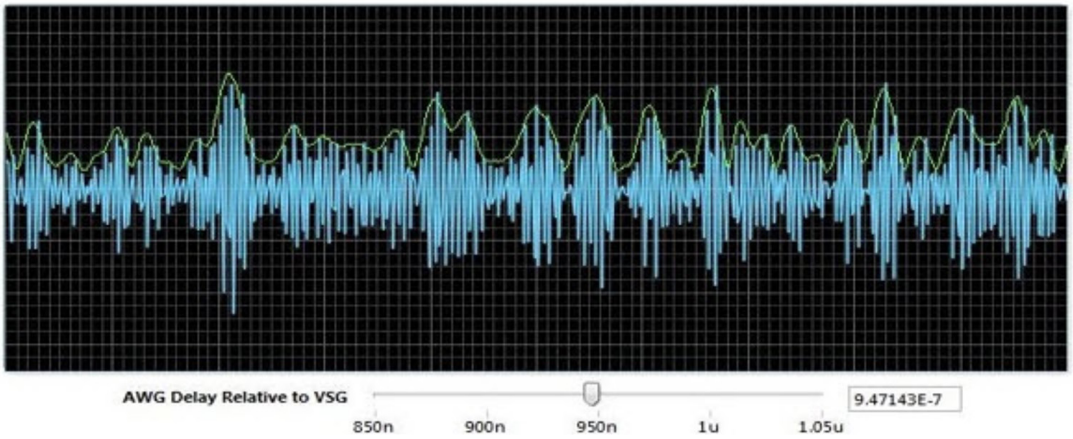

Figure 48: Time alignment between RF signal and envelope supply

Results of ET Using PXI, VST, and AWR Design Environment

The NI VST and PXI were used to optimize the LTE Band 1 (2.14GHz) PA using MaXentric's MaXEA 1.0 modulator. The MaXEA 1.0 is a 30 V integrated envelope modulator with greater than 70% modulator efficiency, capable of outputting up to 7W of average envelope power. The modulator was designed to support signals with high PAPRs such as those used in LTE and 5G and is compatible with various PA technologies such as LDMOS, GaN, GaAS, and more.

A consequence of high data-rate communications such as LTE, LTE-A, and future 5G systems offering greater spectral efficiency based on CA and OFDMA (or other modulation schemes) will be the increase in the PAPR of the time-domain signal. Signals with large PAPR will experience nonlinear distortions at the transmit power amplifier, resulting in in-band distortion and out-of- band spectral leakage, which cause performance degradation, interference to other systems, energy inefficiency, reduced cell coverage, and system capacity loss. Hence, RF components in the transmitter front end must be designed for linearity and efficiency.

This article has described the combined use of circuit/system/electromagnetic co-simulation available in the AWR Design Environment platform, inclusive of AWR Microwave Office, AWR VSS, and AWR AXIEM software, along with a measurement solution based on NI PXI, VST, and LabVIEW software to significantly reduce the optimization and product development time for a wideband ET PA across different bands and applications.

Filter Technologies for 5G Communication Systems

Systems offering large bandwidths through carrier aggregation and ubiquitous coverage through the massive overlapping of microcells will present both in-band and out-of-band interference that must be managed or eliminated. Likewise, implementation of massive MIMO will require compact filtering technology that mitigates the adverse impact of out-of-band interference on the uplink sum rate of maximum-ratio combining (MRC) receivers. This chapter examines the filter design challenges brought on by adopting these new technologies, the factors driving the physical, electrical, and cost restraints for 5G filters, and the supporting simulation technology that will help designers physically realize these components.

Current Mobile Device Filter Technology

Today's 4G (LTE) smartphones support in excess of 30 bands, requiring over 60 filters, many in the form of multiplexers. This number of filters consumes significant space and commands the largest share of the RF expense in the mobile ecosystem, putting considerable cost pressures on component manufacturers. The majority of these components are based on surface acoustic wave (SAW) or bulk acoustic film (BAW) technology. At the lower frequency range, SAW filters meet the requirements for low insertion loss and excellent rejection, covering broad bandwidths at a fraction of the size of traditional cavity and even ceramic filters. Meeting these requirements with the increase in frequency up to 6GHz and mmWave bands is proving to be a challenge for these filter technologies.

A conventional filter stores the energy in the charge on capacitors and current in inductors, whereas BAW and SAW filters store the signal in acoustic resonators. As the name implies, surface acoustic waves propagate in the lateral direction with the shape and center frequency of the passband determined by the pitch, line width and thickness of the interdigital transducers (IDT) (Figure 49).

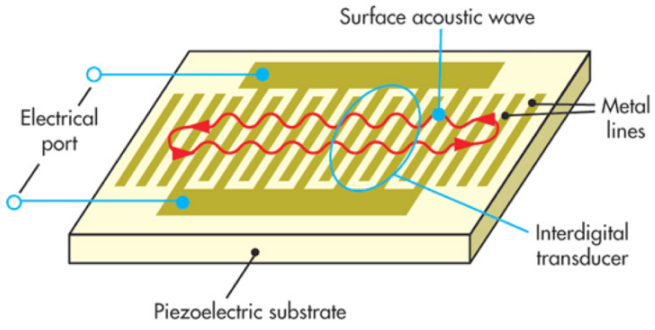

Figure 49: Basic structure of a SAW filter

Because they are fabricated on wafers, SAW filters can be created in large volumes at low cost and filters/duplexers for different bands can be integrated on a single chip with little or no additional fabrication steps. Their key advantages are low cost, good relative bandwidth, and flexible port configurations.

However, due to the degradation in selectivity at higher frequencies, SAW filters have limited use above ~2GHz and are mostly used for applications with modest performance requirements such as global system for mobile communication (GSM), code-division multiple access (CDMA), and 3G receiver front ends, duplexers, and filters. SAW devices are also highly sensitive to temperature as the stiffness of the substrate material decreases with higher temperatures, resulting in a diminished acoustic velocity and degraded RF performance. Typically, SAW filters operate in the mobile environment from 600MHz to 2GHz, whereas BAW filters operate between 1.5GHz and 6GHz, putting them in the range for the lower 5G bands.

Temperature-compensated SAW (TC-SAW) filters are fabricated using a more complex and costly layer structure to increase the substrate stiffness at higher temperatures and extend their operating range. Since the process doubles the number of required mask layers, TC-SAW filters are more expensive to manufacture, but they are still less expensive than BAW filters. In comparison, BAW filters require about 10 times more processing steps than SAW filters. While BAW technology yields approximately 4 times more parts per wafer, it still has a higher cost per filter compared to SAW[1].

1. Robert Aigner, "SAW, BAW and the future of wireless", EDN (edn.com/Home/PrintView?contentItemId=4413442)

BAW filters fall into two general architectures, solidly mounted resonators (SMRs) and film bulk acoustic resonators (FBARs). With BAW filters, an electric field excites an acoustic wave which travels in a vertical direction through the body of a piezo-electric substrate, as shown in Figure 50. The resonant frequency is determined by the thickness of piezoelectric layer, which must be controlled to high accuracy. The result is a device with lower loss, higher Q, better power handling, and sharper corners (greater selectivity) compared to SAW filters operating at the same higher frequencies.

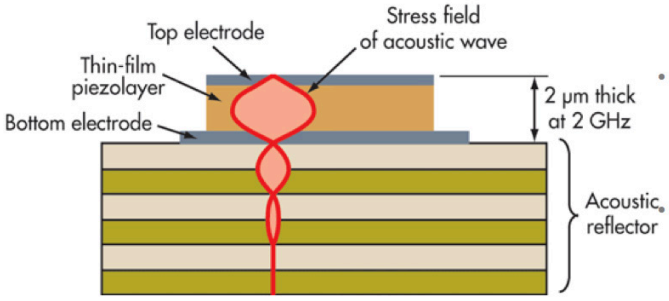

Figure 50: Cross-section of a BAW device

In the case of FBAR filters, the resonator is surrounded by an air interface created through etching or micro-machining. In contrast, acoustic reflectors below the bottom electrode of BAW-SMR filters allow them to be optimized for wideband performance in frequency regions where FBAR filters are more technically challenged. Although BAW-SMR and FBAR filters are more expensive to manufacture, their performance advantages are better suited for most LTE bands in addition to the PCS band, which has a narrow transition range of only 20MHz between transmit and receive paths.

The construction of both BAW filter types allows them to handle higher RF power levels than SAW filters. They have less temperature variation than SAW devices, although not as good as a TC-SAW. The silicon dioxide (SiO2) used in the reflector reduces the overall temperature drift of BAW significantly below what either traditional SAW or FBAR filters can achieve. Since the BAW-SMR resonator sits on a solid substrate, it can dissipate heat more effectively in comparison to FBAR, which dissipates heat laterally through a much smaller edge surface. This allows BAW devices to achieve higher power densities, allowing devices to handle upwards of 10 W, ample power for small-cell base station applications.

Leading SAW filter manufacturers include Qorvo, Qualcomm/TDK-EPCOS (RF360 Holdings), Murata, Panasonic (integrated into front-end module from Skyworks), and Taiyo Yuden, whereas the high-volume BAW supply chain is dominated by Qorvo and Broadcom (Avago)[2]. Akoustis Technologies recently started shipments of its patented single-crystal BAW filter prototypes targeting 5.2GHz for 802.11ac Tri-Band WiFi routers. The company expects to be first to market with 5.2GHz BAW filters and is preparing to begin commercial production during the first half of 2018.

Various manufacturers use AWR Design Environment platform, specifically AWR Microwave Office circuit design software and AWR AXIEM and AWR Analyst™ EM simulators to support their SAW/BAW filter design activity. With customized simulation libraries that implement acoustic wave filters using mathematical models directly in AWR Microwave Office software, filter designers are able to focus on the combined electrical performance of the SAW/BAW devices with any off-chip resonators and electronic packaging.

Some of these devices have been implemented as PCells along laminate and low-temperature co-fired ceramic (LTCC) design kits for further product development and module integration. For SAW/BAW filter designers, AWR software offers:

- Complete front-to-back design flow in one integrated tool
- Integrate acoustic to electrical models
- Polymorphic/dynamic model support
- Sophisticated interconnect routing and modeling
- EM stack-ups with built-in shape pre-processing
- Integrated ACE automated circuit extraction and AWR AXIEM and Analyst EM simulators
- Multi-technology device/module design flow

2. edn.com/design/analog/4442660/2/A-major-change-in-smartphone-RF-filters-and-front-ends-as-5G-approaches

Spectrum and Architecture

The FCC has proposed RF bands for 5G of 3.5-6GHz, 27-40GHz, and 64-71GHz. Each band will undoubtedly present its own set of issues and solutions for components in the radio design. As a result, this significantly expanded spectrum is expected to result in a greater diversity of filter solutions than those serving the current mobile communication bands.

When allocating the band spacing for a new standard, the 3GPP must strike a balance between efficient use of available spectrum and the current capabilities of radio technology, including the state of filter design with regard to performance, cost and size. With 5G, the need for bandwidth has motivated the 3GPP to push for advances in radio access technology into the mmWave spectrum as well as select unused bands between frequencies that have been authorized for public safety and defense applications. As radio technology evolves, planners will look to maximize the use of this very valuable spectrum by limiting the unused space (guard bands) between adjacent bands, as shown in Figure 51.

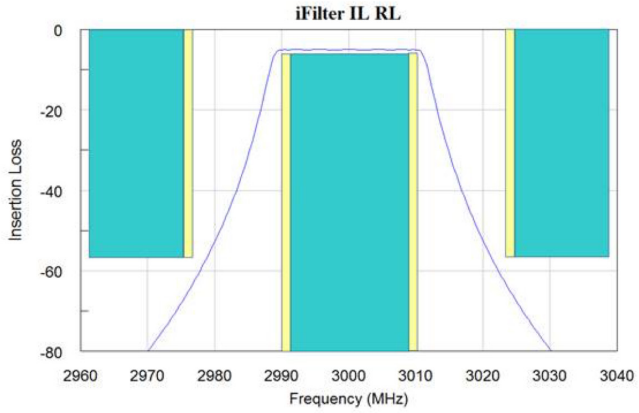

Figure 51: General filter S21 frequency mask showing passband and guard bands as simulated in AWR Microwave Office software

High-performance filtering is critical as spectral crowding increases the need for interference mitigation and bandwidth utilization drives the need to reduce or even eliminate guard bands. Supporting technology will require very low-loss, raising the filters with exceptionally steep filter skirts (high selectivity), high rejection, and very little temperature drift. In addition to these stringent requirements, increased parasitics and substrate losses associated with the filtering device and its packaging (laminate) at mmWave frequencies will most certainly degrade performance unless properly addressed.

For the new 3.5-6.0GHz 5G bands, the frequencies are close enough to the current mobile high-band that systems can employ a similar set of radio solutions. While the higher (6GHz) frequencies will challenge the performance levels for current off-the-shelf components, the basic radio architectures employed in current systems are expected to work. From a filter perspective, the incremental higher frequency will be an additional barrier to SAW filters, which already struggle at the 2.5GHz band. This leaves the field open for BAW and TC-BAW filters. However, the performance degradation of the current BAW technology at higher frequencies may disqualify these types of filters as well.

Filter technology will also be driven by size and integration concerns, which will be influenced by the system architecture. To illustrate, consider the receiver portion of a 4G base station that could be configured along two main architectural paths: an IF sampling receiver with heterodyne mixing stages down-converting the carrier frequency to the IF sampled by the ADC and a direct down-conversion receiver in which the carrier frequency is converted through quadrature demodulation into two baseband signals for digital conversion.

Because each of the radio blocks represent a discrete or lightly integrated component, the heterodyne architecture offers certain flexibility, allowing a relatively straightforward design to be easily modified for different wireless standards and carrier frequencies. While the architecture is robust and well documented, designers must still address a number of concerns that will impact the filtering. These concerns include device linearity (spurious products from nonlinear components), size constraints, and complexity. Due to the large number of discrete components required, heterodyne systems can consume large board areas and become cost challenging with low-volume components.

These drawbacks are multiplied when designing multiple antenna systems. The challenge of addressing space and cost pressures is compounded by the complexities introduced with the architecture advances of carrier aggregation, phased array antennas and massive MIMO. As a result, the design and product development effort becomes a formidable task requiring considerable engineering support starting with simulation.

AWR VSS system design software enables system designers to tackle these challenges with the ability to investigate different architectures and study the impact of individual component specifications on the overall system performance. Combined with AWR Microwave Office software and AWR AXIEM and AWR Analyst EM simulators, designers have a seamless path from initial system architecture development to component specification to physical realization and verification.

A standard example featuring a preconfigured single conversion heterodyne receiver and a direct-conversion receiver illustrates two popular architectures, providing system designers with an excellent guide to developing their own virtual system design bench, as shown in Figure 52. The received signal in each case is made up of a 16QAM signal at 27GHz (close to the 28GHz band currently being considered by Verizon for 5G) along with an image signal at 7GHz. The same image rejection and LPFs are used in both the single conversion heterodyne and direct conversion top-level systems.

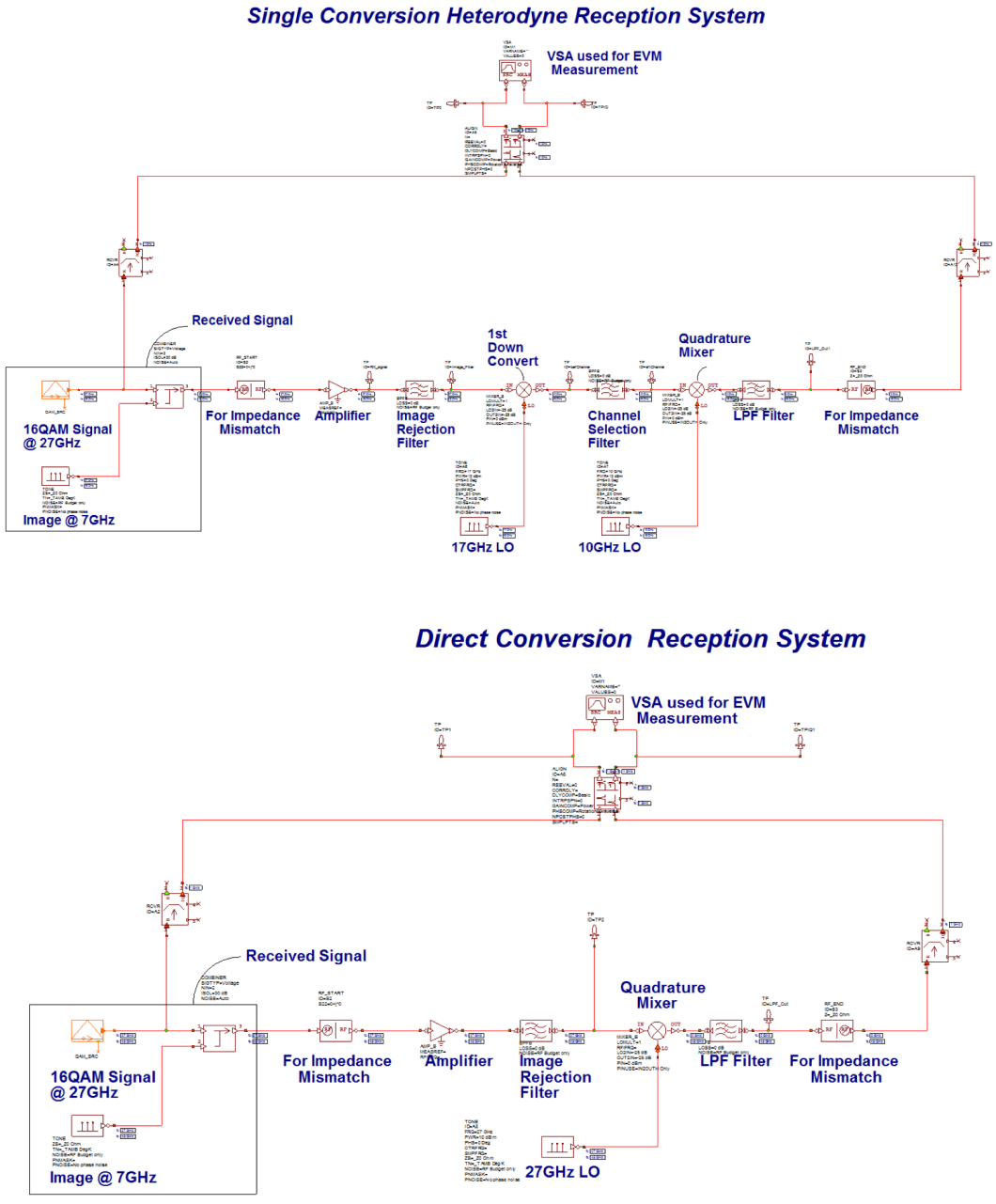

Figure 52: Two different system architectures in standard AWR VSS example illustrate (filter) component specification impact on system performance for both heterodyne (top) and direct-conversion receivers (bottom)

The desired response of the filter (low-pass Butterworth) used in both of these systems is easily defined by the user with real-time visual inspection through the property definition dialog box shown in Figure 53. Designers specify the expected or desired filter characteristics based on information from vendors or based on system requirements which can then be passed along to the filter manufacturers. Alternatively, designers can substitute real measured or data from circuit/EM level (physical model) simulation directly into a system analysis.

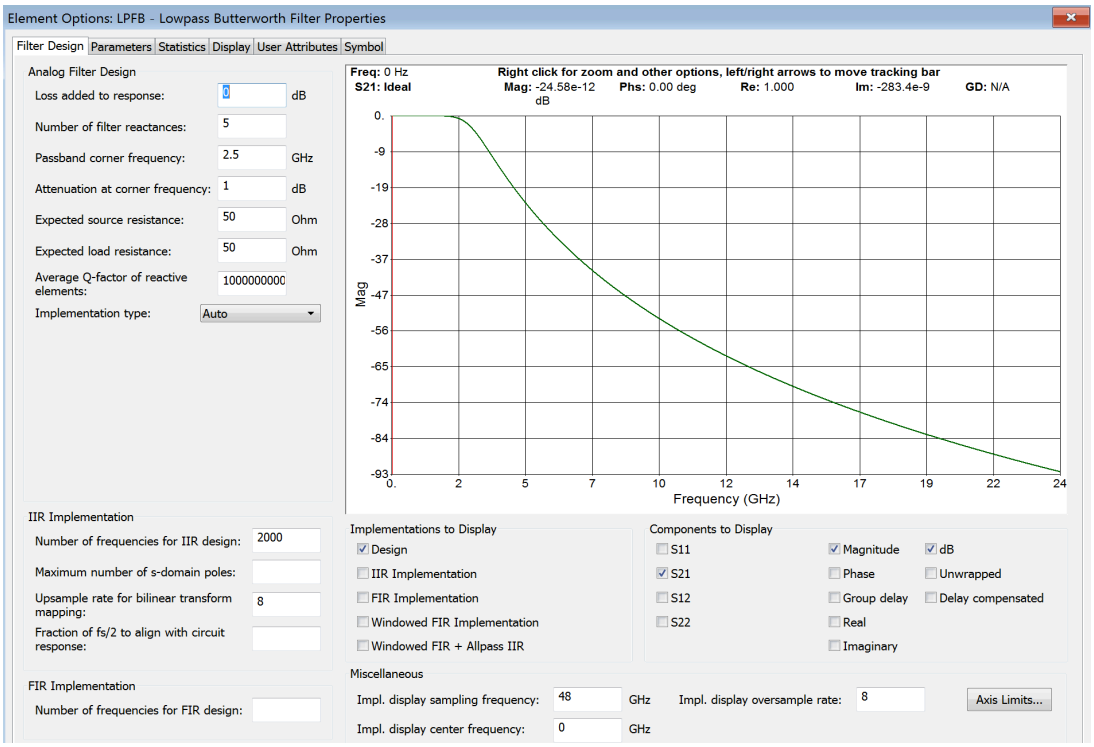

Figure 53: Properties definition for LPF element used in heterodyne and direct-conversion system architectures

Two alternative radio approaches gaining attention include cognitive and reconfigurable software defined radios (SDRs) and tunable filters. With SDRs, all the filtering is done after the A/D conversion on the receive side and before the D/A on the transmit side. The current state of the art in silicon can address the filtering, however this approach consumes power (tens of watts) in contrast to passive filters which consume zero power. In addition, the front-end amplifier would be vulnerable to any potentially strong out-of-band signals and the ADC would be converting the entire received spectrum. A tunable band select filter before the LNA would address out-of-band signals, while a tunable anti-aliasing filter before the ADC would greatly improve the power efficiency[3].

In addition to the use of CA and mmWave spectrum, 5G networks will make use of greatly improved antenna array technology, requiring additional filter solutions. Massive MIMO, which may contain 100 or more antenna elements may offer an order of magnitude improvement in spectral efficiency (60-110 of bit/s/Hz/cell, under ideal conditions, compared to ~ 3 bit/s/Hz/cell) over a 4×2 MIMO[4]. One concern for massive MIMO implementation is the complexity and quantity of components per RF chain including broadband high-resolution analog digital converters (ADC and DACs), highly linear PAs with linearizing control circuits, and a large number of filters with strong out-of-band suppression to address any interfering signals. Reducing interference as early as possible in the receiver chain is a favorable approach to achieving the objectives of MIMO antennas, simultaneously increasing interference robustness while decreasing power consumption.

As the number of MIMO base-station antennas (M) increases, studies have shown that the necessary out-of-band attenuation provided by the bandpass filters (BPFs) increases proportionately to the square root of the M[5]. This implies a practical limit on the number of broadcast satellite (BS) antennas due to the increase in BPF design complexity and power consumption. Insufficient out-of-band attenuation would result in aliasing of the filtered out-of-band interferers into the useful band at the output of the analog-to-digital converter (ADC), thereby corrupting the received baseband signal.

3. Steven Mahon, "The 5G Effect on RF Filter Technologies", IEEE Transactions on Semiconductor Manufacturing, Volume: 30, No. 4, November 2017
4. Emil Bjorson, "How much does Massive MIMO Improve Spectral Efficiency", ma-mimo.ellintech.se/2016/10/18/how-much-does-massive-mimo-improve-spectral-efficiency
5. Sudarshan Mukherjee and Saif Khan Mohammed, "How Much Bandpass Filtering is Required in Massive MIMO Basestations?", IEEE Transactions on Vehicular Technology, Volume: 66, Issue: 5, May 2017

Physical Design at mmWave

Taking advantage of mmWave spectrum will require addressing poor individual component performance and the technological challenges of applying current mobile radio solutions above 20GHz. Compounding these issues, when the mm-wave specific bands are defined, the standards will most likely require the filters to preserve as much bandwidth as possible, calling for high selectivity.

FBARs operating in frequency range of 5-20 GHz have been reported in literature[6,7]. Due to their high Q factor, these filters offer low insertion loss for decent system performance and can be designed integrated with MMIC and other technologies to reduce cost and size and provide low-power consumption. In general, the use of mmWave frequencies will likely require different filter technology than the acoustic wave filters currently used in mobile devices at cellular frequencies. Due to the need for RF chain optimization and proper addressing of the interactions between elements, there will be more integrated approaches for filtering–and the overall jump in complexity for 5G subsystems will place greater demands on design teams.

As frequencies increase toward the mmWave range, the RF wavelength becomes small enough that filters based on EM techniques are feasible. Waveguide and cavity filters are two most common high performing filter types between 20GHz and 80GHz. These filters have dimensions in centimeters rather than the required millimeters, However, there are many efforts to miniaturize these filters at mmWave frequencies.

The wavelength size for the EM wave being filtered is still large with respect to the filter's physical size requirements so it is likely that these mmWave filters will be larger than the lower band acoustic filters, which may be permissible if a different radio architecture can reduce the quantity of filters required. Otherwise, alternative construction must be developed.

Likely candidates are filters based on substrate integrated waveguides (SIW), shown in Figure 54, which offer a planar construction that can be easily incorporated into monolithic microwave integrated circuit (MMIC), RFIC, and PCB substrates with existing interconnect structures, and have also been demonstrated using standard CMOS technology. GaAs and indium phosphide (InP) technologies offer better performance than the CMOS process because of higher breakdown voltages, higher electron mobility, as well as high cutoff frequencies (fT) and good noise performance. MMICs also offer high quality passives. However, major drawbacks of the III-V semiconductor technologies include high cost, a low level of integration, and high-power dissipation.

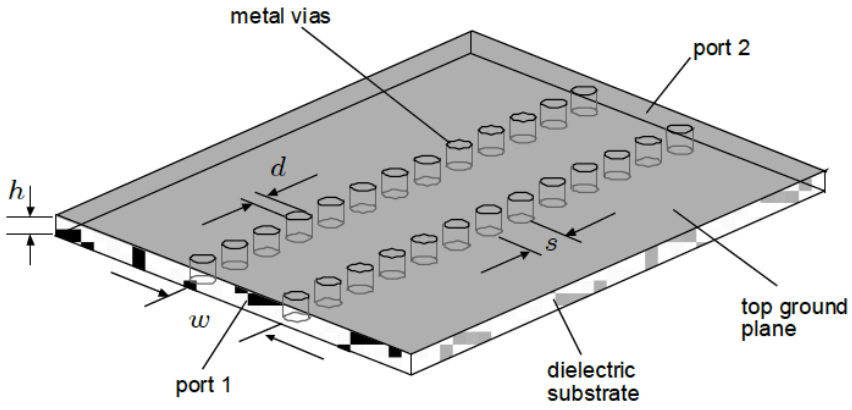

Figure 54: Typical construction of an SIW

The main advantages of CMOS include low cost, integration of digital, analog, and RF functionality into a single IC, plentiful number of manufacturers, and cutoff frequencies beyond 100GHz. Because of the low resistivity of Si substrates (typically 10Ω-cm) and metal losses, on-chip passive components exhibit low Q-factors and suffer from high losses in mmWave circuits, degrading BPF insertion loss and out-of-band rejection.

6. K. Umeda, H. Kawamura, M. Takeuchi, and Y. Yoshino, "Characteristics of an AlN-based bulk acoustic wave resonator in the super high frequency range," Vacuum, vol. 83, no. 3, pp. 672–674, 2008
7. N. I. M. Nor, K. Shah, J. Singh, N. Khalid, and Z. Sauli, "Design and analysis of film bulk acoustic wave resonator in Ku-band frequency for wireless communication," in Proceeding of SPIE, Active and Passive Smart Structures and Integrated Systems 2012, 83411R, vol. 8341, 2012

The size of a mmWave passive filter based on distributed transmission (example filter in AWR Microwave Office software is shown in Figure 55) is smaller than a filter at microwave frequencies, supporting integration with other circuits on a single chip. The Q-factor of a monolithic transmission line (TL) is directly proportional to the square root of its operating frequency. As a result, the Q-factor of a TL is enhanced with increasing frequency. Consequently, TLs are broadly used and preferred as resonators for mmWave passive filter design. At mmWave frequencies, reactive elements required for matching networks and resonators become very small. Quasi-transverse EM (quasi-TEM) TLs are easily scalable in length and can realize small reactances.

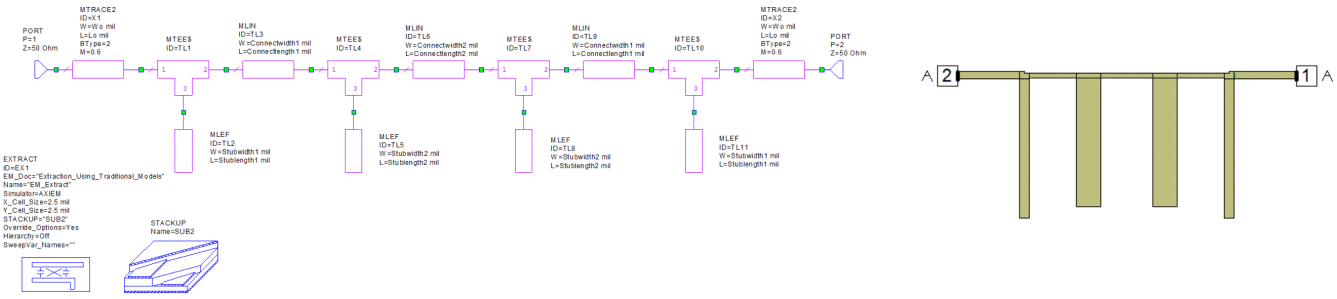

Figure 55: Microstrip bandpass filter example based on transmission lines and open-circuited stubs that reduces in size at mmWave frequencies

For 5G filter designers, the challenges are compounded by an increase in potential interferers due to the adoption of massive MIMO and network cell densification, guard-bands that are reduced or eliminated, and carrier aggregation demands of greater selectivity and mmWave spectrum. As current radio and acoustic filter technologies struggle with performance at these higher frequencies, designers will need to explore a wide range of alternatives. Simulation software, which includes system, circuit, and EM analysis will play a critical role in the success of these new filter technologies.

Advances in System-Level Simulation to Support 5G

The exploration phase for high-performance 5G communication systems is well under way with ongoing investigations into enabling technologies that will support the use of more spectrum and mmWave frequencies, smaller high-density cells, improved device power efficiency, new modulation schemes for diverse device coexistence, and high directivity OTA transmission made possible through the implementation of massive MIMO antenna arrays and beam steering technologies.

5G On the Way

The goals for 5G communications are very ambitious: 10,000 times more traffic, 1,000 times increased capacity, much lower latency, very high peak and sustained data rates, much longer battery life, and lower device cost. As the infographic in Figure 56 conveys, the planned requirements for 5G mobile networks include:

- Peak data rate: 10 gigabits per second
- Reaction speed (latency): less than 1 millisecond
- Network reliability: 99.999%
- Number of devices: more than 1 million per square mile
- Energy efficiency: 10% of current consumption
- Max speed of reliable coverage: 300 miles per hour

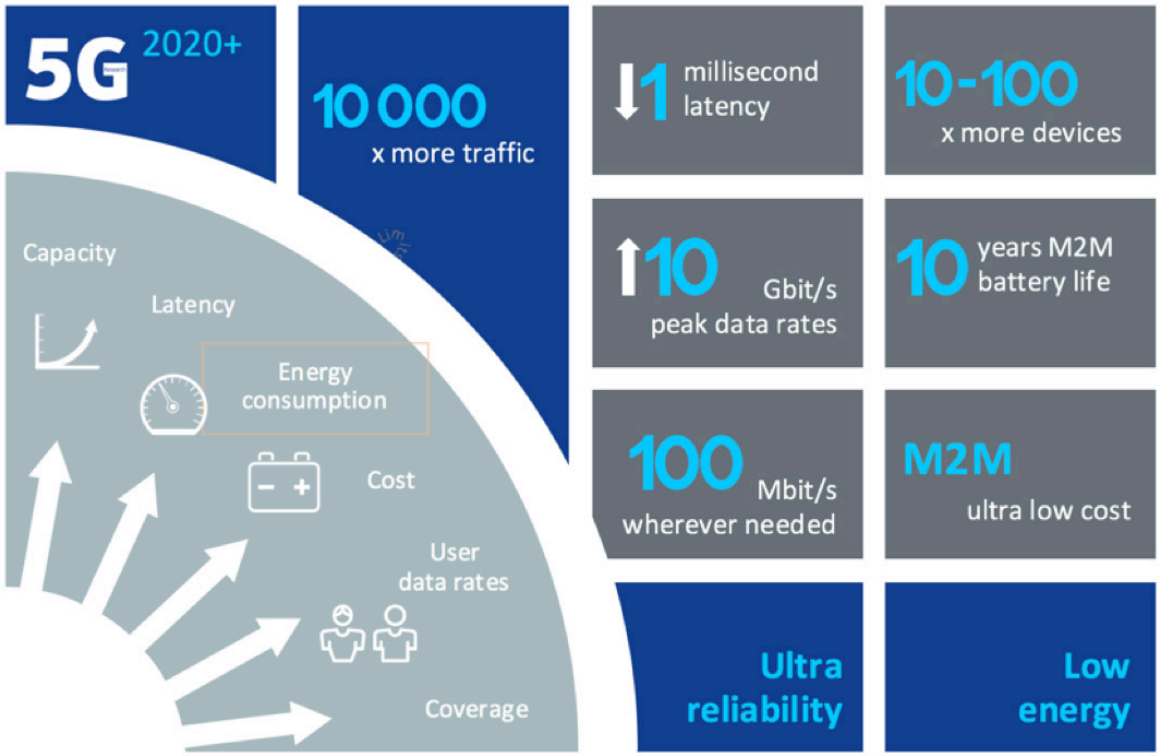

Figure 56: Goals for high-performance 5G (image courtesy of Nokia Bell Labs)

Unique 5G Design Challenges

In support of 5G, the range of mobile communication frequencies will be extended to include new spectrum allocations below 6GHz, as well as higher frequency bands that will complement the lower bands by providing additional system capacity and very wide transmission bandwidths on the order of 1GHz or more for bands above 30GHz. These higher frequency ranges will provide the very wide bandwidths necessary for extreme data rates in dense deployments. However, since frequencies above 30GHz have inferior propagation properties (higher loss), the lower bands will be more commonly used, serving as the backbone for 5G mobile communication networks.

Massive MIMO and Beamforming Antenna Arrays

Massive MIMO and beamforming signal processing is expected to play a critical role in 5G as it greatly enhances coverage and user experience across the entire range of frequency bands. Massive MIMO, a term coined by the 5G community to describe antennas with many elements (up to 128), will contribute significantly to the required 5G capacity increase. Massive MIMO will employ beamforming technology, which will then enable 5G systems to pinpoint and steer the signals to specific users and track these users so they always have good coverage. It will also enable simplified receivers on the user equipment side.

Another benefit offered by beamforming is the ability to transmit considerably less power due to the array gain, which in turn results in certain reductions in hardware complexity. For example, the power amplifiers (PAs) and supporting circuitry in a traditional base station dominate power consumption at about 1kW for three sectors because of their need to provide high-RF output power and their low efficiency when operating at considerable back off to achieve linearity requirements [1]. In Massive MIMO a similar range can be covered with a total power consumption of 15W for 100 antennas. Massive MIMO also helps counteract the impact of the higher propagation losses at mmWave frequencies by directing energy more efficiently over the channel.

In addition, beamforming improves the radio environment by limiting interference to small fractions of the entire space around a transmitter and likewise limiting the impact of interference on a receiver to infrequent stochastic events. The use of beamforming will also be an important technology for lower frequencies; for example, to extend coverage and to provide higher data rates in sparse deployments.

Another goal is to provide within the MIMO technology itself spatial-multiplexing capabilities that increase user throughput. By using arrays with hundreds of antennas at base stations that simultaneously serve many tens of low-complexity terminals in the same time frequency resource through closed-loop spatial multiplexing/de-multiplexing (multi-user MIMO precoding/decoding), a 10x or more increase in gross throughput can be achieved with massive MIMO. Perhaps even more important is the significant gain in reliability due to flattening out of deep fades, hardening of the channel, and array gain [2].

MIMO RF-System Design and Analysis Using VSS

In order to cope with moving terminals, the base station employing beamforming must be able to track the terminal (user device) and adaptively steer its beam in the direction of the terminal. Such adaptive beamforming can be implemented with a phased-array antenna, which consists of various interconnected individual transmitters. With a variable and intelligent arrangement of the individual transmitters, the resulting antenna pattern achieves high directivity and the resulting beam can be flexibly adjusted to moving users and varying capacity needs.

Achieving the goals for massive MIMO poses several unique design challenges. Any large antenna system, and especially a MIMO system, is complex to design and difficult to analyze. As communications systems move to higher and higher frequencies, RF impairments become ever more significant. MIMO system modeling includes antenna elements in the phased array as well as the RF links of the individual elements. Since each element has its own RF links in MIMO, it is important to include the RF link impairments in the overall performance of the antenna so that meaningful results are obtained that closely match the final measured results of the device once it is built. The effects of the specific RF links for each of the elements in the antenna pattern of the overall system need to be investigated. This design process will also define the matching network requirements for the system.

New phased-array modeling capabilities in the AWR Design Environment platform, specifically AWR VSS system design software, provide ease of configuration and reduced overhead, as well as shorter design and simulation times. These capabilities enable designers to configure the array's geometry using either a standard layout pattern or a custom-created one. The radiation patterns of individual elements can be specified via simulations or real-world measurements and can be included in the performance evaluation of the phased array. Such an approach yields much more accurate results compared to simple, idealized, isotropic sources. Furthermore, the system simulator can model the individual RF components in the phased array so that designers can obtain a realistic performance of the overall system. The following example demonstrates these new capabilities in the design of a 4X4 phased-array antenna.

MIMO System Design Example

This example examines a base-station MIMO. There is a source, which goes to a transmitter phased array, then to a channel, and then to a receiver antenna. Looking at the transmitter phased array in Figure 57, it can be seen that it is a simple 4X4 phased array containing 16 elements. Each of the elements has its own RF link. One of the challenges of designing systems is the impedance matching between the power amplifier and the antenna.

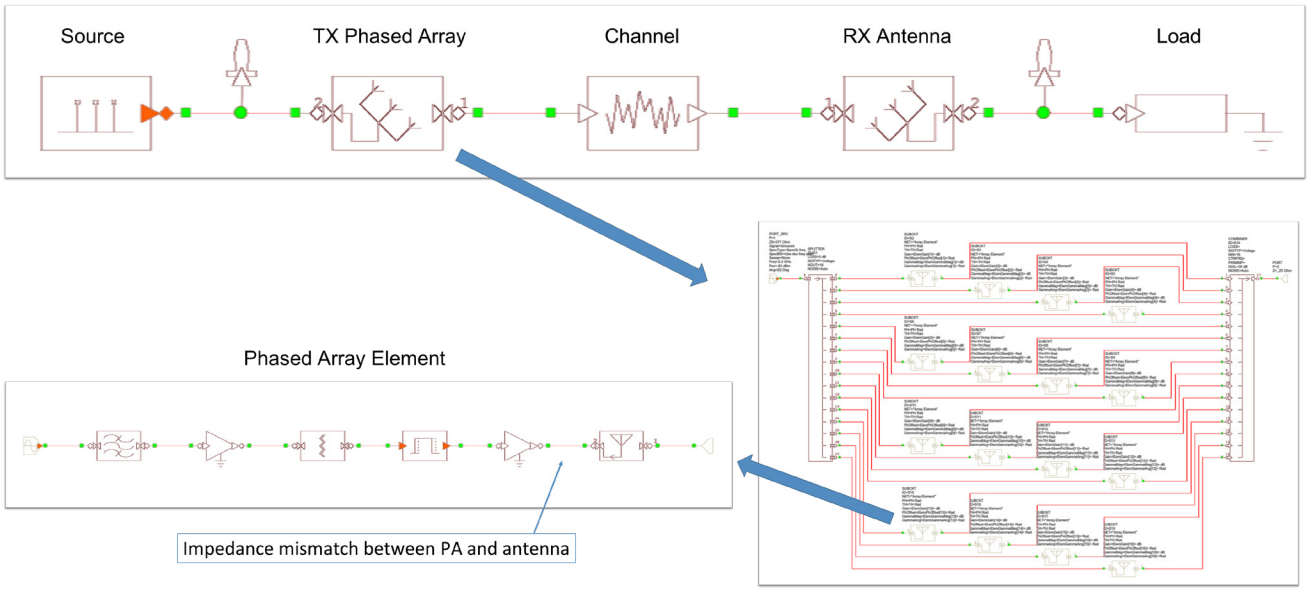

Figure 57: One of the challenges of designing systems is the impedance matching between the PA and the antenna

While traditional approaches may be sufficient for smaller phased arrays, larger, more complex arrays require significantly more processing time and power. The new phased-array functionality in AWR VSS enables users to design and analyze very large phased arrays with thousands of elements and facilitates the implementation of various array geometries, tapers, imperfections, and degradation. AWR VSS software offers enhanced modeling of element radiation patterns and mutual coupling, as well as characterization of RF links for individual array elements.

It is well known that the impedance mismatch between the PAs and their corresponding antenna element varies based on the scan angle of the array. In this example, the designer investigated the impedance mismatch between the power amplifier and the antenna by setting a range of impedance values on a Smith chart and then using AWR VSS software to evaluate the performance of the design over the range of impedance values. Different measurements were run and evaluated, and from the measurements the requirements were drawn for the matching networks (Figure 58).

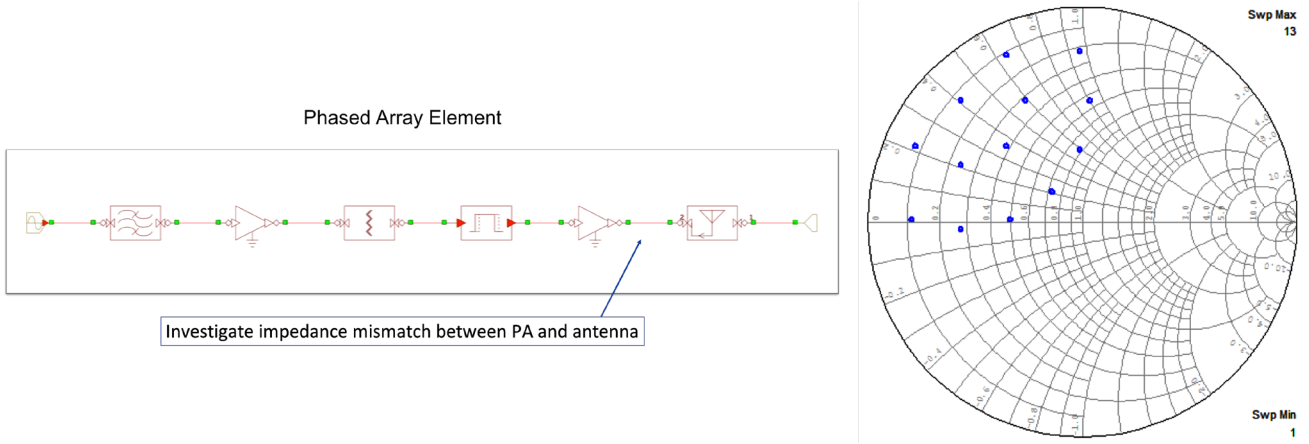

Figure 58: The impedance mismatch between the PA and the antenna was investigated by setting a range of impedance values on a Smith chart

A simple 4x4 rectangular array with λ/2 element spacing was used for the phased-array configuration in this case, and a Dolph-Chebyshev gain taper and patch elements were used for the antenna array elements. The blue curve on the left in Figure 59 shows the array response when there is perfect matching between the PA and the antenna elements. The graph on the right in Figure 59 shows results for each of the impedance points on the Smith chart from Figure 58. It can be seen that there is a wide variation in mismatch effects. Both the main lobe and side lobes change significantly in terms of main lobe gain, beam width, and side lobe suppression.

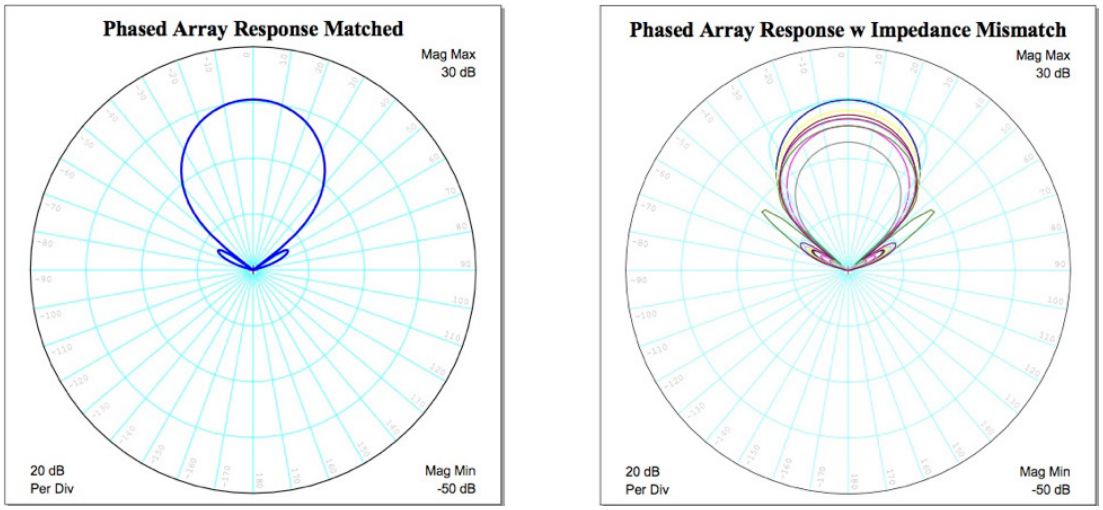

Figure 59: The blue curve on the left graph shows the array response for perfect matching between the PA and the antenna elements and the right graph shows results for each of the impedance points on the Smith chart from Figure 58

One quantity that can be calculated is the antenna array response; however, much more can be gleaned through system-level measurements. The same system can be driven with modulated signals, system-level measurements for EVM, ACPR, and more can be performed, and measurement contours can be plotted on a Smith chart. The performance of matching networks can be investigated, and these system-level measurements can be used to derive the requirements for the matching networks, as shown in Figure 60.

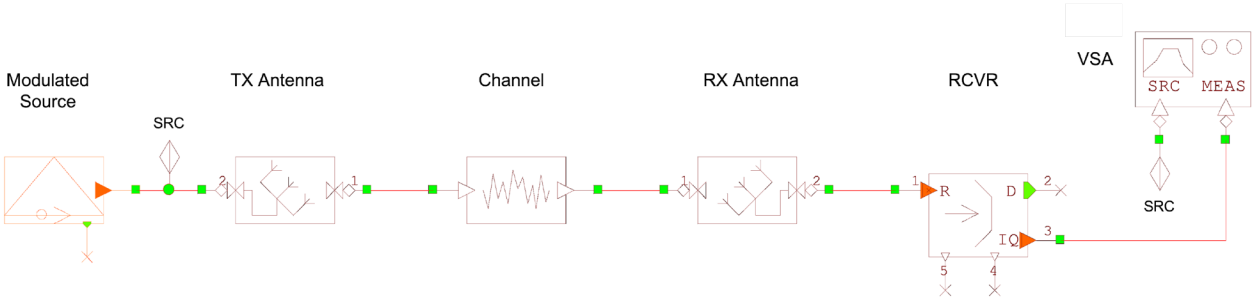

Figure 60: Along with antenna array response, system-level measurements can be taken from the same system

AWR VSS software also offers an automated analysis flow, enabling users to define the system architecture (modulation and more), configure the antenna array, set up the RF links, define gamma or impedance points that will be used for analysis, configure desired measurements, and, finally, run the automated analysis.

EVM and ACPR or other measurements are calculated. The results of the automated analysis are shown in Figure 61 with ACPR contours on the left and EVM contours on the right. The measurement contours are plotted on a Smith chart, and regions where the requirements are met are identified, giving the definitions for the matching networks. The designer is now able to go back and intelligently design the matching networks, ensuring that the overall system will perform well.

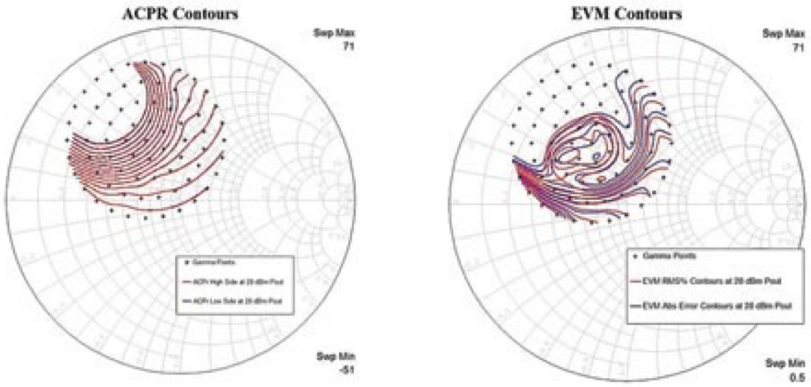

Figure 61: Results of the automated analysis with ACPR contours on the left and EVM contours on the right

Emerging technologies being developed for 5G communications and new modulation schemes are being considered. The simulation capabilities in AWR VSS software help designers overcome the associated design challenges with new advances in phased-array design and analysis and the ability to capture the real-world interactions that occur between phased-array antennas and their driving circuitry.

While the antenna example discussed is simple, there was actually a large amount of processing and analysis behind the final design. The capabilities in AWR VSS software enable users to design very large phased arrays and simplify array design and configuration. Element radiation patterns for individual elements and mutual coupling are included, as well as the RF model links for individual array elements. AWR VSS software enables designers to evaluate the effects of matching networks in overall system performance, including array response and system-level measurements that will be used for evaluating the overall system. Automated analysis enables users to quickly configure a complex 5G system for particular requirements and obtain results in a short amount of time in order to follow up with further design work.

5G/MIMO Design With Circuit/Antenna In-Situ Simulations

EM simulation software is commonly used to simulate antennas with multiple feeds, including phased arrays, stacked radiators with different polarizations, and single apertures with multiple feed points. These types of antennas are popular for communication systems where MIMO and polarization diversity antenna configurations are being rolled out.

The beam of multiple-feed antennas is controlled by changing the phase and amplitude of the signals going into the various feeds. An accurate simulation of such a system must account for the interaction that occurs between the antenna elements and the driving feed network. The problem for simulation software is that the antenna and the driving feed network influence each other. The antenna's pattern is changed by setting the input power and relative phasing at its various ports. At the same time, the input impedances at the ports change with the antenna pattern. Since input impedance affects the performance of the nonlinear driving circuit, the changing antenna pattern affects the overall system performance.

Until now, engineers have been forced to simulate the coupled circuit/antenna effects manually using an iterative process. For example, first the antenna is driven with idealized sources with known phasing at the input ports. The impedance of the ports is then used as the load impedance for the driving circuit. The process is then iterated until convergence is reached. This procedure is awkward and time consuming. Fortunately, there is a faster, more accurate way to attain the final result.

The in-situ measurement feature in Microwave Office circuit design software enables communication between the circuit and antenna, thus automatically accounting for the coupling between the circuit and the antenna in an easy-to-use framework. The designer identifies the antenna data source, the circuit schematic driving the antenna, and the measurement under consideration; for example, the power radiated over scan angle. This concept is illustrated in this section using two phased-array examples in which the antennas are simulated in the AWR AXIEM 3D planar and AWR Analyst 3D FEM EM simulators.

Patch Microstrip Array Optimized Using Microwave Office Software

In this example a 4x4 patch array that is driven by a corporate feed network with a phase shifter and attenuator at each element is simulated. A MMIC PA is placed at each element before its corresponding phase shifter. The array is only simulated once in the EM simulator. The resulting S-parameters are then used by the circuit simulator, which also includes the feed network and amplifiers. As the phase shifters are tuned over their values, the antenna's beam is steered. At the same time, each amplifier sees the changing impedance at the antenna input it is attached to, which affects the amplifier's performance. The PAs are nonlinear, designed to operate at their 1dB compression point (P1dB) for maximum efficiency. They are therefore sensitive to the changing load impedances presented by the array.

The combined circuit and EM simulations are necessary for a number of reasons. First, the EM simulation is necessary because the antenna elements interact with each other, which can significantly degrade the antenna's performance. An extreme example of this is scan blindness, where the interaction between the elements causes no radiation to occur at certain scan angles. The coupling between the elements can also lead to resonances in the feed network. In order to optimize the feed network to account for deficiencies in the antenna, the entire array combined with the entire circuit must be optimized. It is critical to simulate the feed network itself since resonances can build up due to the loading at the antenna ports.

Another often neglected but important point is that the PA driving the antenna requires a nonlinear circuit simulation. It is therefore important that the antenna's S-parameters include a DC simulation point and values at the various harmonics used in the harmonic balance simulation. Otherwise it is possible to have unpredicted degradations in system performance due to poor matching at the harmonic frequencies or inaccurately specified DC biasing.

Figure 62 shows the 4x4 patch antenna array. Each patch is fed individually by a pin going to the ground below. The port is placed at the bottom of the pin. AXIEM software, which is used for the planar EM simulations, has the ability to ground a port with a metal strap, which is used as the pin.

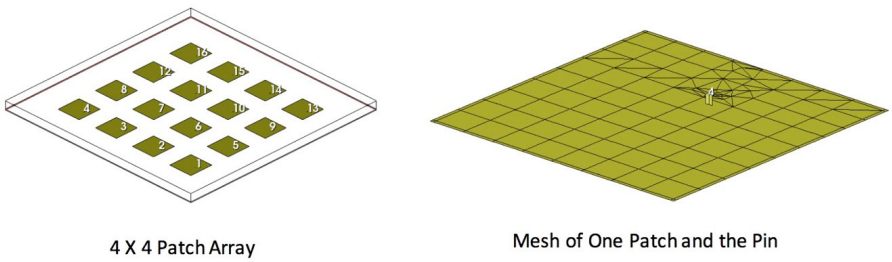

Figure 62: A 4X4 patch array (left), where each patch is fed by a pin coming up from the bottom ground plane. The right picture shows the mesh of one element, and the driving pin to the ground plane

This type of simulator is ideal for planar patch arrays that may require a 3D EM simulator depending on the structure details, since the patch is not in a package and radiation effects are therefore included automatically. It should be noted that the simulation techniques described in this paper do not depend on a specific EM simulator, since third-party simulated or measured S-parameter data can be used to represent the antenna response. The corporate feed network is shown in Figure 63.

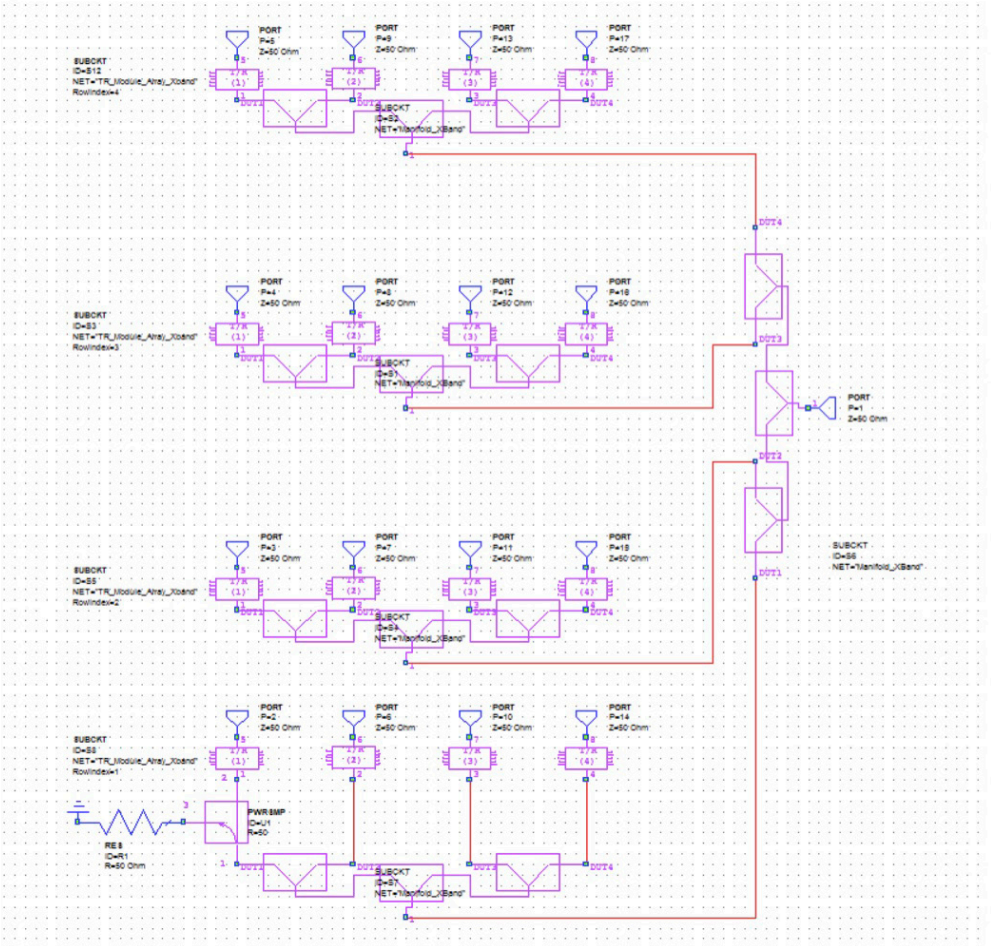

Figure 63: Corporate feed network for the patch array. Each element is driven by a MMIC amplifier, and controlled by a phase shifter and attenuator

The power is input from the right side. Wilkinson dividers are used to split the signal and feed the 16 patches. Figure 64 shows the feed for a typical patch.

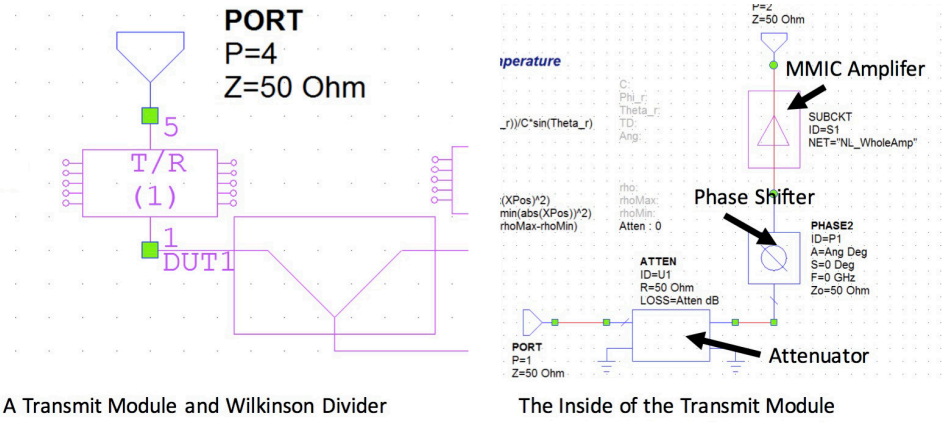

Figure 64: The left picture shows one Wilkinson divider and the transmit module, which contains the phase shifter, attenuator, and a MMIC amplifier

The transmit module and Wilkinson divider are shown in detail on the right side of Figure 64 and the inside of the transmit module on the left side. Each transmit module has a phase shifter, attenuator, and MMIC amplifier chip. The beam is steered by setting the phase and attenuation going into the MMIC amplifier and then sending the resulting signal to the patch. The phase and attenuation are controlled by variables in the software, which can be tuned and optimized as desired. In this manner, the beam can be scanned. Figure 65 shows the 3D view of the MMIC amplifier, which is a two-stage, eight-field effect transistor (FET) amplifier designed to work at X-band.

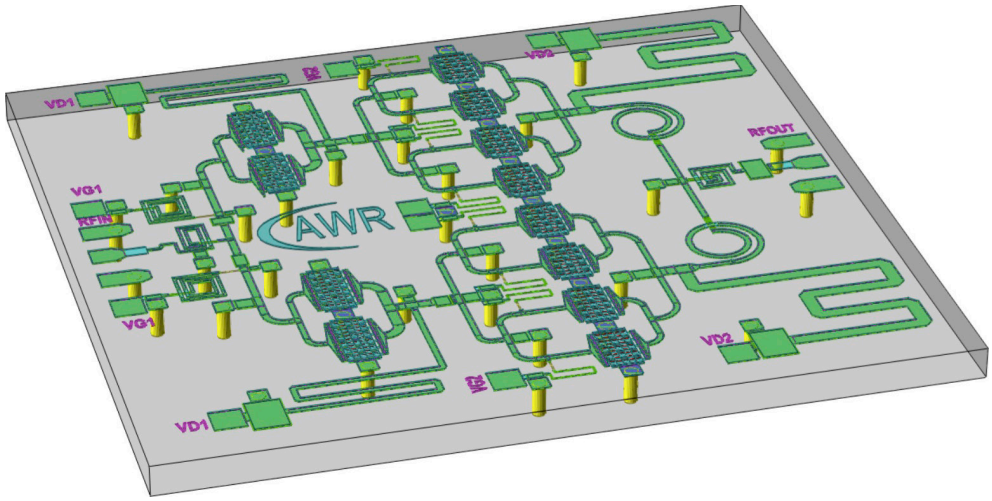

Figure 65: 3D layout view of the designed MMIC amplifier

In this example, the feed network is simulated entirely in the circuit simulator. A more realistic example would simulate the layout of the feed network in an EM simulator to make sure the models are accurate and there is no unintended coupling between sections of the network.

Typical circuit simulation results are shown in Figure 66. The system is designed to work at 10GHz. The purple curve shows the input impedance for an isolated patch from 6-14GHz on a 50Ω normalized Smith chart. The marker shows the normalized impedance at 10GHz. The four crosses show the input impedance of four typical elements at 10GHz. Note that the interaction between the elements in the array shifts the input impedance of each element from that of an isolated patch. The green contours are load-pull simulations for the MMIC amplifier, showing the power delivered to a load. The shifting of the impedances of the antenna feed results in a 0.5dB degradation of power to the elements. (Figure 66 power contours are in 0.5dB increments.)

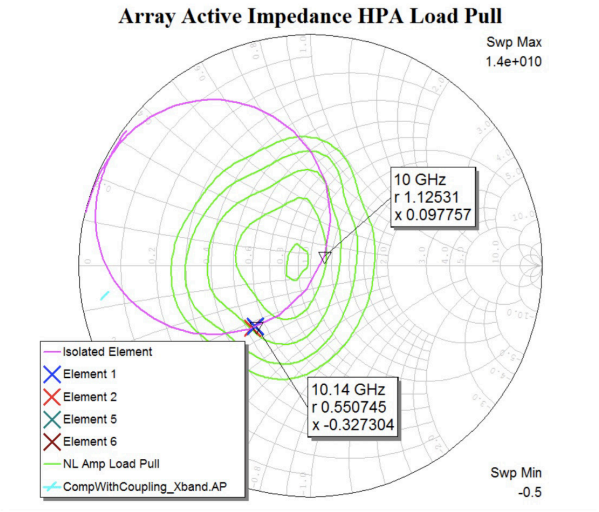

Figure 66: The Smith chart shows the Input impedance to an isolated element and to elements when the entire array is simulated. Load pull contours for power getting to the load are also shown

Examples of the antenna pattern are shown in Figure 67. The beam is steered by controlling the relative phasing and attenuation to the various transmit modules. In practice, the harmonic balance takes substantial time to run with 16 power amplifiers. Therefore, the beam is steered with the amplifiers turned off. The designer then turns on the power amplifiers for specific points of interest. Note: the far-right image in Figure 67 shows a second lobe created when the main lobe is at a near grazing angle.

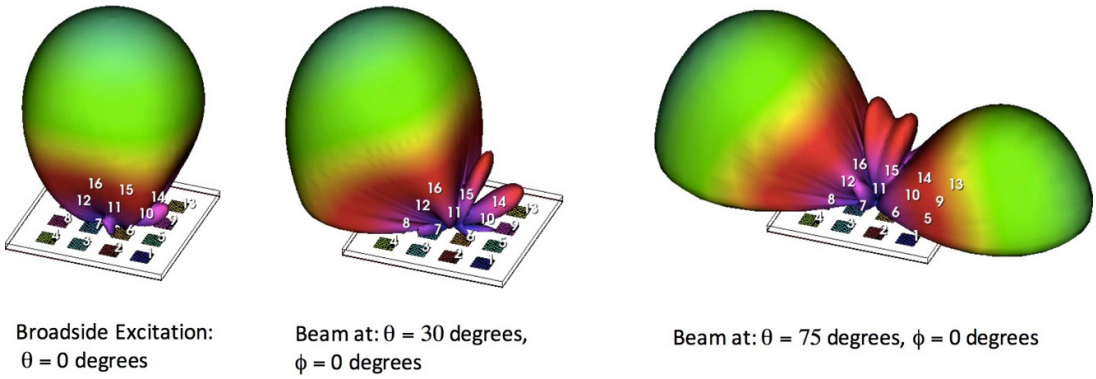

Figure 67: The beam of the array as it is scanned through typical values of theta and phi

This second example is an 8x8 patch array. Anything that can be tuned in AWR Microwave Office software can also be optimized. For example, in Figure 68, the antenna pattern is optimized for a certain scan angle. In the interests of time, the amplifiers are not included in the optimization. At the end the amplifiers are turned on to see the amount of degradation. The plot is of the total power in the beam, scanning in the theta direction with phi at 0°. The blue bars show the optimizer goals for the measurement. The purple pattern is the original broadside pattern. The optimizer changes the phase and attenuation at the feeds to the patches. The resulting blue curve meets the optimization goal of scanning at 20° with acceptable side lobe levels.

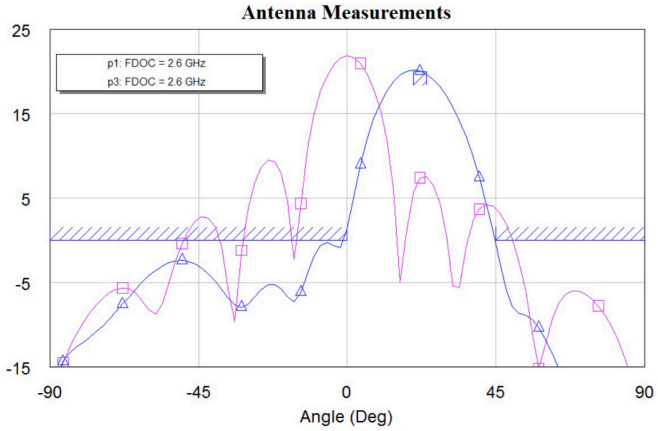

Figure 68: The antenna pattern is optimized to be below the blue bars

Designing antennas with multiple feed points for communications or radar systems requires simulation of the interaction that occurs between the circuit, typically a highly nonlinear power amplifier, the feed network, and the antenna. The beam is steered by the circuitry, and as the beam changes the input impedance or input characteristics of the antenna change, which effects the circuit. The circuit and the antenna are connected, so both must be included in the simulation.

The traditional method of simulating antennas with multiple feeds is to simulate the coupled antenna/circuit effects manually using an iterative process that is time consuming and frustrating. AWR Microwave Office circuit and antenna simulation are coupled together, enabling arrays to be easily excited from the amplifier and feed network. The load impedances of the array are incorporated into the circuit simulation. This automates the process, saving design time and delivering products to market faster.

MIMO and Beam-Steering Modeling in Support of 5G

5G represents the next milestone in mobile communications, targeting more traffic, increased capacity, reduced latency, and energy consumption through various technologies such as massive MIMO and beam-forming antenna arrays, mmWave spectrum use, and carrier aggregation. Initial deployment is expected to begin in 2020, and, according to Nokia, there will be some 5G communications implemented in the 2018 winter Olympics.

Physical technologies required for 5G realization are increased spectrum and new circuitry (amplifiers, passives, and antennas), as well as efficient power schemes for amplifiers in mobile and base stations and smaller cells in distributed systems.

Improved antenna systems are a critical enabling component of the proposed new 5G communications standards currently under development. As shown in Figure 69, high data rates, increased capacity, and low power specifications for 5G will require that communication system antennas be designed for maximum efficiency and throughput with narrow, directed beams. As a result, RF system engineers need to include the antenna characteristics in their simulations to correctly design the entire transmit/receive system.

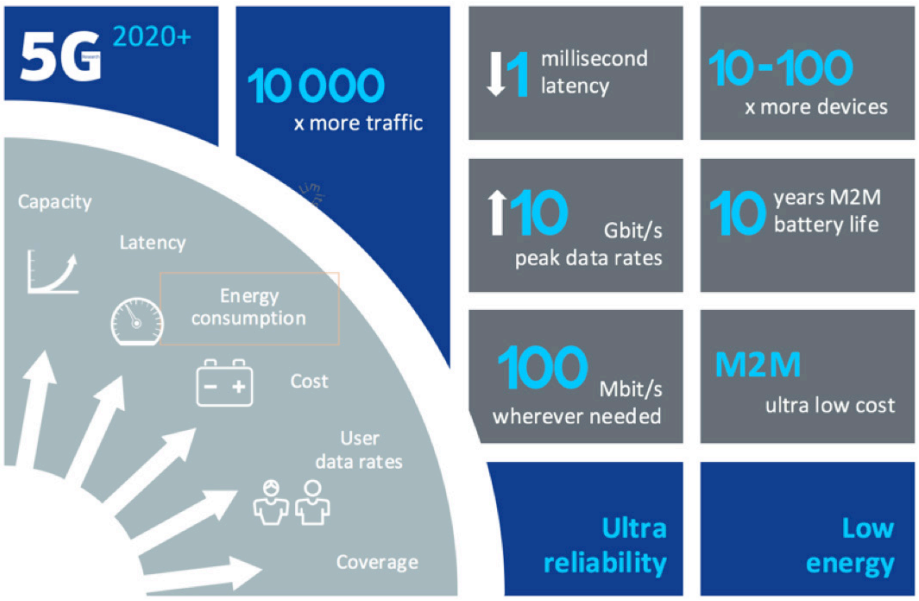

Figure 69: Goals for high-performance 5G (image courtesy of Nokia Bell Labs)

New antennas geometries such as MIMO/Massive MIMO and integrated phased arrays will be required for 5G. As Figure 70 shows, it is important to remember that MIMO does not go from a single transmit antenna to a single receive antenna, but rather the output goes to multiple receivers, making 5G antenna design very complex.

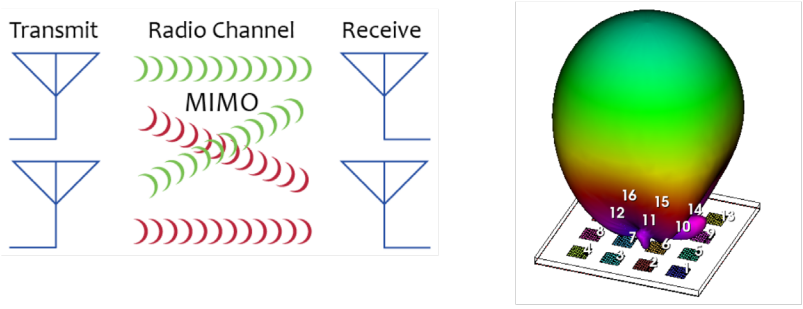

Figure 70: MIMO and beam-forming array antenna configurations for 5G

MIMO and Beam Steering Model Technology

The potential of massive MIMO will bring over 10x in capacity improvement and over 100x reduction in power consumption. Figure 71 shows how MIMO antenna arrays enable more efficient transmission of power with higher capacity.

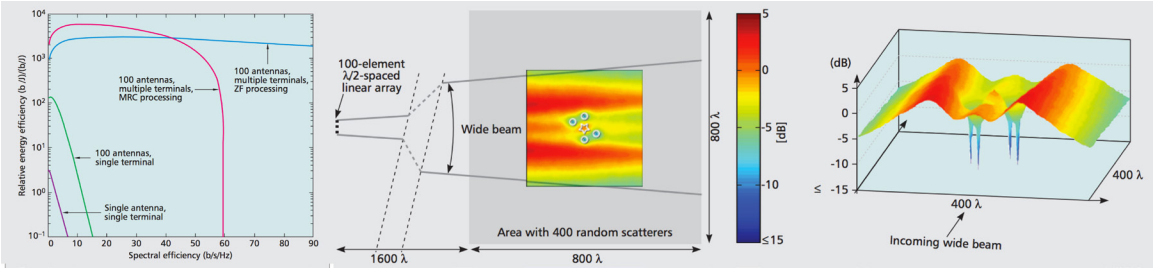

Figure 71: MIMO antenna arrays enable more efficient transmission of power with higher capacity. (Courtesy of IEEE Communications Magazine)

As a result of the complexities of 5G antenna design, RF system engineers will need to include the antenna characteristics in their simulations to correctly design the entire transmit/receive system. AWR Design Environment software, inclusive of AWR Microwave Office circuit design software, AWR VSS system design software, and AWR AXIEM planar and AWR Analyst 3DFEM EM simulators, helps engineers develop the technologies that will make these advances possible.

This application note presents several practical examples commonly encountered by the RF systems engineer and showcases advances in MIMO and beam-steering model technology within AWR VSS system design software. Detailed examples of the models being utilized in real-world systems are shown, including:

- Individual antenna patterns for array models
- Coupling of nearby elements
- Modeling of different array geometries, including imperfections and defects of elements
- Active impedances observed at each element of the array
- Different RF links for each element.

Phased-Array System Design in AWR VSS Software

In VSS the recently enhanced beam-steering behavioral model provides accurate characterization for a distributed feed architecture. User can define the desired splitter/combiner architecture, along with the desired beam angle and observation angle. The model automatically calculates the phase and the input power required for each element and gives the user the array performance. The phased arrays may be investigated in transmit or receive mode or combined to model a complete transmit and receive chain and evaluate the end-to-end system performance.

The MIMO model provides the flexibility to further define the RF link connected to each antenna element, including the filtering and amplification for each element. A common application would be studying requirements for amplifier performance in an array where the center elements are being excited at higher power. Furthermore, such setup would allow users to investigate array operation when elements are excited with non-correlated signals, resulting in higher cross-talk and more demanding designs. Classically, designers would use an EM simulator and antenna software for the phased array itself. As a system engineer designing the RF link, it is important to include the effects of the antenna and the phased array into the system-level design. Figure 72 shows a simplified link in AWR VSS software.

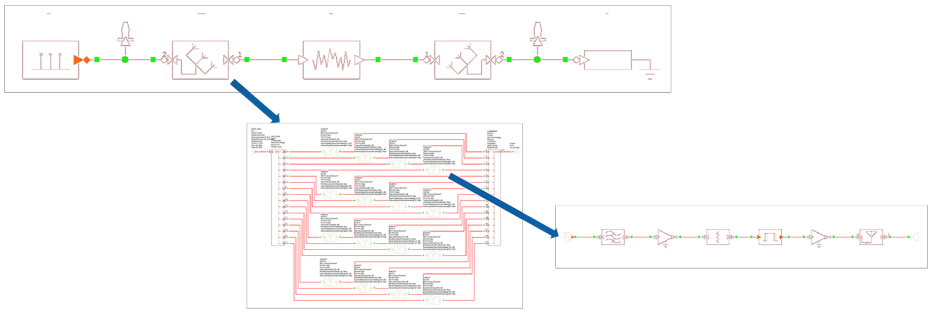

Figure 72: System-level phased-array design of the RF link

RF Link Characterization

In AWR VSS software the flow for modeling a phased array has been greatly automated. Users can put real antenna patterns into the element, and can actually couple the elements to get coupling effects for issues like nearest neighbors. In addition, the RF links can be individually modeled for each array element.

Figure 73 shows the RF link characterization capability in the software. Rather than having to write text files manually, a new AWR VSS measurement automatically generates the data-file model of the phased-array element RF link. The user starts with the RF link design (top-right) and uses a link characterization measurement to extract the RF link characteristics and save them to a file. The results are then used in the phased-array model.

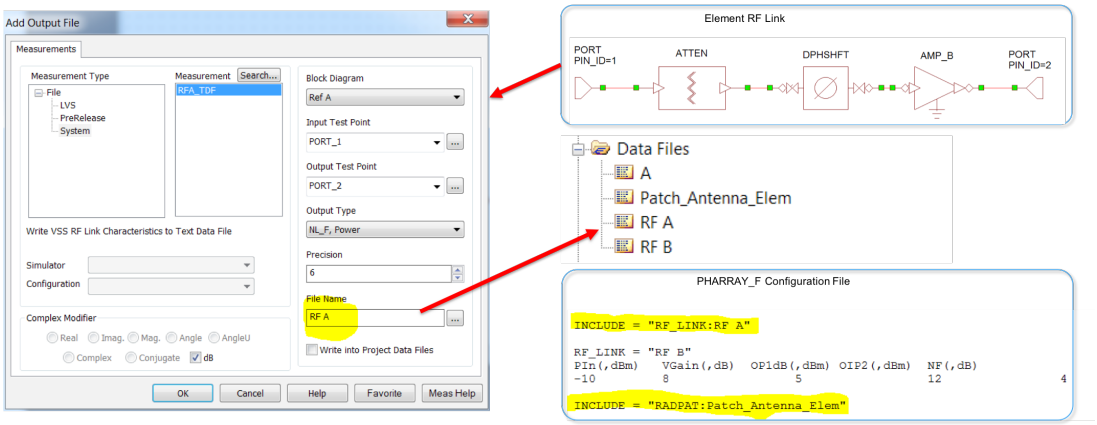

Figure 73: VSS phased-array element with RF link characterization

Element Phased-Array Pattern Measurement

The phased-array element in the Microwave Office circuit simulator can use real antenna patterns, derived from an EM simulator, as shown in the simple patch antenna example in Figure 74. The user designs the element and measures the radiation pattern in either AWR AXIEM or AWR Analyst EM simulators. The antenna patterns in the phased-array element within the simulator come either from an EM simulator or from measured data. The input impedance is input into the phased-array element, which produces the pattern. Then the software automatically generates the data file for the pattern, which is then put into the element.

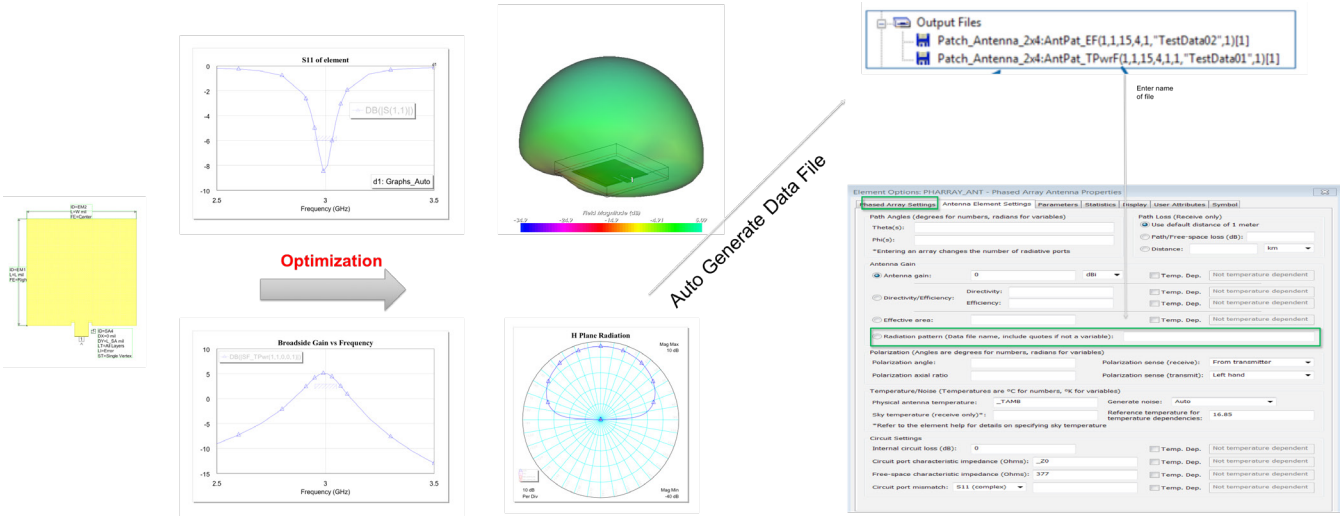

Figure 74: The element is designed, and the radiation pattern is EM simulated in AWR AXIEM or AWR Analyst software, which then automatically generates the data file for input into the element

Phased-Array Element Design

If antenna elements have not been designed yet, users can take advantage of AWR AntSyn™ software, which offers automated antenna design, synthesis, and optimization. With this tool designers can define their specifications and the software will provide the best antenna designs based on those requirements. It will often suggest antennas that the designer might not have considered, but that the software has determined might be better for the particular application (Figure 75).

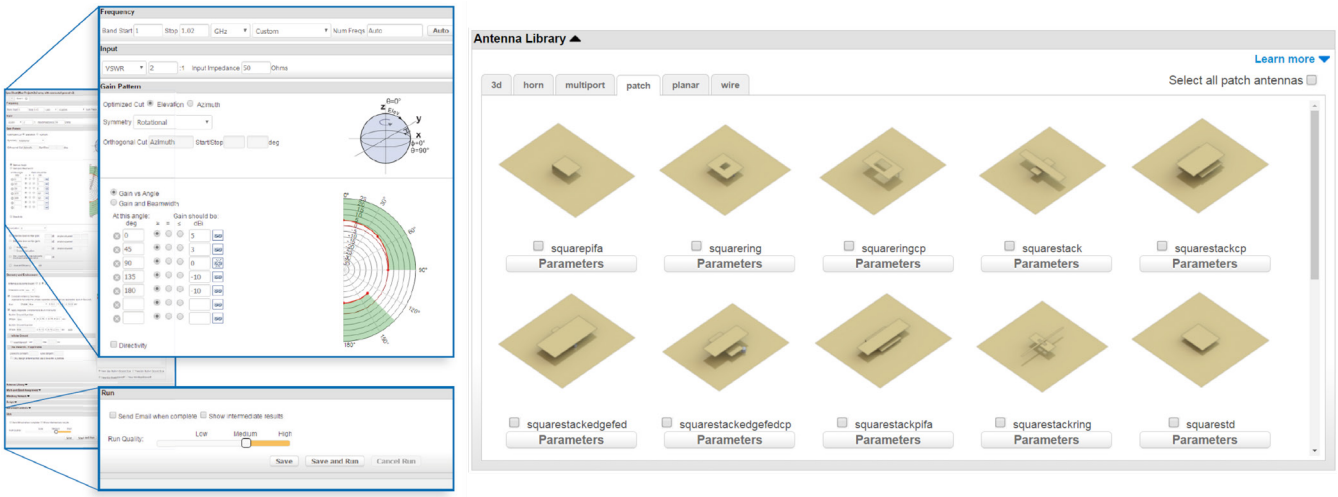

Figure 75: AntSyn software takes antenna specifications as input and produces designs based on the input requirements

This is another example of means for getting the patterns of the elements in the antenna design. Figure 76 shows how AWR AntSyn software provides an output antenna pattern file that can be imported into the AWR VSS phased-array model.

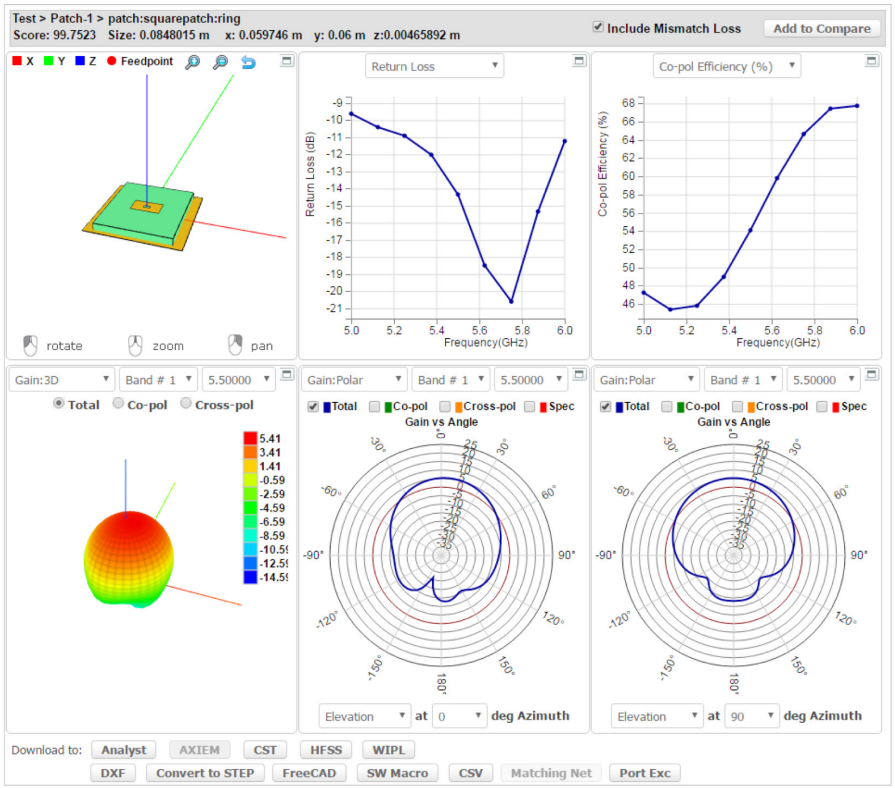

Figure 76: An AntSyn antenna pattern file can be imported into the AWR VSS phased-array model

Element Radiation Patterns

The antenna pattern and input impedances can be affected by cross-coupling between neighboring elements. In an effort to have more realistic effects in the system element, AWR VSS software enables designers to include coupling between elements. Looking at the 8 x 8 array in Figure 77, clearly the elements in the center have more neighboring elements than the ones in the corners or around the edges. In this example, elements are divided into three categories: elements that are on the interior of the array, elements at the edge of the array, and four elements at the corners. These categories can be used to model the specific mutual coupling that is observed by each type of element, resulting in better evaluation of the array response.

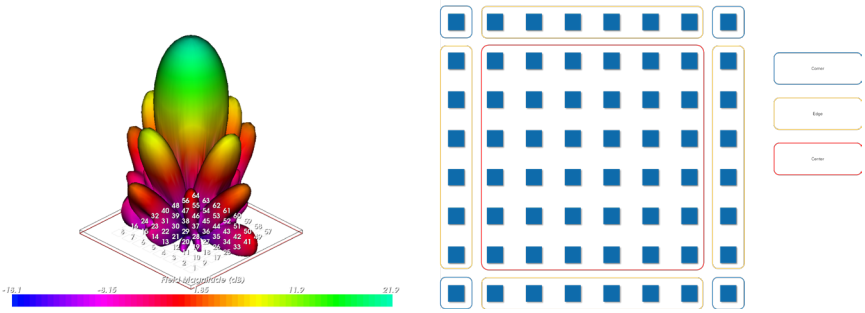

Figure 77: The coupling elements for center, edges, and corners of the array (left) and resulting EM simulation (right)

In the phased-array element in the system simulator, users can define which pattern and/or which active impedance should be used. The VSS phased-array model can use different patterns for each element, which can be calculated using EM simulations, and mutual coupling effects coming from neighboring elements.

The AWR VSS system model supports a number of different architectures, including standard array geometry configurations such as lattice (rectangular/triangular) and circular (with multiple concentric circles), as shown in Figure 78. Custom configurations such as multi-panel arrays and pseudo-random arrays are also available within AWR VSS software (Figure 79).

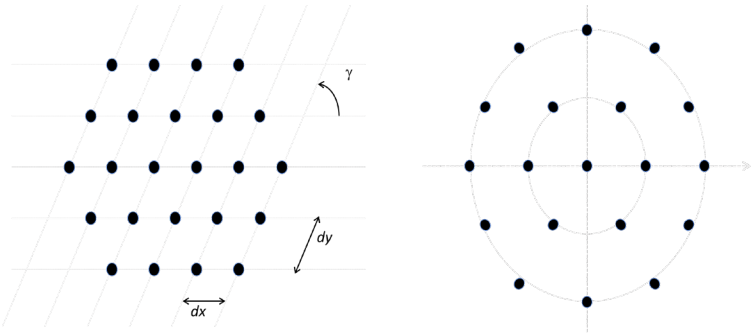

Figure 78: VSS standard array geometries: lattice (left) and circular on the (right)

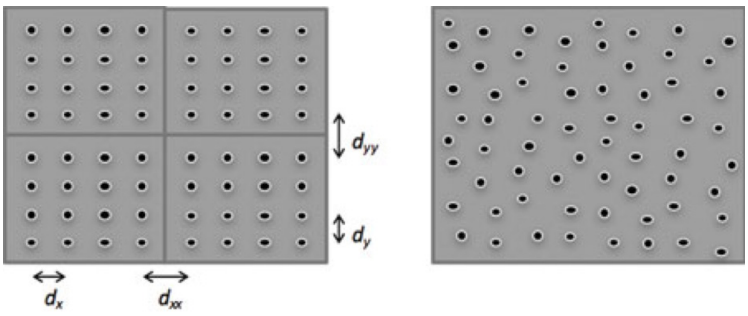

Figure 79: Custom array configurations: multi-panel (left) and pseudo-random (right)

As part of the model, users can do an element failure analysis. When the elements fail, the array response will degrade. With AWR VSS software users can see how the pattern is degrading before the design is in trouble. Figure 80 shows a rectangular (16 x 4) array with λ/2 spaced elements. Element failure results in side lobe response degradation.

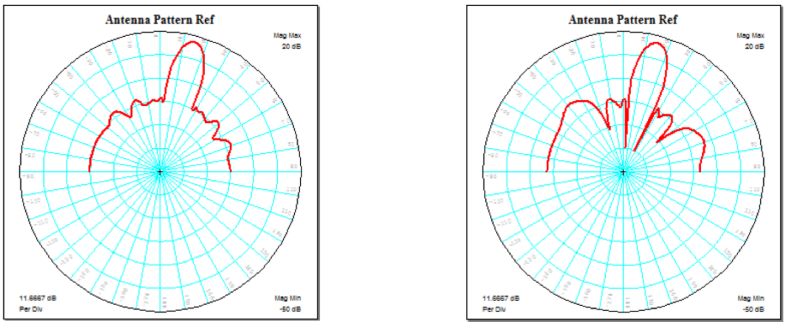

Failure rate = 2% (element #9)

Failure rate = 5% (element #9, #36, #55)

Figure 80: Element failure results

In-Situ Analysis

Figure 81 shows the in-situ analysis capability in AWR Microwave Office circuit simulator, which, as the beam is scanned, models the power amplifiers and automatically accounts for the coupling between the input impedance of the antenna and the power amplifier. As the designer scans the beam by changing the phase and amplitude at each element, the software recalculates with harmonic balance the power amplifier performance. The AWR AXIEM 3D planar simulator within AWR Microwave Office circuit design software also offers phased-array simulation capabilities. As can be seen in Figure 81, the antenna array pattern is being EM simulated by AWR AXIEM software.

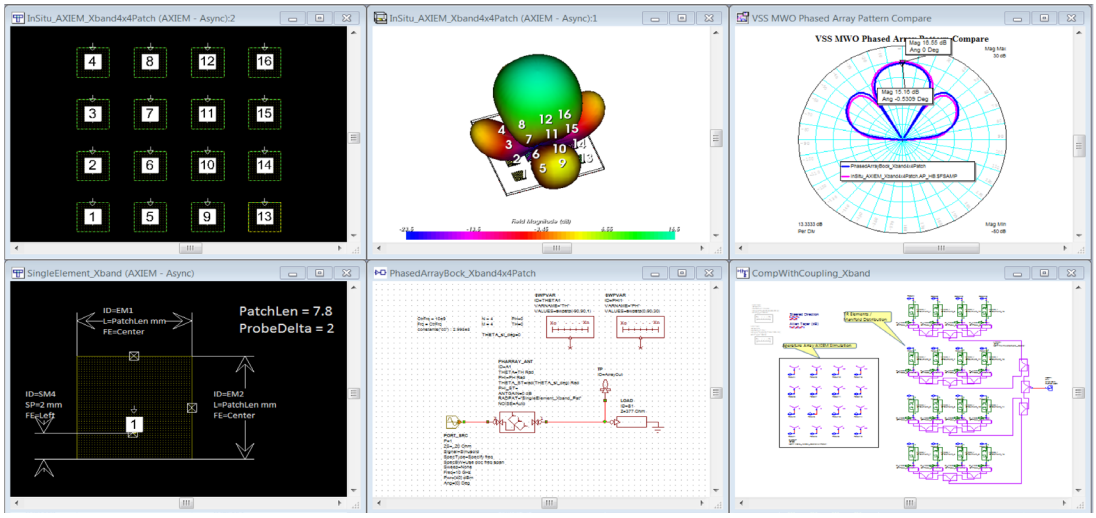

Figure 81: Antenna array pattern being simulated in the AWR AXIEM EM simulator embedded within AWR Microwave Office software

What makes these antenna patterns so difficult is that because the elements are being driven by power amplifiers in saturation, as the beam is scanned, the load impedance to the power amplifier changes and therefore the input impedance to the elements changes. A classic example of this is where designers taper the power coming into the antenna so the most power goes to the center elements with less power to the outside elements, which lowers the side lobes. This drives the power amplifiers of the elements in the middle to saturation much more than the ones on the outer part of the array, possibly resulting in different performance than expected.

Multi-Beam Support

In AWR VSS software, designers can simulate multiple beams using the phased-array element, which supports a variety of ways of doing this, including analog, digital, and hybrid beamforming, as well as single beam versus multi-beam and beam sweeping. Figure 82 shows how AWR VSS software enables designers to have multiple beams at different angles coming out of the same array.

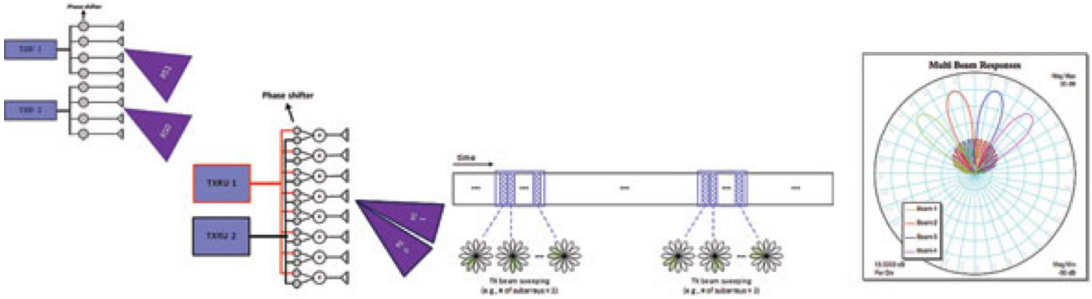

Figure 82: VSS software provides a variety of ways for simulating multiple beams

In the analog beam-steering method, the RF carrier is sent in and branched out to the elements with an analog phase shifter at the RF frequency of each element. The designer then scans while changing the phase at that center frequency. The advantage of this technique is that it is relatively simple, however, it is not very accurate. A newer method is digital beam forming, where at baseband the designer digitally processes the signal, then upconverts it, getting a much more accurate steer on the beam. The problem with that is that now each element must have a separate feed, making the feed structure coming into each element much more complex and requiring upconversion at each element. As arrays are getting bigger, hybrid architectures are employed as a mix of digital and RF beamforming.

LTE Multi-Beam Example

Figure 83 is an LTE multi-beam example using VSS. On the left a subcircuit labeled “4 LTE signals” can be seen. That subcircuit contains four LTE signal sources transmitted out of the same phased array, with each signal broadcast at a specific beam angle aimed at four different receivers. As the designer changes the beam angles, the performance of each receiver can be monitored and the system throughput can be displayed, showing the effect of beam steering and beam placement. VSS enables designers to see how accurately they need to control the beams in order to achieve acceptable power and data throughput. They can also monitor a number of other measurements, such as ACPR, EVM, constellation, and more.

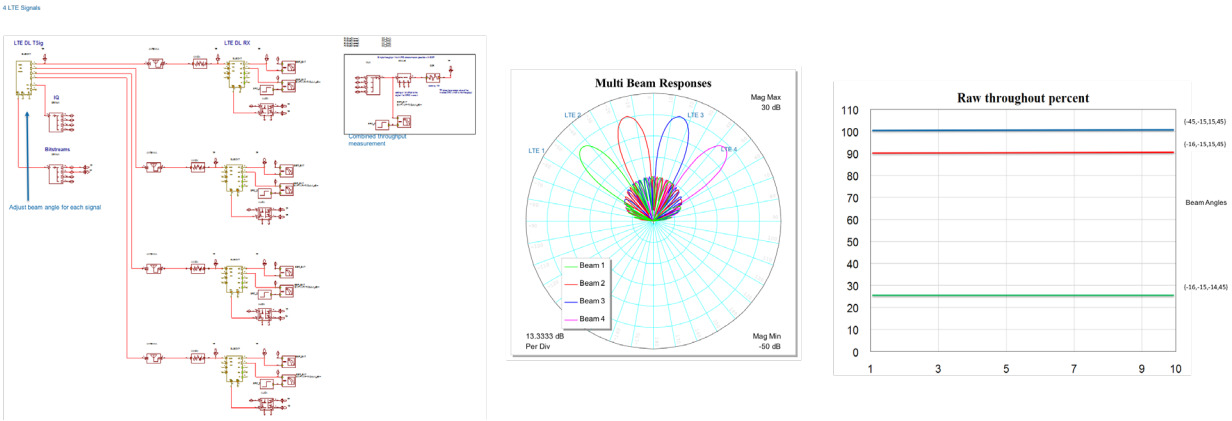

Figure 83: LTE multi-beam example.

28GHz Phased-Array Transceiver Example

Figure 84 is a VSS mockup of a 4x4 phased array prototype developed by IBM and Ericsson. Designers can run multiple tests to evaluate the performance of gain control, beam steering control, as well as array response over a range of frequencies.

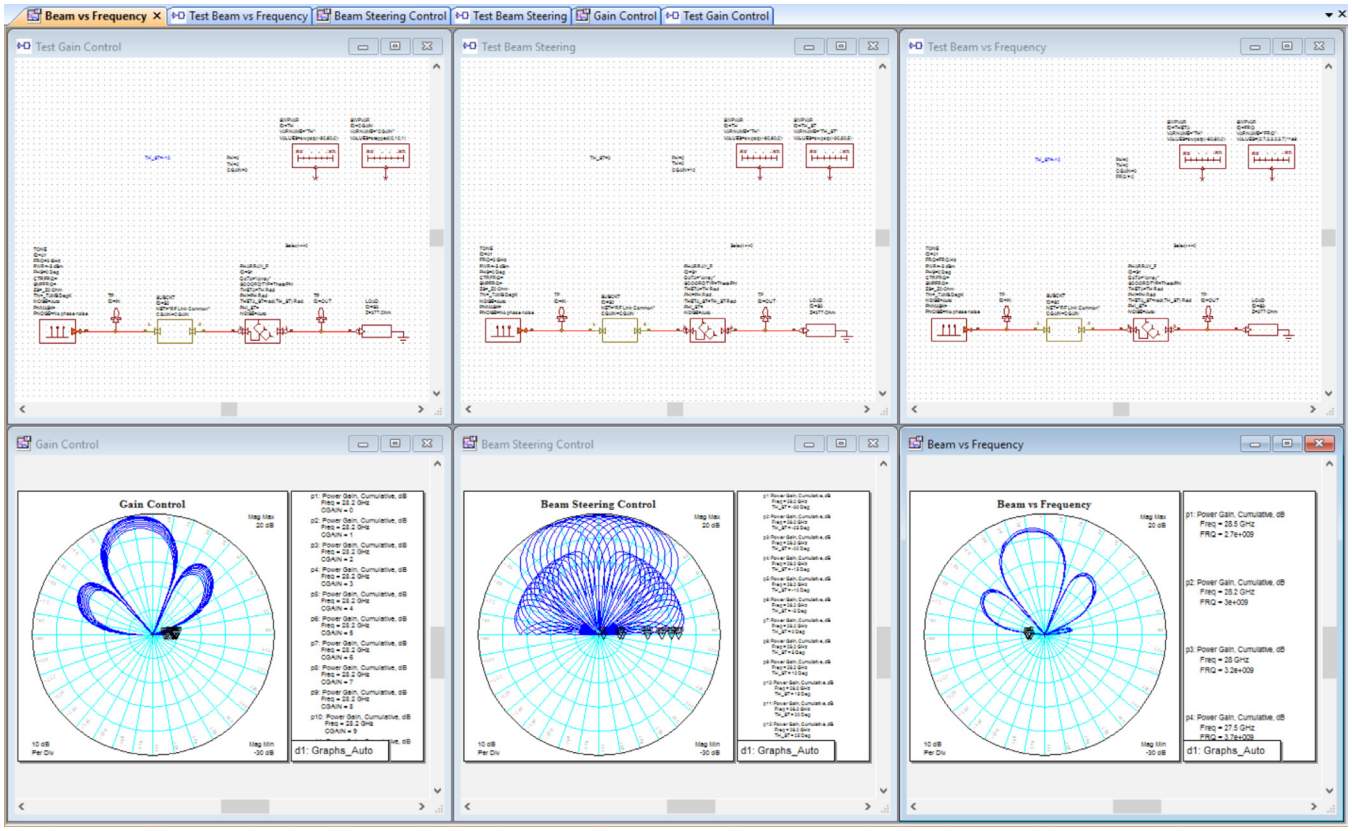

Figure 84: 28GHz phased-array transceiver in VSS software

AWR Design Environment software provides a powerful framework for simulating complex 5G MIMO systems with multi-beam and beamforming capabilities. The AWR AXIEM and AWR Analyst EM tools can be used for designing and evaluating the phased-array elements and their interactions. Element radiation patterns are included in phased-array system analysis. The effect of realistic RF links is included in the phased-array assembly to achieve realistic performance evaluations. A complete communication system can be modeled, inclusive of modulations, baseband processing, TX/RX links, noise effects, and propagation.

Conclusion

This 5G primer discusses some of the technical issues driving 5G NR development and provides several RF front-end, antenna, and system design examples based on the simulation technology within the AWR Design Environment platform developed to enable designers to overcome these issues. 5G NR exploits new modulation schemes, the use of aggregated bands in the sub-6GHz and mmWave spectrums, and MIMO/beam-steering antenna technology to achieve the performance goals of this next-generation communication network. The examples presented help demonstrate the modeling, simulation, and design automation capabilities in AWR software that support amplifier, filter, and phased-array antenna design for mmWave 5G applications. To learn more about the breadth of AWR software products available for 5G, visit www.awr.com/5g.